Final Technical Report

Fuel-Efficient Platooning in Mixed Traffic Highway Environments

Award: DE-EE0008470

United States Department of Energy (DOE)
Energy Efficiency and Renewable Energy (EERE)

October 1, 2018 through September 30, 2021

Recipient Organization:

American Center for Mobility (ACM)
2701 Airport Dr.
Ypsilanti, MI 48198

Principal Investigator:

Reuben Sarkar,
reuben.sarkar@acmwillowrun.org
734-223-9010

Subrecipients/Partners:

Auburn University

University of Michigan-Dearborn (UM-D)

United States Army Combat Capabilities Development Command (DEVCOM) Ground Vehicle Systems Center (GVSC)

National Renewable Energy Laboratory (NREL)

Michigan Department of Transportation (MDOT)

DOE Project Team:

Program Manager: David Kirschner
Contract Specialist: Patrick Mayle
Contract Officer: Angela Bosley

Submitted On: December 8, 2021

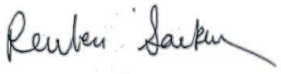

Acknowledgments: This material is based upon work supported by the U.S. Department of Energy's Office of Energy Efficiency and Renewable Energy (EERE) under the Award Number DE-EE0008470.

David Kirschner (DOE-National Energy Technology Laboratory-Pittsburgh); Mark Smith and Michael Laughlin (DOE-Vehicle Technology Office); David Bevly and Mark Hoffman (Auburn University); Sridhar Lakshmanan and Paul Richardson (University of Michigan-Dearborn); Andrew Kotz and Jeff Gonder (National Renewable Energy Laboratory); Mark McKaig and Scott Heim (Ground Vehicles Systems Center); Collin Castle and Michele Mueller (Michigan Department of Transportation); Dennis Winslow (Intertek); Reuben Sarkar, Dhiren Verma and Beth Jakubowski (ACM).

American Center for Mobility
2701 Airport Dr.
Ypsilanti, MI 48198
(734) 472-0102 – Office Number

Table of Contents

1 Cover Page Data Elements 6

2 Executive Summary 7

2.1 Introduction 7
2.2 Objectives 9
2.3 Approach 9
2.3.1 Testing Overview 10
2.3.2 Fuel Consumption Measurement 14
2.3.3 Outlier Removal 19
2.3.4 Effect of Sensor Performance on Platooning 22
2.3.4.1 Dynamic Base Real-Time Kinematic Positioning (DRTK) 22
2.3.4.2 Delphi Electronically Scanning Radar (ESR) 23
2.3.5 Modeling and Simulation 25

3 Accomplishments 27

3.1 NCAT 2019 Results 27
3.2 ACM 2019 Results 29
3.3 NCAT 2020 Results: H-Infinity Control 31
3.3.1 Establishing Ideal Platoon Performance 33
3.3.2 Cut-ins and Merges with H-Infinity Control 35
3.3.3 Controller Development Prior to ACM 2021 Testing: NMPC 38
3.4 ACM 2021 Results 40
3.4.1 Cut-ins and Merges with NMPC Platoons 42
3.5 V2V Communications Subsystem Performance 43
3.5.1 Occlusions 43
3.5.2 Rain 45
3.5.3 Antenna Position 46
3.5.4 RF Interference 51
3.5.5 GPS Outage 52
3.5.6 Road Curvature 53
3.5.7 Grade 54
3.6 Effect of Sensor Performance on Platooning 55
3.6.1 Effect of Faulty Radar on Platooning 55
3.6.1.1 Sensor issue 55
3.6.1.2 Control effects 56
3.6.1.3 Dynamic effects 56
3.6.1.4 Fuel Effects 57
3.6.2 Effect of Degraded GPS on Platooning 58
3.6.2.1 Sensor issue 58
3.6.2.2 Control effects 59
3.6.2.3 Dynamic effects 60
3.6.2.4 Fuel Effects 61
3.6.3 Effect of Radio Interference 61
3.6.3.1 Sensor issue 61
3.6.3.2 Control Effect 62
3.6.3.3 Dynamic Effect 63
3.6.3.4 Fuel Effect 63
3.7 Modeling and Simulation 64
3.7.1 Modeling 64
3.7.1.1 Test road 64

3.7.1.2 Sensors 65
3.7.1.3 Weather Conditions 67
3.7.1.4 Control and Actuation 68
3.7.1.5 Vehicle Dynamics 69
3.7.2 Simulation 70
3.7.2.1 Scenario A 71
3.7.2.2 Scenario B 74
3.7.2.3 Scenario C 74
3.7.2.4 Scenario D 77

4 Conclusions 80
4.1 Overall Testing Performance 80
4.2 Influence of Cut-Ins and Merging 80
4.3 Influence of Grade 80
4.4 V2V Communications Subsystem Performance 82
4.5 Effect of Sensor Performance on Platooning 82
4.6 Modeling and Simulation 82

5 Recommendations 83
5.1 For Real-World Fuel-Efficient Platoon Control 83
5.2 On Allowed Platoon Headway Variance 83
5.3 V2V Communications Subsystem Performance 83
5.4 Effect of Sensor Performance on Platooning 83
5.5 Modeling and Simulation 84

6 Products 85
6.1 Publications/Presentations 85
6.2 Patents Applications/Inventions 86
6.3 Works Cited 86

1 Cover Page Data Elements

Please see the above Title Page for all the necessary data elements referenced in the reporting requirements checklist for RD&D awards.

2 Executive Summary

2.1 Introduction

Platooning has become a focus area for heavy-duty vehicle fuel savings during highway driving. Often, the platoon formation is controlled by a system called Coordinated Adaptive Cruise Control (CACC). CACC platooning seeks aerodynamic fuel economy benefits while simultaneously decreasing driver strain by setting and maintaining a desired headway from preceding vehicles. Under close following conditions, the controller must exhibit robust characteristics during testing to be considered safe.

Specific to this study, real-time vehicle to vehicle (V2V) communication shares vehicle state information among members of the same platoon, enhancing control response as the platoon members adjust to surrounding vehicles. Trucks not on the leading or trailing edge of the platoon exhibit benefits stemming from a push effect from the truck behind and a pull effect from the truck preceding it.

The aerodynamic drag reduction for heavy-duty platoons is reasonably well-understood. If all other loads remain consistent, the lowering aerodynamic drag reduces the required vehicle power and leads to holistic fuel-/energy-efficiency gains. However, the influence of disturbances on the platoon energy efficiency is not negligible. Due to the cooperative nature of platooning, disturbances impose greater control demands on platoon members relative to single vehicle driving scenarios, particularly in the presence of velocity and grade changes. These new control demands could jeopardize the platooning efficiency benefits.

Velocity and grade disturbances correspond to vehicle cut-ins/merges within the platoon and hilly terrain, respectively. These two disturbances may be treated as distinct problems to solve. In the case of velocity disturbances, the string-stability of the platoon must be analyzed.

This work examines experimental platooning investigations at the National Center for Asphalt Technology (NCAT) and the American Center for Mobility (ACM) utilizing both a PID-based CACC and an alternative control design. These controllers were developed by the Global Positioning System (GPS) and Vehicle Dynamics Lab (GAVLAB). This work utilizes various heterogeneous platooning of up to four class-8 truck configurations to better understand fuel economy benefits experienced by each truck in varied, real-world platoon scenarios. The novelty of this study comes from the heterogeneous nature of the trucks, a thorough exploration of longitudinal truck spacing/positioning, and the purposeful subjection of the platoon to vehicle cut-in and grade disturbances. These novelties combine several main factors affecting fuel economy during platooning as seen in Figure 1.

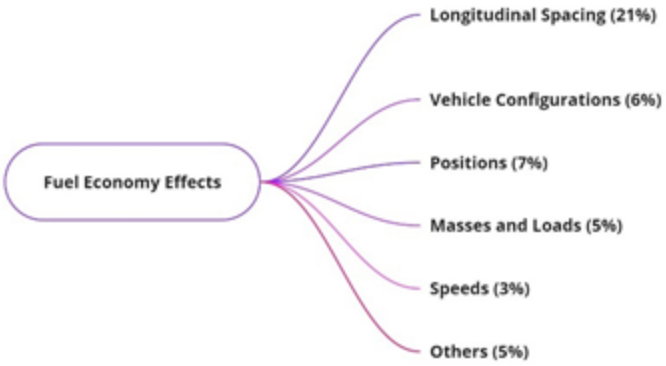

These disparate factors influencing platoon energy efficiency are isolated in this experimental campaign through strict procedural design. A baseline condition is established for each truck while operating in isolation. Platooning energy savings are then calculated relative to baseline operation for each vehicle at each test track. This work then establishes an ideal experimental case to which platooning benefits from non-ideal scenarios can be compared. This ideal scenario includes perfect alignment of trucks and near zero grade changes. An ideal cycle provides a standard of optimal (yet realistic) platooning conditions for future testing and analysis. This study compares each platoon configuration's energy utilization against ideal platooning performance as an assessment of platoon effectiveness. The aim of this study is to realize the truck platooning benefits for different types of trucks as they operate in various truck-trailer-configuration combinations in ideal scenarios and compare those results to drive cycles containing additional exogenous disturbances, such as grade changes and curves.

In addition, V2V communications is an important element of CACC (Francisco and Vicente 2019) as well as higher-level autonomy. This study also properly characterizes the behavior of the communication channels and networks that are used to enable this inter-vehicle communication, for optimization of future network planning and layout.

Platooning systems critically rely on information from several sensors: radar, radio communication, and global positioning. The performance of these sensors and communications can impact measurements and coordination critical for platooning, and as a result, impact the platoon fuel economy. While a Kalman Filter is introduced to help mitigate poor measurements from sensors, not all bad measurements can be adequately filtered out. We also analyzed the fuel economy of the platoon in the scenarios where the sensors perform sub-optimally, building on prior work:

- Effect of V2V communications on platooning (Bergenhem, Hedin and Skarin, Vehicle-to-Vehicle Communication for a Platooning System 2012) (van Nunen, et al. 2017) (Lyamin 2016) (Yu, et al. 2018) (Zeng, et al. 2019) (Bergenhem, Johansson and Coelingh, Measurements on V2V Communication Quality in a Vehicle Platooning Application 2014),
- Modeling and simulation (Wang, Wu and Barth, Developing a Distributed Consensus-Based Cooperative Adaptive Cruise Control System for Heterogeneous Vehicles with Predeessor Following Topology n.d.) (Wang, et al. n.d.) (Wang, Wu and Barth, A Review on Cooperative Adaptive Cruise Control (CACC) Systems: Architectures, Controls, and Applications n.d.) to study the interplay between V2V communications and control in platooning (Gonçalves, Varma and Elayoubi 2020) (Zhang, et al. 2017),
- Effects of highway traffic conditions and road grade on platooning (Shladover, et al. 2014) (Lu and Shladover n.d.),

- Performance of CACC by varying operational and environmental conditions (Eilbert, et al. 2020) (McAuliffe, et al. n.d.) (Crane, Bridge and Bishop 2018) (Roberts, et al. n.d.),
- Improve V2V reliability for platooning (Sybis, Kryszkiewicz and Sroka 2018), and
- Impact of 5G V2V technology on platooning (Serizawa, et al. 2019) (Nardini, et al. 2018).

We also undertook a simulation and modeling effort to study some of the same effects. The real-world environment being modeled is ACM. It builds on previous simulation work from our group to understand the performance of a two-truck platoon using PreScan simulation software under adverse weather conditions. This work differs from the previous work in that each of the trucks in this simulation utilizes a Dedicated Short-range Communications (DSRC) radio for V2V communications. Furthermore, a 3D map of the ACM has been employed to allow a more realistic analysis of the truck platoon as they navigate the 3D road network. Lastly, sensor noise and sensor failure of the long-range radar and short-range radar have been implemented to add another layer of fidelity to the model.

2.2 Objectives

The objective of this project is to improve multi-vehicle heavy-duty truck platooning efficiency and safety using automated controls, advanced communications, real-world testing, data analysis, and simulation development. The scope of work aims to autonomously control the entire fleet of three following vehicles – throttle, brake, and steering – while optimizing the entire platoon for fuel efficiency and safety. The scope includes baseline and initial testing in which controlled track tests are designed and executed; the development of algorithms and identifying/installing V2V communications required to optimize platoon performance through ramp testing and vertical curvature testing. Also, trucks will be instrumented with new data collection systems. Risk management and safety protocols will be developed prior to roadway testing. Furthermore, the scope includes the program management necessary to verify and report on these tests and evaluations.

2.3 Approach

Since 2015, Auburn University has been developing a platooning system that is referred to as CACC. This CACC system has been validated up to SAE Level 2 autonomy, which means lateral and longitudinal control is operational, but human supervision is required (Ward, Cooperative Adaptive Cruise Control (CACC) in Controlled and Real-World Environments: Testing and Results 2019).

The Auburn test platforms are fairly unique if their autonomy is achieved. Rather than have an actuator physically command an acceleration through a throttle angle, the Auburn system acts as the vehicles automated cruise control (ACC) system. As a result, and as long as the Auburn platooning system has access to the vehicles Controller Area Network (CAN), it can control the vehicle.

The Auburn platooning system also has a fallback method in the case of unexpected behavior. All the CAN traffic being commanded by the Auburn system, must go through the CAN gateway which has an internal physical disconnect switch that will stop all CAN traffic from the Auburn computer. The Auburn hardware setup is shown below in Figure 2. The CACC system relies on several sensors: a Delphi Electronic Scanning Radar (ESR), Novatel ProPak GPS receivers, Memsense (3020) IMU's and Cohda MK5 OBU Wireless radios for V2V communication. The effects of the performance of the MK5 radio, Delphi RADAR and Novatel GPS receiver on semi-truck platooning were studied in this project.

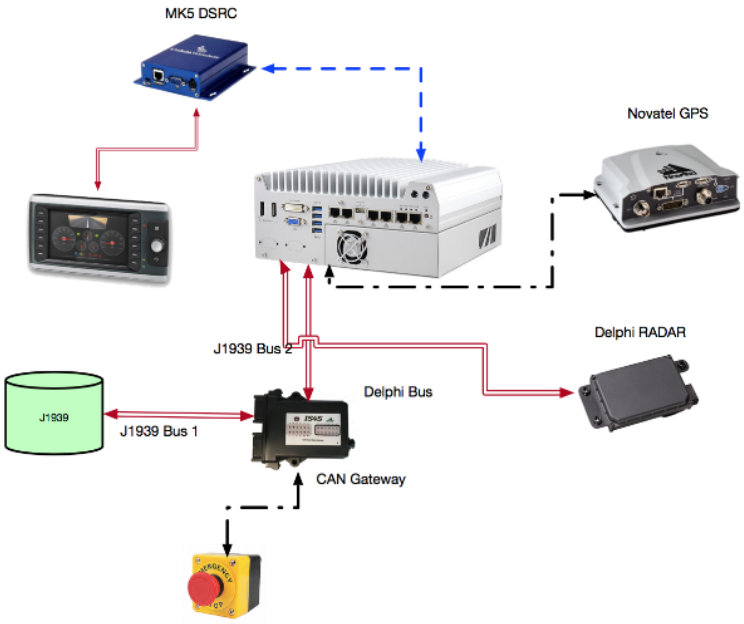

2.3.1 Testing Overview

Testing occurred in two periods (excluding the controller development on US-280 prior to the final phase). Each period was composed of baseline and platoon testing with a variety of platoon configuration at two test tracks: NCAT and ACM. Thus, there were 4 total phases in which fuel consumption was quantified.

The ACM test track located in Ypsilanti, Michigan is a roughly circular loop. The track includes an overpass and tunnel and is about 2.3 miles in length. A satellite view is shown in Figure **3**.

The NCAT test track located in Opelika, Alabama, is capsule shaped and is about 1.7 miles in length with no special considerations such as bridges or tunnels. Figure 4 gives the satellite view of this test track.

The four class-8 trucks consisted of: two 2015 Peterbilt 579s utilizing different engines, namely a Cummins ISX15 and a Paccar MX-13, and two 2009 Freightliner M915A5s, each with a Detroit Diesel S60, where one vehicle was armored and the other unarmored. The Paccar-engine Peterbilt truck is denoted as A1, the Cummins-engine Peterbilt truck is denoted as A2, the armored M915 is denoted as T13, and the unarmored M915 is denoted as T14.

As mentioned before, the platooning control system uses a variety of sensors and algorithms. A DSRC radio established a V2V communication network. The range between trucks was determined using a combination of GPS, radar, and transmitted wheel-speed measurements as the inputs to a Kalman-Filter estimator. Control of the trucks is accomplished by sending commands over the vehicles' CAN's using the architectures in place for Adaptive Cruise Control (ACC). A central, standalone computer running Robotic Operating Software (ROS) unites all the sensors and systems and runs the control and estimation algorithms.

The DSRC network used Cohda Wireless MK5 OBU's. Each radio was connected to a pair of antennas mounted left and right on the truck cab for diversity. The antennas used were the ECOM6-5900's from MobileMark, 5.9 GHz dipole antennas with 6 dBi of gain and the antenna pattern shown in Figure 5.

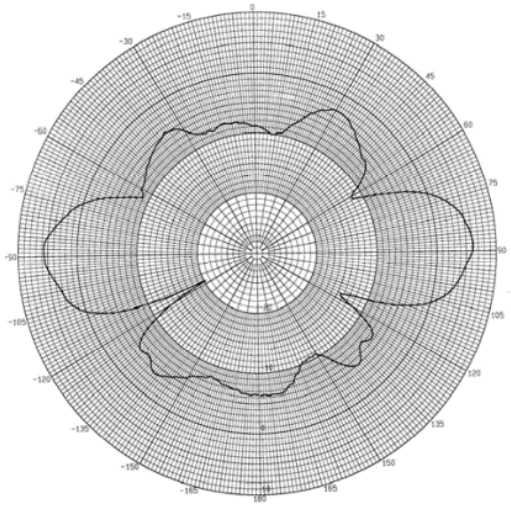

While we chose to use dipole antennas for availability reasons, it is worth noting that there are several interesting attempts at designing DSRC-specific antennas such as (Liou and Mao 2017), (Ekiz, et al. 2014) and (Onishi, et al. 2013).

The trucks were equipped with electrically assisted steering wheels to enable level II autonomy, although for this testing the trucks were manually steered.

All vehicles were warmed up with one hour of track operation prior to any fuel quantification, enabling fluid and tire temperatures to reach equilibrium. Any gaps in testing were limited to under thirty minutes or else the trucks would require another warm-up period.

Various platooning configurations were considered during the creation of the testing matrix for each testing campaign. Standalone baseline runs were conducted where trucks operated in isolation to prevent any aerodynamic effects from other trucks on the track. Subsequently, two and four–truck platoon configurations were examined at various longitudinal spacings. This work employs the moniker "2T" to represent a two-truck platoon (either A1 leading T14 or T13 leading A2), while "4T" designations imply four-truck operation (in the following order: A1, T14, T13, A2). Numbers at the end of these designations (for example, 4T 50) indicate the following distance from the preceding truck in feet. The different 2T and 4T platoons are illustrated in Figure 6.

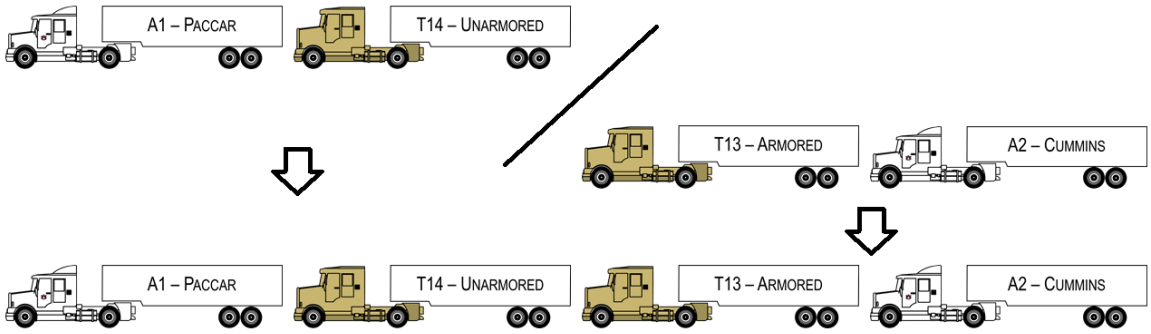

In addition to baselines, 2T, and 4T runs, cut-in and merge runs were performed. Cut-ins are distinguished from merges in this work by only one criterion: a cut-in involves detection of a vehicle by range estimation (the same algorithms for platooning gap estimation) while a merging vehicle communicates its intentions to the platoon pre-emptively via a V2V radio in the merging vehicle. Thus, in merge cases, the platoon preemptively opens a gap for the incoming vehicle, whereas the platoon senses and reacts to a cut-in event.

Fuel results for cut-ins and merges were performed during three of the four testing periods: NCAT 2019, NCAT 2020, and ACM 2021. A schematic of the cut-in and merging strategy is shown in Figure 7. Note the sharp drop in perceived headway when the cut-in vehicle is detected, accompanied by the fuel command reaching zero.

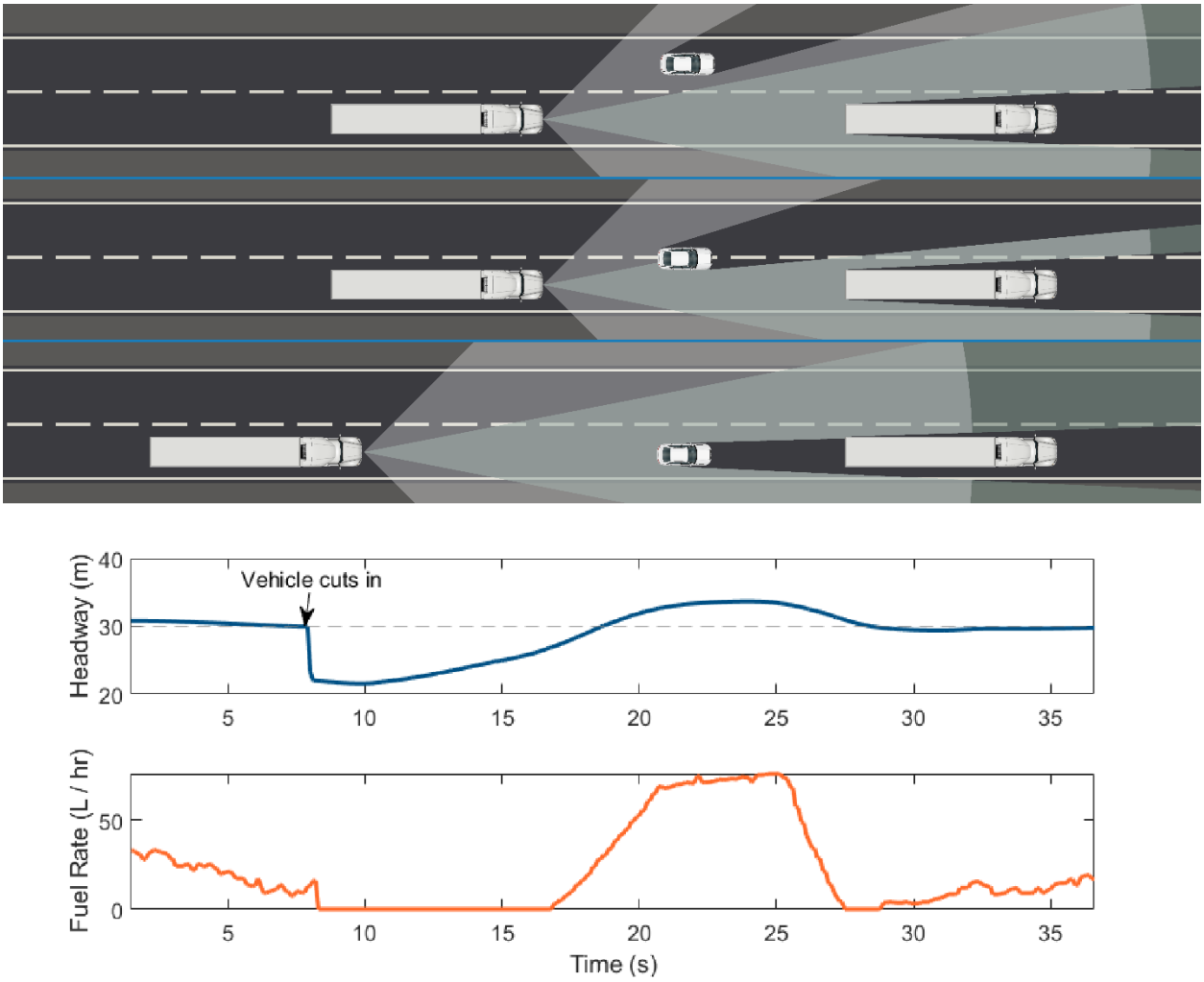

2.3.2 Fuel Consumption Measurement

Initially, redundant fuel consumption measurement methodologies were outfitted on the trucks during the test campaigns. In the early test stages, both gravimetric measurements and AVL KMA fuel flow data were collected (Figure 8). With the four-truck testing however, timing was very tight to weigh all four tanks without violating the maximum 30 minutes of downtime.

All trucks were outfitted with AVL KMA fuel flow meters. Due to differences in the fuel flow pathways of the trucks, the implementations were different for the Peterbilts versus the M915s. On the Peterbilts, a housing was fabricated for the KMA, and the secondary tank plumbing was rerouted to the KMA and an auxiliary fuel tank.

KMA logging issues during several of the test campaigns led the team to investigate the calculated CAN fuel rate's accuracy. The CAN calculated fuel quantification agreed well with the KMA and gravimetric methodologies, facilitating its use for all fuel consumption results.

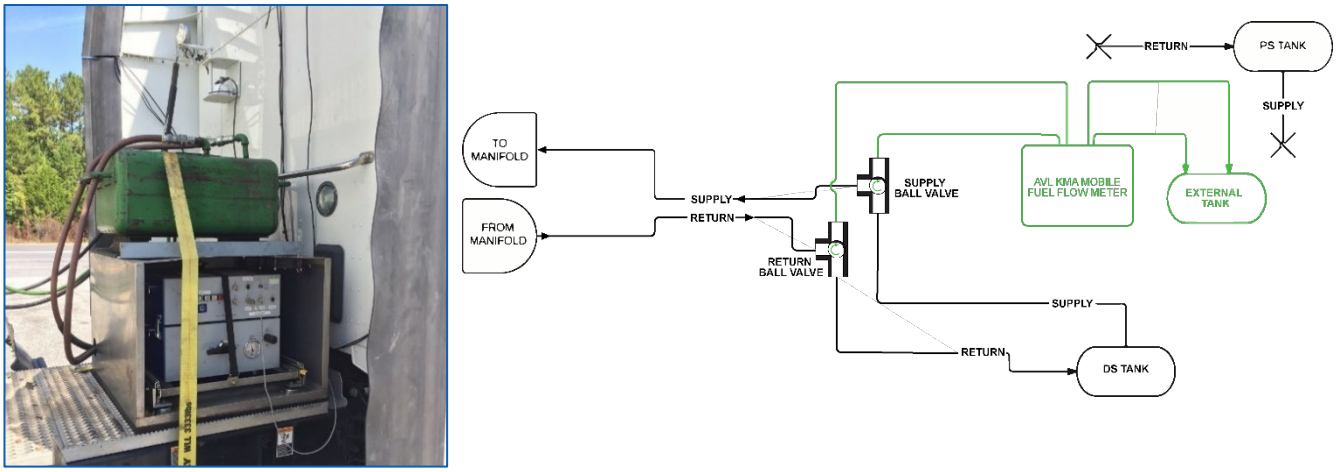

Figure 8: KMA and Gravimetric weigh tank setup

Many difficulties were encountered in this setup. The original solenoids for fuel switching did not sufficiently resist backflow, leading to short-circuiting of the fuel flow from auxiliary tank to primary. Unfortunately, this issue was not immediately detectable and the NCAT 2019 and ACM 2019 campaigns could only rely on CAN fuel data. Subsequent testing replaced the solenoids with remotely operated ball valves.

For NCAT 2020 and ACM 2021, the J1939 reported CAN fuel flow rate was recorded, timestamped and measured via ROS on the Auburn CACC computer. The AVL KMA fuel flow measurement was recorded on a separate system using the AVL Device Control Software, into an unsynchronized Comma Separated Values file. As a result, a time alignment procedure had to be developed. The process began by dividing a day's worth of KMA data into "runs", a manual process illustrated in Figure 9.

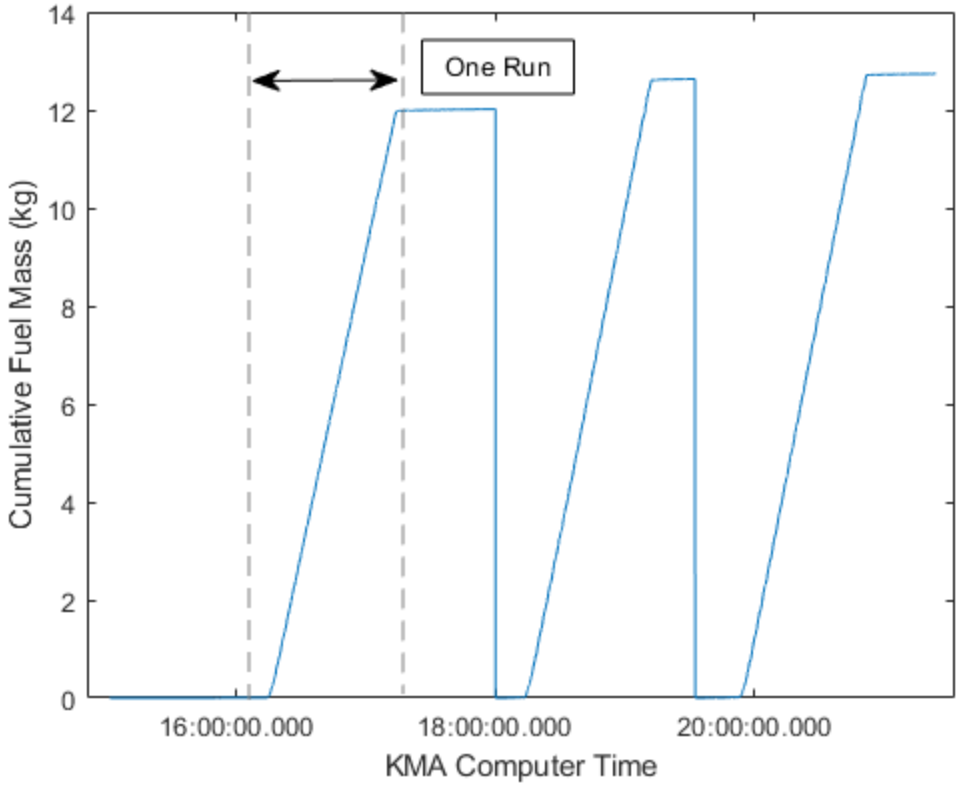

Next, the data had to be named accordingly and cross-correlated with the CAN fuel rate data stream to identify the time offset between the start of the CAN data and the start of the KMA data. The sample rate of the KMA data is 1 Hz, whereas the J1939 stream was recorded at 10 Hz. Due to the mismatch in sample rate between the two signals, the KMA data was up sampled to 10 Hz rather than down sampling the CAN fuel rate. By up sampling instead of down sampling, the time offset calculation had higher resolution and high frequency parts of the CAN fuel rate were preserved. Using the MATLAB function *xcorr*, cross-correlations were calculated for the up sampled KMA fuel volume flow and the CAN fuel rate. Due to occasional incorrect lag calculations, other peaks in the cross-correlation were also used where necessary, as is shown in Figure 10.

Not all data was taken for cross correlation: as a point of reference, of 129 CAN datasets from NCAT 2020, 86 were deemed well aligned, which was easily done visually.

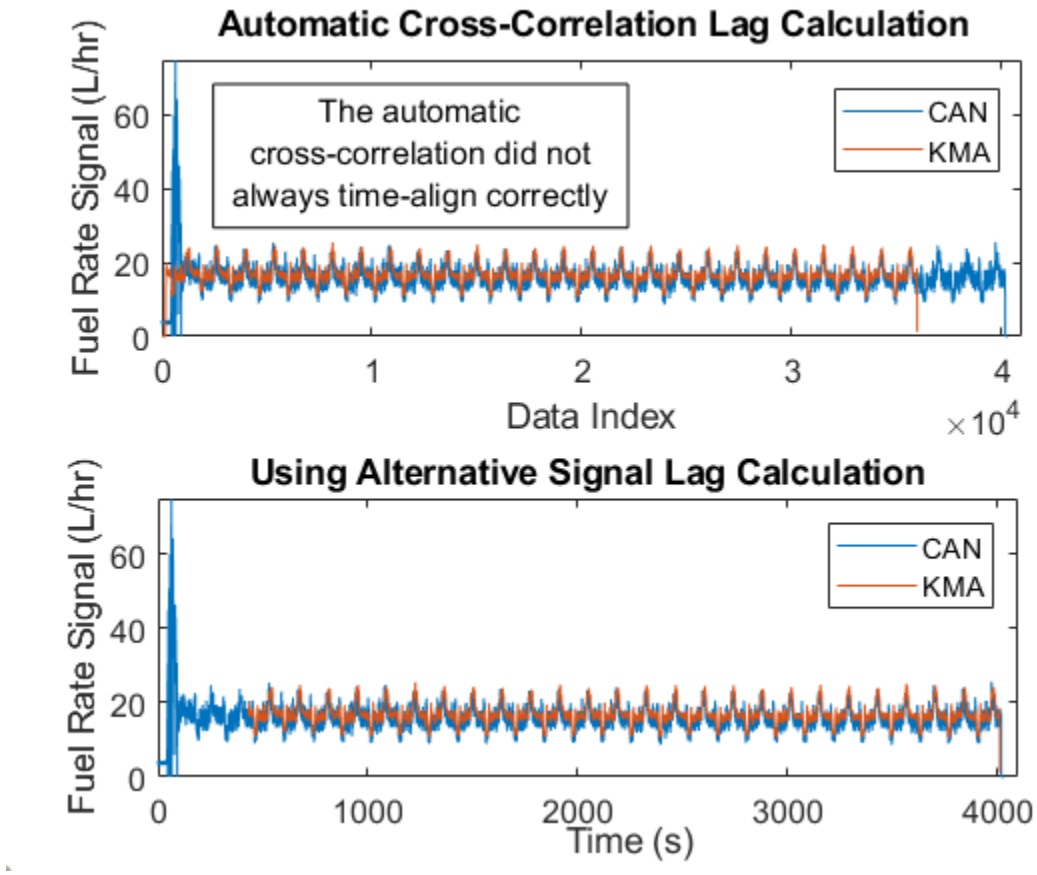

Figure 10: Cross-Correlating KMA and CAN fuel rate signals to time align them sometimes required manual intervention

Using these approved datasets, the final calibration process was undertaken. CAN data was divided into laps using GPS in a process similar to that in (Stegner et al. 2021). Because the KMA time vector was corrected to the same time as the CAN time in the previous step, the KMA signals could also be divided into laps in the same way, demonstrated in Figure 11. The KMA data stream was only temporarily up sampled for the previous time-alignment step, so here the original 1 Hz data was used, now having an offset applied to its time vector.

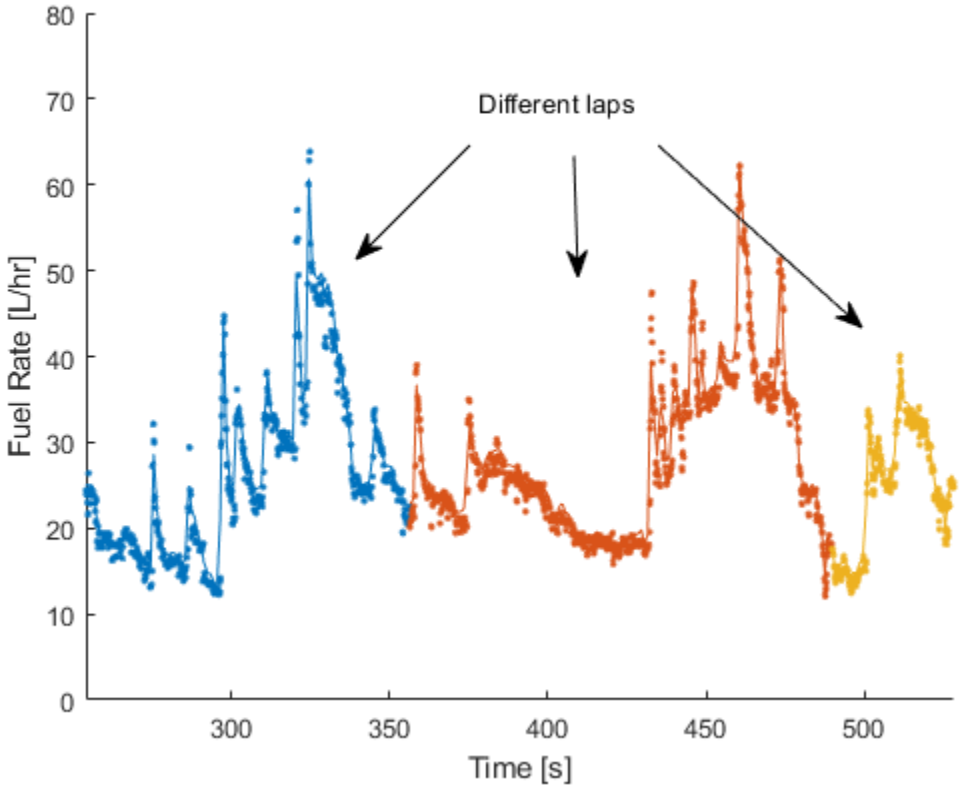

Figure 11: KMA and CAN fuel rates divided into laps and plotted on their own time vectors to verify cross-correlation

Finally, for each of these laps, the cumulative fuel used was calculated and binned, and CAN fuel use was divided by KMA fuel use to get a ratio of the two. Because it was unknown if the volume flow signal from the KMA represented an aggregate over the last sample period of KMA flow data or merely a point sample, the cumulative volume signal from the KMA was used instead in comparison to trapezoidal integration of the CAN fuel rate.

Outlier rejection was performed on the population of CAN to KMA ratios, treating any ratio greater than 3 scaled median absolute deviations (MAD) from the median as an outlier. In general, this process resulted in few laps being rejected, and mostly only partial or clearly erroneous laps, which was the main motivation for outlier rejection in the first place.

Having removed outliers, the CAN to KMA ratios of each run of each truck were then aggregated into a single vector per truck, from which the mean ratio was calculated. NCAT (Figure 13) and ACM (Figure 12) were correlated separately. The results are shown in Table 1.

Table 1: CAN to KMA fuel use ratios at each track

CAN/KMA	A1	A2	T13	T14
NCAT 2020	0.929	0.934	0.940	0.937
ACM 2021	0.936	0.962	0.966	0.962

At NCAT, where there was less velocity variation and control aggressiveness, the correlations were near 0.93 for most trucks. In contrast, at ACM, the correlations were closer to 0.96 for the following vehicles:

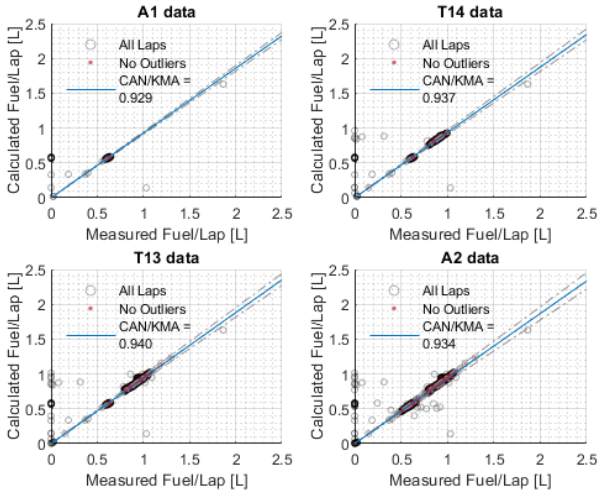

Figure 13: NCAT CAN vs KMA fuel per lap

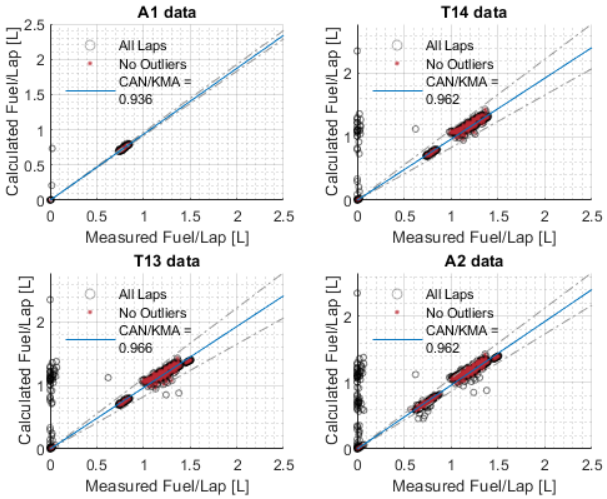

Figure 12: ACM CAN vs KMA fuel per lap

2.3.3 Outlier Removal

A significant effort was expended to remove outliers from the data population, leaving only experimental runs that truly represent a driving cycle for the trucks. The process proved necessary during analyses and was applied to the current data to remove laps containing testing errors. These errors consisted of GPS drops, vehicles kicking out of CACC mode mid-run, and other equipment malfunctions. Plotting vehicle speed versus track distance allows these errors to become apparent as seen in Figure 14 where each trace represents one lap during an arbitrary test run.

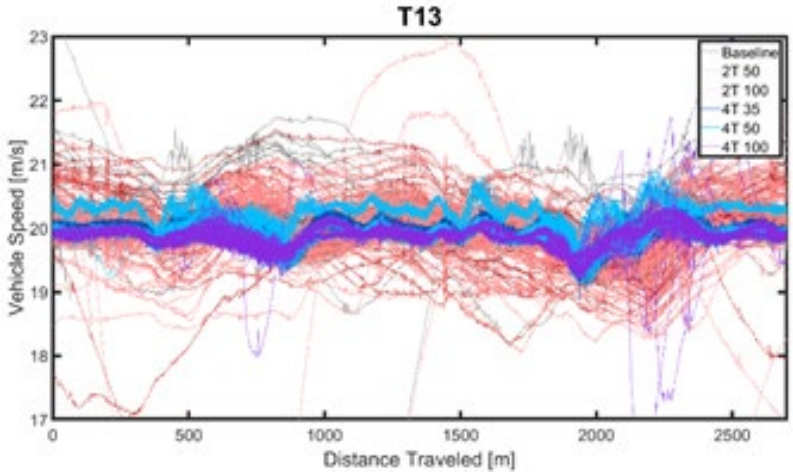

Figure 14: Speed Traces for T13 before the Outlier Removal Process, NCAT 2020

The color scheme for this experiment will remain consistent throughout the content of this paper. While errors are not as prevalent (or potentially nonexistent) in A1's runs, they are more obvious

when other trucks are considered, particularly for those further back in platoon order, T13 and A2. It is expected A2 will experience the greatest number of excursions due to the accordion-like nature of speed variances imposed on the platooning trucks. Depending on the controller design, speed dithers can be passed down from the lead truck to the last follower truck in compounding fashion, and the expected quantity of outlier behavior caused by testing errors increases as you go down the platoon. To automate the procedure and remove observer bias, bounds were set on the speed data, acting as limits that the speed traces must fall between. These bounds were calculated at each time step for each lap, each truck, and each configuration. The bounds used in the outlier removal process were ±2 standard deviations away from the mean of the speed traces at each time step. T13's 2T 100 bounds are illustrated in Figure 15.

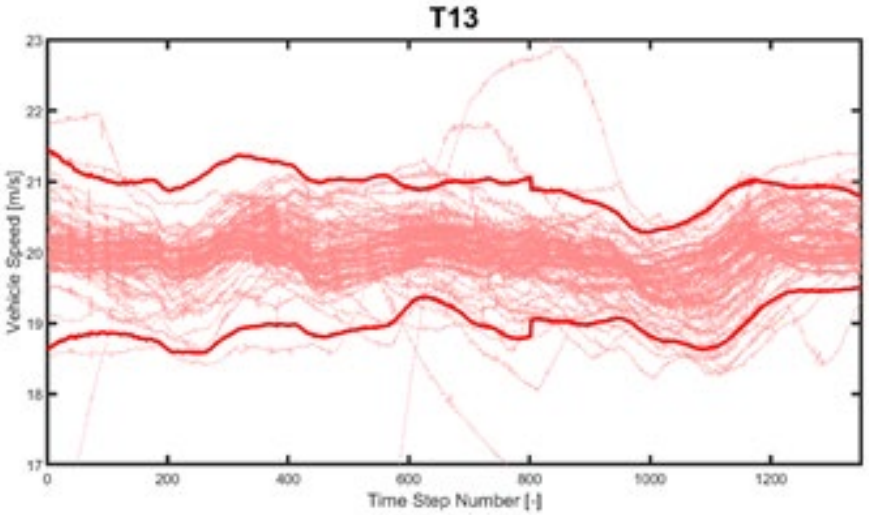

Figure 15: T13 2T 100 Speed Traces with Upper and Lower Bounds (in bold) before the Outlier Removal Process, NCAT 2020

Each truck-configuration combination received its own set of bounds so that four-truck platoons (typically noisier, containing more variance) did not influence the outlier removal for baseline (least noisy, lowest variance) runs. Laps containing more than 10% of their time steps outside those bounds were removed. The process then iterates, recalculating fresh standard deviation bounds while the 10% limit remained the same. A mathematical model for the removal criteria can also be written as Equation 1.

$$\left[\left(\sum_{i=1}^{N} t_i > +2\sigma_i\right) + \left(\sum_{i=1}^{N} t_i < -2\sigma_i\right)\right] > N * 0.1 \quad (1)$$

where: N = total number of time steps for an arbitrary lap [-]

t_i = any given time step in that lap [s]

σ_i = standard deviation at that time step [m/s]

If the sum of time steps for an arbitrary lap outside the standard deviation boundaries is greater than 10% of the total number of time steps, the lap is removed. This process was iterated until zero laps were removed from any truck-configuration combination for data recorded at both NCAT and ACM. NCAT data took 11 iterations to eliminate all outliers while ACM required 16. This was

expected due to the increased transiency experienced by all trucks at ACM. A breakdown of how many laps removed from the total data population during each iteration is shown in Figure 16.

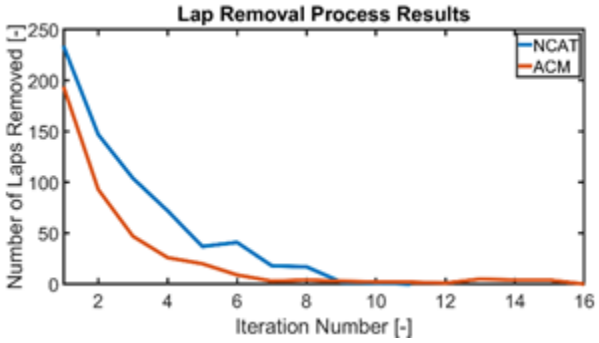

Figure 16: Breakdown of Lap Removal Process, How Many Laps Removed at Each Iteration, NCAT 2020

The data sets considered in Figure 16 each contain more than 2,800 laps. The automated, iterative outlier removal never removed more than 20% of any data population. This methodology proved to be an effective and repeatable way to remove outlier data for the experimental runs conducted at both tracks. Figure 17 shows the remaining population of T13's 2T 100 laps after iterating through the outlier removal process.

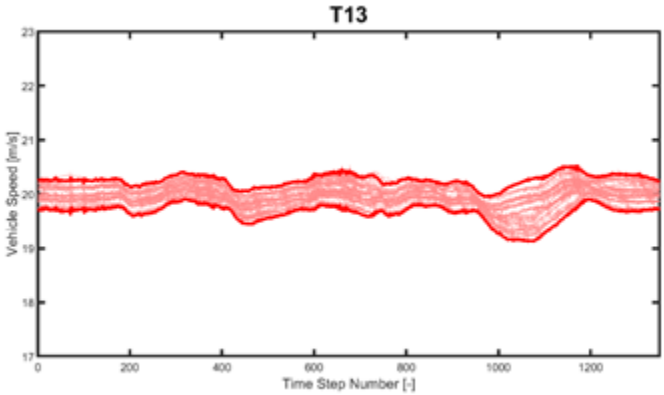

Figure 17: T13 2T 100 Speed Traces with Upper and Lower Bounds (in bold) After the Outlier Removal Process, NCAT 2020

This process does not remove every outlier in the data since it will not catch laps containing short segments of outlier behavior. However, this method does eliminate significant amounts of variance due to erroneous occurrences during testing. Figure 14 shows the speed traces for T13 at NCAT before the removal process and Figure 18 shows the speed traces after the removal process.

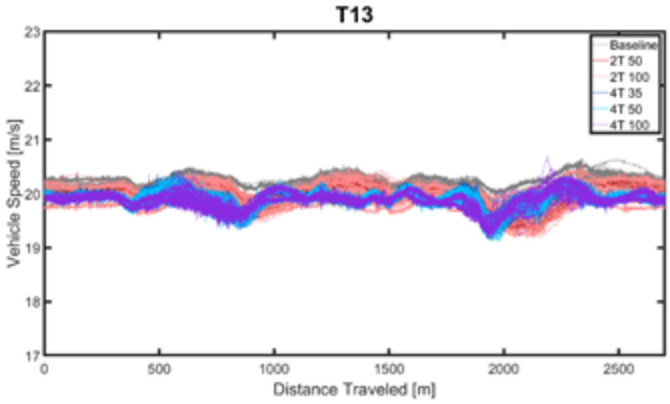

Figure 18: Outlier Removal Process Results for T13 Speed Traces, NCAT 2020

2.3.4 Effect of Sensor Performance on Platooning

The performance of the CACC system depends heavily on the reliability of the underlying V2V communications network. Using data recorded on precision-instrumented trucks at both ACM and NCAT test tracks, we provide an understanding of various effects on V2V network performance:

- Occlusions - non-line-of-sight (NLOS) between the Tx and Rx antenna may cause network signal loss.
- Rain - water droplets in the air may cause network signal degradation.
- Antenna position - antennas at higher elevation may have less ground clutter to deal with.
- RF interference - interference may cause network packet loss.
- GPS outage - outages caused by tree cover, tunnels, etc. may result in degraded performance.
- Road curvature - curves may affect antenna diversity.
- Road grade - antenna may have limited vertical coverage

2.3.4.1 Dynamic Base Real-Time Kinematic Positioning (DRTK)

GPS is the core measurement used in the Auburn platooning system. GPS allows for radar measurement initialization, provides centimeter to sub-centimeter accuracy range measurements, and allows for time-differenced carrier phase measurements to be used for accurate odometry measurements. While GPS alone does not provide an inter-vehicle range measurement, the use of V2V communication allows for raw GPS observables to be combined into a range measurement.

While GPS is a highly reliable measurement, it can suffer from atmospheric errors, receiver clock biases, multipath errors and more. To help reduce these errors, there are static GPS receiver on earth, called base stations, that broadcast GPS corrections to atmospheric errors. These corrections are referred to as real-time kinematic (RTK) positioning.

DRTK operates on the same principle as RTK. A GPS pseudo-range measurement can be formulated as:

$$\boldsymbol{\rho_a} = \|\boldsymbol{r_a}\| + \boldsymbol{c}(\boldsymbol{\delta t_a} - \boldsymbol{\delta t}) + \boldsymbol{\lambda}(\boldsymbol{T} + \boldsymbol{I}) + \boldsymbol{M_\rho} + \boldsymbol{\epsilon_\rho}$$

Where $\|\boldsymbol{r_a}\|$ is the true range from the receiver to the satellite, c is the speed of light, $\boldsymbol{\delta t}$ and $\boldsymbol{\delta t_a}$ are the receiver and satellite clock errors, T and I are the tropospheric and ionospheric affects, respectively, $\boldsymbol{\lambda}$ is the carrier frequency, M is multipath error, and $\boldsymbol{\epsilon_\rho}$ is measurement error. An important note is that atmospheric affects are considered to be constant within a certain region, usually within a few kilometers.

The details of the DRTK algorithm is beyond the scope of this paper, but a concise summary is included herein for thoroughness. If two vehicles are platooning with V2V communication, and the pseudo-ranges are passed from leader to follower, the following vehicle can difference the two values, $\boldsymbol{\rho_a}$ and $\boldsymbol{\rho_b}$, at which point the atmospheric errors will be cancelled, and a relative position vector (RPV) $\vec{\boldsymbol{\rho}}_{a/b}$ is returned. This RPV solution can be anywhere between centimeter to decimeter level accurate. This means the DRTK solution has an extremely low variance and can be used as a "truth" measurement for inter-vehicle distances. Figure 19 presents the DRTK solution overlaid on the best estimate of the inter-vehicle distance, or headway.

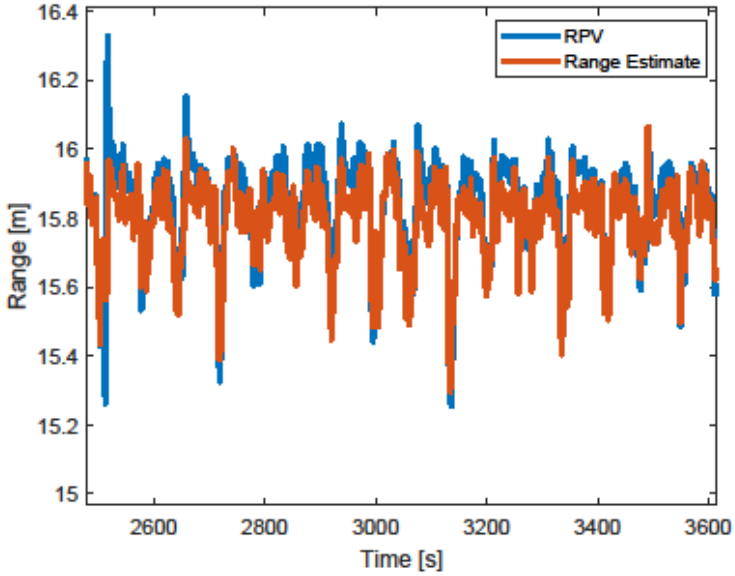

Figure 19: Accuracy of RPV vs Range Estimate

The GPS measurement is extrinsic and not inertial, so it is unaffected by engine, powertrain, and road vibrations. Therefore, static data from the NCAT test track allowed for a statistical categorization of the measurement. The noise characteristics for the GPS measurement are $\boldsymbol{\sigma} = \boldsymbol{.125m}$ and $\boldsymbol{\mu} = \boldsymbol{0}m$.

2.3.4.2 Delphi Electronically Scanning Radar (ESR)

The Delphi RADAR is another critical sensor for the CACC system. Delphi ESRs provide a measurement of range, range rate, and an estimated bearing between the radar and target object. Delphi ESRs have 64 channels, which means 64 separate radar data points are retuned. Each point has a unique radar track between 1-64, with each track having an associated range, range-rate and bearing. Selecting the correct radar track is done by using the DRTK measurements to create a "bounding box" on the trailer of the lead vehicle. Each radar track is then sequentially checked to see if it falls within the bounding box.

Figure 20 depicts range returns that were used by the platooning system at the NCAT test track, as well as a subplot of the track ID that was used for the range update. While the measurement

may seem “noisy”, most spikes are caused by a change in the ID selection for the range measurement. Figure 21 provides a look at the data at a smaller timescale to show that the range measurement variance falls within the expected range.

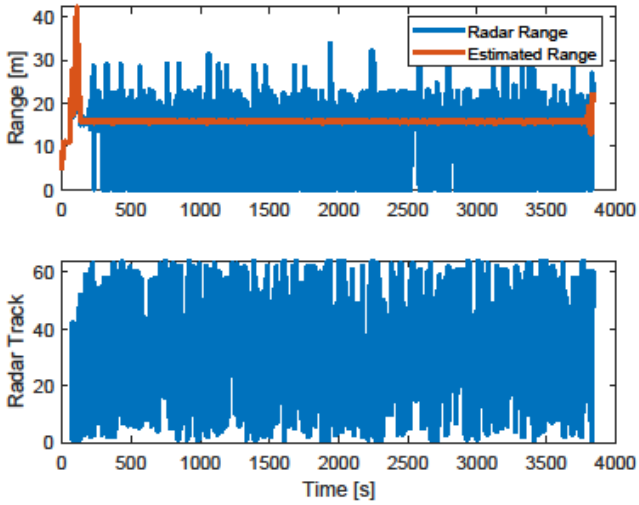

Figure 20: High-level radar range vs time

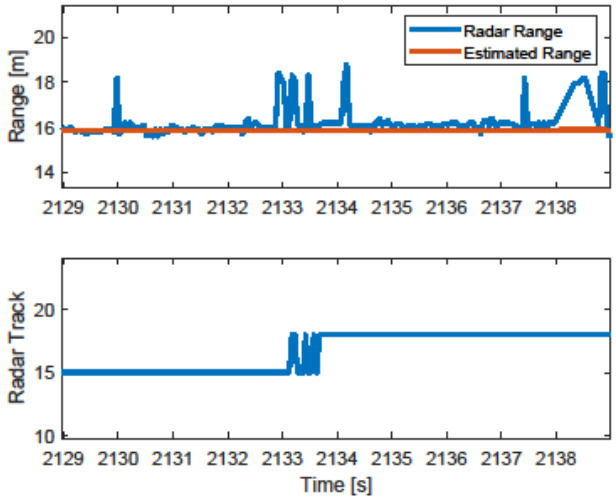

Figure 21: Selected radar range vs time

While vibrations can cause reductions in the Probability of Detection (PD) for a target due to shifts in the radar echo phase (Longman 2019), the actual measurement is relatively unaffected. This allows for a mean and standard deviation value to be established for the sensor. According to the Delphi datasheet, the noise characteristics on the range measurement are $\boldsymbol{\sigma = 0.25m}$ and $\boldsymbol{\mu} \in [\boldsymbol{-0.0125m}, \boldsymbol{+0.0125m}]$.

2.3.2.3 Dedicated Short-Range Communications (DSRC)

The DSRC protocol is used for communication in the 5.9GHz frequency range, at a varied power level of up to 23dBm (SAE V2X Core Technical Committee n.d.). Cohda MK5 OBU (On-board units, Figure 22) are used as the backbone RF interface via a custom (non-standard) wave service

message, that includes a payload of GPS constellation data, vehicle acceleration or deacceleration (breaking) status, and current velocity. These messages are broadcast, such that any other truck convoy within range receives these communications, which are interfaced to the rest of the system via an UDP socket connection.

Figure 22: DSRC Cohda MK5 OBU radios

2.3.2.4 Sensor Fusion

For many of the cases investigated herein, a sensor that is performing sub-optimally will be compared against an estimated range value. This estimated range is a combination of all available range and range-rate measurements on the platooning vehicle. These measurements are DRTK range, RADAR range and range-rate, and relative wheel speeds. The combination of these measurements is commonly referred to as sensor fusion, and in this instance is achieved through the use of a Kalman Filter (KF).

A Kalman Filter is a probabilistic filter that uses measurement noise characteristics as well as the process model uncertainty to optimally estimate the system states. The system states estimated in the Auburn CACC are $\hat{x} = [r \quad \dot{r} \quad \beta]^T$ which are the inter-vehicle range, range rate, and bearing, respectively. These states are outlined by Figure 23:

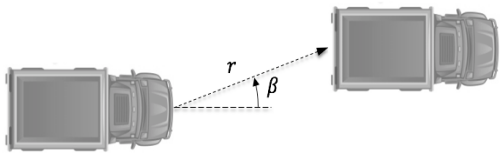

Figure 23: Estimated vehicle states.

While the full derivation of the KF is beyond the scope of this paper, it is important to note two design decisions. First, in the case that the Auburn platooning system loses radar line-of-sight and also loses radio communication, the Kalman Filter will assume a constant range-rate and continue to predict the states. The second design decision was the selection of the sensors, which is critically important because the KF weighs sensor noise variance verses the process uncertainty and the covariance of the estimated states. Because the platooning system has slow dynamics and a driveline model which is largely linear, the process uncertainty remains small. However, the Delphi RADAR and Novatel GPS receiver were specifically chosen because of their measurement stability and accuracy, which allows for accurate centimeter level ranging.

2.3.5 Modeling and Simulation

In addition to field experiments, using modeling and simulation, we have also analyzed scenarios for leader-follower vehicle convoys that have the potential to be unsafe, hazardous, or even fatal in order to provide insight on dangerous driving conditions for autonomous vehicle platoons. These scenarios were created in a simulation software called PreScan and are made to reflect

the behavior of the vehicle dynamics and sensor characteristics of a real-world vehicle convoy. Encouraging results of our earlier study referenced earlier (Lakshmanan, et al. 2019), have motivated us to study how implementing these new features to our models will affect the truck platoon. Safety margins are paramount for the success of AVs. The question this paper desires to answer is under what conditions would it be unsafe to deploy a vehicle convoy without a DSRC communication link, and how can a DSRC communication link be utilized as a failsafe for the platoon.

The communication protocol implemented in this study to connect semi-trucks within the platoon is known as DSRC. The message being sent over the DSRC network is a Basic Safety Message (BSM). BSMs are SAE J2375 compliant and contain customizable message parameters that can be changed to fit a multitude of AV safety applications (Li, et al. 2014) (emergency vehicle response, vehicle/traffic light cooperation at intersections, accident avoidance on roadway through vehicle connectivity and alert messages, etc.). A BSM consists of data frames, which in turn are composed of other data frames or data elements. A basic vehicle state data frame containing data elements such as a message identifier, time, position, motion, and other data elements is mandatory for any application (Delgrossi and Zhang 2012). A BSM may also contain a vehicle safety extension data frame which contains data elements such as event flags, path history and path prediction. In this experiment, both the vehicle state data frame and safety extension frame are sent over the DSRC network, however only positional data is utilized within the receiving vehicles actuation system.

In addition to a communication link between AVs, other systems are implemented to keep AVs moving in the desired trajectory. ACC and CACC (Qing and Sengupta 2003) control systems are currently the prevailing systems used for maintaining a safe headway. A typical ACC unit operates by taking range, Doppler velocity and azimuth angle information from two millimeter-wave (operating at 24 GHz) Doppler radars and outputs vehicle throttle percentage and braking pressure to the engine and braking system. In our modeling and simulation experiment, one long range radar with a narrow beam is used to maintain the desired headway with the vehicle ahead of it and one short range radar with a wide beam is used to detect vehicle cut-ins from adjacent lanes. Through both of the radars outputs, a reliable system for headway control is achieved using an ACC system (Shladover, et al. 2014). CACC systems utilize the outputs from the same radars but also fuse incoming data from a V2I, V2V or vehicle-to-anything communication link to add another layer of reliability in AVs. A pseudo CACC system is implemented in this experiment.

3 Accomplishments

The test matrix as it was completed during each year is shown in Figure 24. There were two 2T configurations, one led by A1 and the other by T13. All cut-in and merge runs were 4T platoons at 100 foot gap. Each "run" is a one-hour continuous test.

NCAT 2019					ACM 2019					NCAT 2020					ACM 2021				
	A1	T14	T13	A2		A1	T14	T13	A2		A1	T14	T13	A2		A1	T14	T13	A2
Baselines	4	11	2	10	Baselines	6	5	4	4	Baselines	7	6	7	10	Baselines	14	5	7	17
2T-50	3		2		2T-50	8		3		2T-50	5		2		2T-50	4		2	
2T-100	4		1		2T-100	5		5		2T-100	3		5		2T-100	3		3	
4T-35	2									4T-35	3								
4T-50	3				4T-50	3				4T-50	5				4T-50	3			
															4T-75	3			
4T-100	3				4T-100	6				4T-100	2				4T-100	3			
Cut-In	3									Cut-In	2				Cut-In	3			
										Merge	1				Merge	2			

Figure 24: Fuel test matrix as completed, showing the number of each run

3.1 NCAT 2019 Results

The controller used during the 2019 NCAT testing campaign was used previously by (Smith et al. 2019). In brief, the controller used PID control with feedforward, and was not designed to cope with grade and cut-ins in a fuel-efficient manner. The controller was less efficient during cut-ins in prior two-truck mixed traffic testing (McAuliffe et al. 2020). This PID controller was employed in the initial testing campaign as a point for reference for the nonlinear model predictive controller being developed for phase two testing. The PID controller operating on the relatively flat terrain of NCAT served as the baseline controller for this study. Subsequently, platoon efficiency with the PID controller was investigated on the highway loop at ACM in 2019.

Headway statistics for NCAT 2019 testing are shown in Table 2. In general, standard deviations in headway were under 2 meters.

Table 2: Headway statistics for NCAT 2019 testing

	T14 (ft, +- std)		T13 (ft, +- std)		A2 (ft, +- std)	
2T-50	49.9	0.3			49.9	0.7
2T-100	100.1	0.7			100.1	1.0
4T-35	35.1	0.7	35.1	1.0	35.1	1.6
4T-50	49.9	0.3	49.9	0.7	49.9	2.0
4T-100	100.1	0.3	100.1	2.0	100.1	2.3
CutIn	49.9	0.3	49.9	0.7	50.2	2.3

After the completion of the test matrix for NCAT 2019, the average fuel economies for each truck and configuration were calculated to compare the benefits each truck experiences during platooning versus when they operate in a standalone baseline run. Overall, each truck experiences some amount of benefit from joining a platoon of heavy-duty trucks. The only vehicles

that did not experience increased fuel economy are A1 during some configurations and T13 when it led 2T platoons at both 50 and 100 feet. These results are quantified in Table 3.

Table 3: NCAT 2019 Fuel Economy Summary

NCAT Lap Fuel Economy Summary			
Truck	Configuration	Avg Fuel Economy [km/L]	Percent Difference from Baseline
A1	Baseline	5.16	-
	2T 50 *	5.15	-0.19%
	2T 100 *	5.15	-0.11%
	4T 35 *	5.37	4.09%
	4T 50 *	5.24	1.56%
	4T 100 *	5.02	-2.62%
A2	Baseline	5.13	-
	2T 50	5.46	6.35%
	2T 100	5.32	3.72%
	4T 35	5.55	8.19%
	4T 50	5.55	8.25%
	4T 100	5.47	6.55%
T13	Baseline	3.07	-
	2T 50 *	3.01	-1.93%
	2T 100 *	3.03	-1.40%
	4T 35	3.36	9.32%
	4T 50	3.37	9.76%
	4T 100	3.26	5.97%
T14	Baseline	3.07	-
	2T 50	3.52	14.96%
	2T 100	3.53	15.16%
	4T 35	3.35	9.28%
	4T 50	3.24	5.56%
	4T 100	3.37	9.91%

* indicates a platoon leader

The benefits or drawbacks experienced by A1 teetered on the edge of no effect. An interesting note for A1 is that, during experimentation in 4T platoons with shorter following distances, the fuel economy benefits increased. The reasoning behind this phenomenon is the exaggerated “push” effects coming from the trucks behind it due to aerodynamic effects. Next in the platoon order is T14, which followed behind A1 in every platooning configuration, whether it be 2T or 4T. While fuel consumption was reduced through platooning benefits, T14 consumed less fuel per km in 2T configurations than it did in 4T. Benefits of 5-15% strongly indicate platooning allows for increased energy efficiency by a following vehicle.

T13, the leader of a 2T platoon and positioned third in a 4T platoon, displayed similar behavior to A1 when leading and similar behavior to T14 when following, which is to be expected. A2 followed in every configuration except baseline operation and experienced anywhere between 3.7-8.25% fuel economy benefits while cooperating in a platoon with the other trucks. 4T benefits outshine benefits seen in 2T configurations as a result of an increased aerodynamic wake width created by the three preceding vehicles in 4T platoons. This wake width grows larger as you move further down the platoon of trucks. A wider wake allows for the truck to move laterally further distances before losing the aerodynamic benefits. As seen with most of the trucks, as the headway increased, the fuel economy benefits decreased for most trucks.

The cut-in strategy at NCAT in 2019 was designed for safe operation first. In fact, it was tuned more conservatively than would likely be seen in a real-world application. The algorithm notably reduced the fuel economy benefits in a prior fuel study on the effects of cut-in conducted in (McAuliffe et al. 2020). Nevertheless, fuel results were collected using the strategy without tweaks to the controller, since the purpose of year 1 was baselining.

3.2 ACM 2019 Results

The PID controller employed at ACM in 2019 was identical to the one used at NCAT in 2019. It was found quickly that a four-truck platoon was quite difficult to maintain around the grade-varying ACM test track with the PID control strategy. Compounding velocity errors were passed through the platoon due to the influence of grade. Some changes to the control strategies were made to improve performance over the heavy grade:

1. Retarder and brake torque thresholds were raised. Raising these values allows more headway variation before the platooning vehicle brakes. It was only a stopgap measure to be able to maintain the platoon.
2. Additionally, the lead truck’s stock cruise control led to difficulties in the string-stability of the platoon, so the lead truck was driven manually for all four-truck platoon results.

Headway statistics for ACM 2019 indicated control issues for all vehicles. The helpful effect of a lead truck being driven manually versus the stock ACC is evident in comparison of T14’s 2T deviation with its 4T deviation. They are otherwise identical runs for T14, except the leader is driven manually on the 4T run and ACC on the 2T. The standard deviation in headway is over twice as high when A1’s stock ACC was active, as shown in Table 4. Also, compared to the NCAT 2019 results in Table 2, the headway variation is much higher at ACM, especially for the third and fourth platooning vehicles.

Table 4: Headway statistics for ACM 2019 testing

	T14 (ft, +- std)	T13 (ft, +- std)	A2 (ft, +- std)
2T-100	100.1 5.9		100.4 4.9
2T-50	57.4 13.8		49.9 3.9
4T-100	100.1 2.3	100.1 6.6	99.4 15.1
4T-50	49.9 2.0	49.9 4.6	50.9 12.5

The average fuel economies for each truck and configuration at ACM in 2019 were calculated to compare to baseline operation of the trucks on the same track. Year 1 ACM results show that, with the introduction of significant grade changes, the fuel economy of the following trucks cannot be easily predicted compared to the baseline. In many configurations, the fuel economy benefits from aerodynamic effects outweigh the increased transiency due to an increased grade profile. This can be seen in Table 5.

Table 5: ACM 2019 Fuel Economy Summary (* indicates platoon leader)

ACM Lap Fuel Economy Summary			
Truck	Configuration	Avg Fuel Economy [km/L]	Percent Difference from Baseline
A1	Baseline	4.72	-
	2T 50*	4.12	-12.71%
	2T 100*	4.57	-3.21%
	4T 50*	4.85	2.75%
	4T 75*	-	-
	4T 100*	4.60	-2.51%
A2	Baseline	4.73	-
	2T 50	5.17	9.33%
	2T 100	4.80	1.46%
	4T 50	4.24	-10.36%
	4T 75	-	-
	4T 100	3.87	-18.15%
T13	Baseline	3.01	-
	2T 50*	3.03	0.67%
	2T 100*	3.02	0.44%
	4T 50	2.98	-0.89%
	4T 75	-	-

	4T 100	2.67	-11.14%
T14	Baseline	3.03	-
	2T 50	2.99	-1.32%
	2T 100	3.04	0.23%
	4T 50	3.45	13.86%
	4T 75	-	-
	4T 100	3.22	6.27%

Fuel economy results for ACM 2019 are scattered due to the grade disturbances. The PID controller design did not provide the platoons with high fidelity string stability and caused significant transient behavior in the speed traces of all vehicles following A1. One issue many researchers are discovering is, at some point, the aerodynamic benefits of platooning do not outweigh the energy expended to maintain a constant following distance. The extra effort the truck makes oftentimes results in reduced fuel economy relative to the individual truck baselines, rendering platooning effort/benefits futile. This, however, is a result of the PID control strategy as will be discussed in the ACM 2021 results.

3.3 NCAT 2020 Results: H-Infinity Control

A new controller was implemented for the 2020 NCAT testing. In platooning, string stability is a measure of how a platoon of vehicles reacts to a disturbance introduced into the system. For a string stable system, if a headway error is introduced to the lead vehicle in a platoon, the error will decay for every following vehicle. Conversely, if the system is not string stable, the errors introduced into the platoon will grow for every following vehicle, until there is a collision or the platoon ends.

String stability is typically evaluated through system sensitivity, which is a function determined by the system dynamics. This function then provides a basic measure of string stability. These analyses assume a linear time-invariant system. The original analysis also did not include models for factors such as engine lag, temporal lag due to gear changes, or communication delays. The system sensitivity of the 2019 controller was evaluated and found to exceed requirements for string-stability.

The H-Infinity controller in (Ploeg, van de Wouw, and Nijmeijer 2014) was implemented on the trucks to rectify the system sensitivity issues. The implementation was validated by testing for velocity disturbances (both in simulation and experimentally) before platoon testing proceeded.

Headway statistics for the NCAT 2020 testing are shown in Table 6. The slightly higher standard deviation versus the 2019 controller is caused by the H-Infinity control using a time gap (between platooning vehicles) rather than a distance/headway gap. Velocity variations change the headway setpoint in meters.

Table 6: Headway statistics for NCAT 2020

	T14 (ft, +- std)		T13 (ft, +- std)		A2 (ft, +- std)	
2T-50	51.8	0.7			49.9	1.6
2T-100	102.7	0.7			99.1	3.3
4T-35	36.4	0.3	34.8	1.0	33.8	1.0
4T-50	51.8	0.7	50.2	1.3	48.6	1.0
4T-100	101.0	0.3	99.7	1.3	98.4	1.0
CutIn	100.7	0.3	98.1	11.5	98.4	3.6
Merge	99.7	0.7	99.4	7.2	99.1	2.3

2020 NCAT results included updates in the controller strategy that allowed for more optimal following behavior. As a result, many of the platoon configurations produced better fuel economy in year 2 than they did in year 1. With the H-infinity controller, following trucks all operated with better fuel economy than their baseline configurations. The resulting average fuel economy numbers were calculated and tabulated in Table 7.

Table 7: NCAT 2020 Fuel Economy Summary (* indicates platoon leader)

NCAT Lap Fuel Economy Summary			
Truck	Configuration	Avg Fuel Economy [km/L]	Percent Difference from Baseline
A1	Baseline	4.85	-
	2T 50*	4.77	-1.52%
	2T 100*	4.74	-2.15%
	4T 35*	4.85	0.07%
	4T 50*	4.78	-1.39%
	4T 100*	4.72	-2.59%
A2	Baseline	4.81	-
	2T 50	5.34	11.08%
	2T 100	5.21	8.41%
	4T 35	5.46	13.46%
	4T 50	5.63	17.06%
	4T 100	5.40	12.22%
T13	Baseline	2.93	-
	2T 50*	2.98	1.65%
	2T 100*	3.09	5.58%
	4T 35	3.45	17.64%

	4T 50	3.30	12.79%
	4T 100	3.21	9.60%
T14	Baseline	3.11	-
	2T 50	3.25	4.48%
	2T 100	3.29	5.70%
	4T 35	3.60	15.54%
	4T 50	3.34	7.40%
	4T 100	3.33	7.10%

Results for A1 mirrored year 1 findings – energy benefits teetered near zero compared to baseline operation. Similar to year 1 operation, in any configuration, increasing the following distance decreased the fuel economy benefits received by A1 during platooning. This also follows the hypothesis stated earlier in NCAT 2019 that A1 receives more of a pushing effect from the truck behind it when the following truck travels closer to the rear of A1. T14 experienced much of the same behavior. During 2T platooning, T14 does not experience a pushing effect from a following truck, but during 4T platooning, the effect is emphasized due to the two trucks behind it. For this reason, 4T platoons produce better fuel economy results for T14 than 2T formations. T14 and T13 (trucks two and three in the four-truck formations) show increasing headway for trucks located in the middle of a platoon does not benefit them. Rather, the increased headway hinders the fuel economy, demonstrated by the 4T platooning numbers for T13 and T14. Overall, platooning increases the fuel economy of all following vehicles (up to 17.6%), regardless of the exact platoon formation.

3.3.1 Establishing Ideal Platoon Performance

For comparison purposes, an “ideal” performance environment was extracted from NCAT 2020 data. NCAT has two straights that lead into curves containing slight grade changes (uphill in the West curve and downhill in the East). These straights are not equal, however, from an analysis perspective. The North straight is very slightly uphill as opposed to the South straight, which is very slightly downhill. The North straight was chosen to define the “ideal” platooning analysis. The beginning and end of the straight were approximated within 1m. The length of a 4T 100 platoon is ~580 feet (176m). This distance was removed from both ends of the straight to ensure each truck is straight and organized in the platoon and without the influence of hills from either end of the straight. Average fuel rates were calculated for each truck to determine whether this process eliminated these effects. Because A2 is the follower in every platoon, its fuel traces were the most important to examine and are plotted in Figure 25.

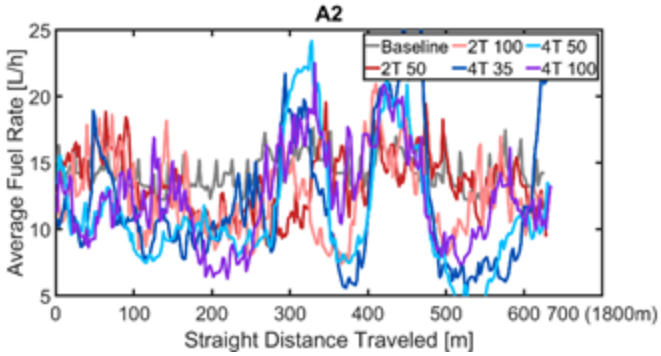

Figure 25: Average Fuel Rate Investigation, NCAT 2020 Straight

The configuration of most concern is 4T 100 where the platoon is the longest. Overall, each configuration's starting fuel rate is nearly identical to its end fuel rate except for 4T 35, which, after examination, is due to a spike at that track location that settles back to 14 L/h immediately after. The significance behind this lies in the fact that the fuel rate of any test vehicle in this study will experience massive spiking above or below the cruising fuel rate when road grade is introduced to the truck's path. Fuel rate traces without these spikes indicate the successful removal of entry and exit behavior. As a result of this investigation, the label of "ideal" straight is applied to this segment of data and the average fuel economies of each truck and configuration were tabulated in Table 8.

Table 8: "Ideal" Performance Fuel Economy Summary, Extracted from NCAT 2020

NCAT Straight (Ideal) Fuel Economy Summary			
Truck	Configuration	Avg Fuel Economy [km/L]	Percent Difference from Baseline
A1	Baseline	5.08	-
	2T 50*	5.09	0.20%
	2T 100*	5.04	-0.77%
	4T 35*	5.22	2.82%
	4T 50*	5.10	0.41%
	4T 100*	5.07	-0.10%
A2	Baseline	5.06	-
	2T 50	5.68	12.24%
	2T 100	5.85	15.51%
	4T 35	6.05	19.53%
	4T 50	6.19	22.32%
	4T 100	5.97	18.01%
T13	Baseline	3.14	-

	2T 50*	3.19	1.76%
	2T 100*	3.04	-2.93%
	4T 35	3.86	23.20%
	4T 50	3.64	16.12%
	4T 100	3.53	12.44%
T14	Baseline	3.27	-
	2T 50	3.49	6.53%
	2T 100	3.56	8.70%
	4T 35	3.94	20.26%
	4T 50	3.59	9.72%
	4T 100	3.59	9.83%

This analysis establishes a theoretically “ideal” platoon performance parameter as a discussion point for future comparisons. The straight section extracted from NCAT data allows a strict view the aerodynamic platooning benefits while undisturbed by other factors like road grade and path curvature. A1 continues to show that increasing headway decreases the fuel economy benefits experienced by the lead truck in both 2T and 4T platoons. T14 does not follow this as closely, but overall fuel consumption decreases greatly during platooning configurations, which can also be seen in T13 data. There is one outlier, T13 2T 100, that is not fully understood. Because T13 leads a 2T platoon, it is possible the aerodynamic benefit did not outweigh the cost of leading. However, the magnitude of decline of fuel economy is not explained by this phenomenon. A2 experienced the largest energy efficiency benefits in every configuration, as expected.

3.3.2 Cut-ins and Merges with H-Infinity Control

Cut-ins and merges were performed in NCAT 2020 with relaxed responses relative to NCAT 2019. Figure 26 shows the differences visually.

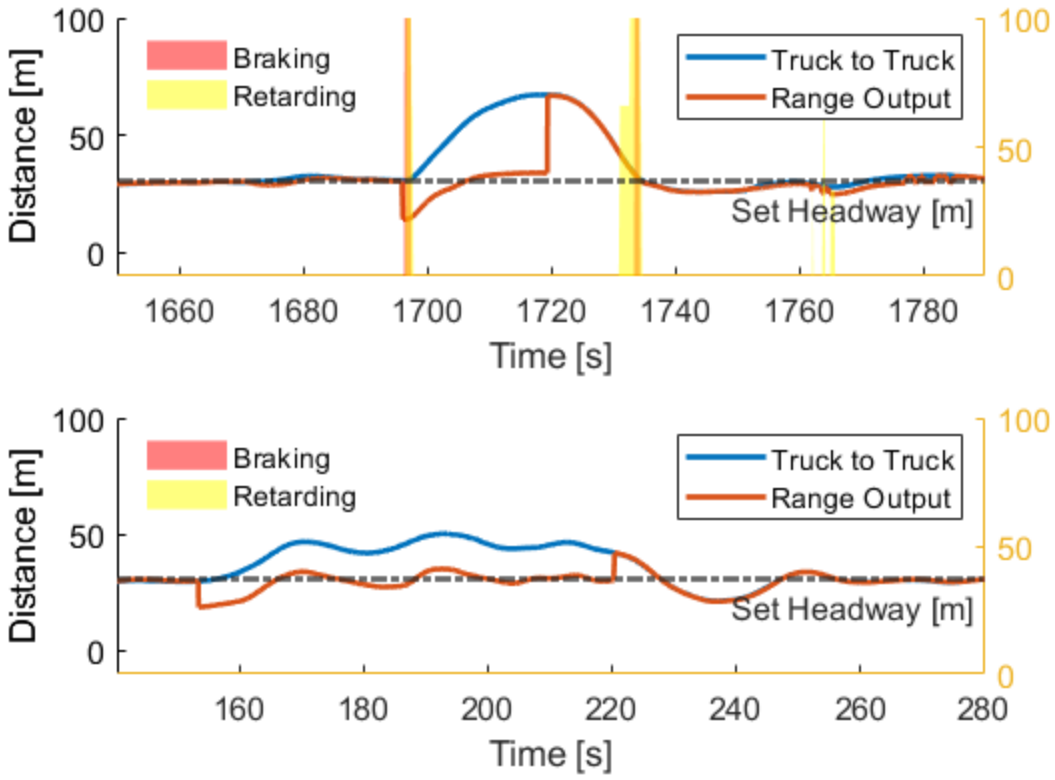

Figure 26: Cut-in strategy at NCAT in 2019 (top) and 2020 (bottom), demonstrating the more conservative strategy of 2020

For the Merge run collected during NCAT 2020 testing, vehicle cut-ins occurred every other lap. This enabled a direct comparison within the run of the effect of cut-ins. Fuel use was summed for each lap for each truck (Figure 27), and a two-sample t-test was performed to determine the difference in fuel consumption for a lap with a cut-in and a lap without.

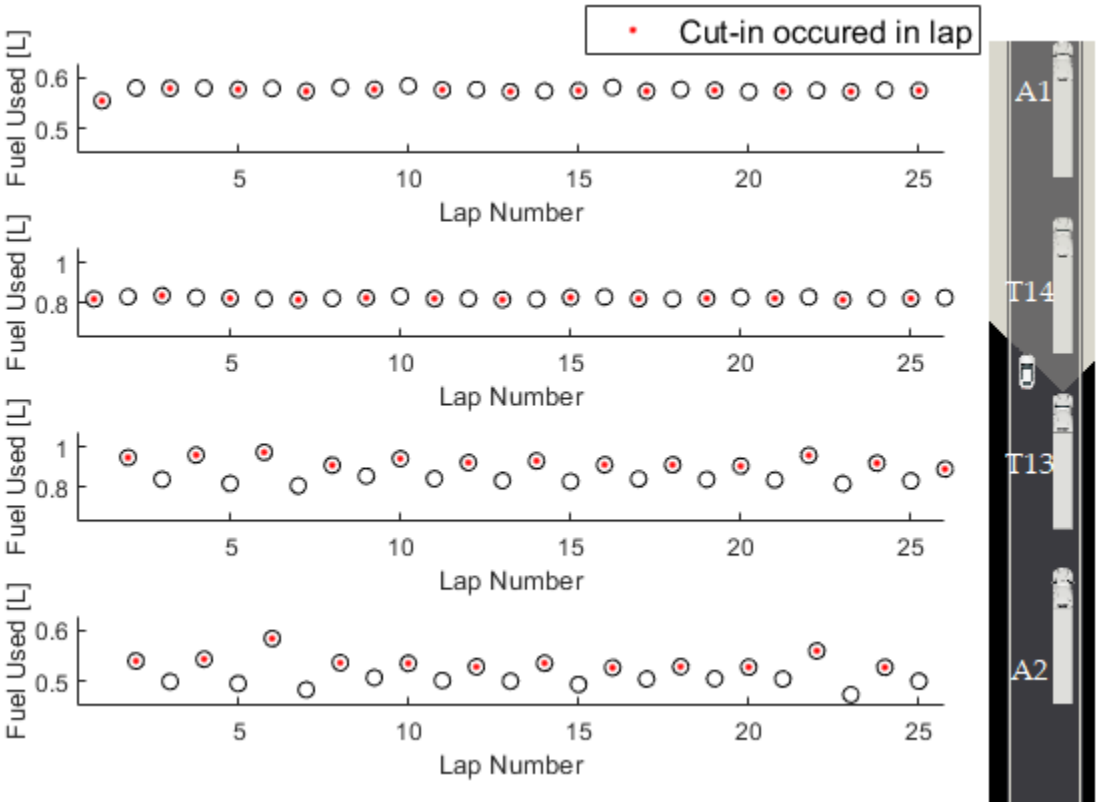

Figure 27: Alternating vehicle cut-ins during NCAT 2020 testing

It was found that for the first two vehicles which did not deal with the cut-in vehicle, only a marginal difference in fuel economy resulted, as is to be expected. However, for the third and fourth vehicles, cut-ins measurably increased the fuel consumption. This impact is quantified in Figure 28.

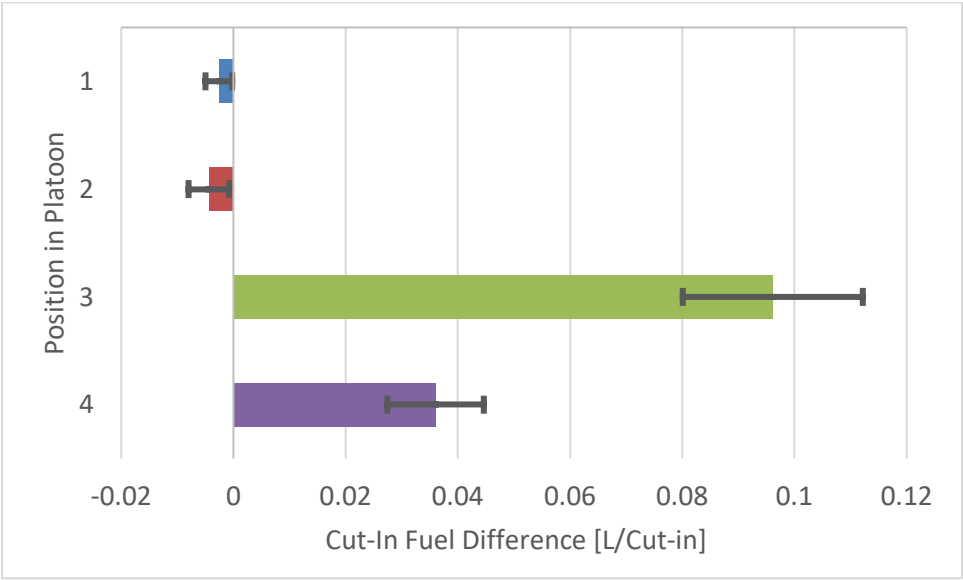

Figure 28: Fuel consumption difference due to a vehicle cut-in at NCAT in 2020

The significance of this result is that for every cut-in, a measurable amount of fuel was consumed to deal with the dynamic changes the cut-in required. For practical significance of this result, it is proposed that there is a “tipping point” where the number of cut-ins has nullified the benefit of platooning. Using the idealized platooning fuel economy benefits and the prediction that each cut-in will consume a consistent amount of fuel, the tipping point can be estimated.

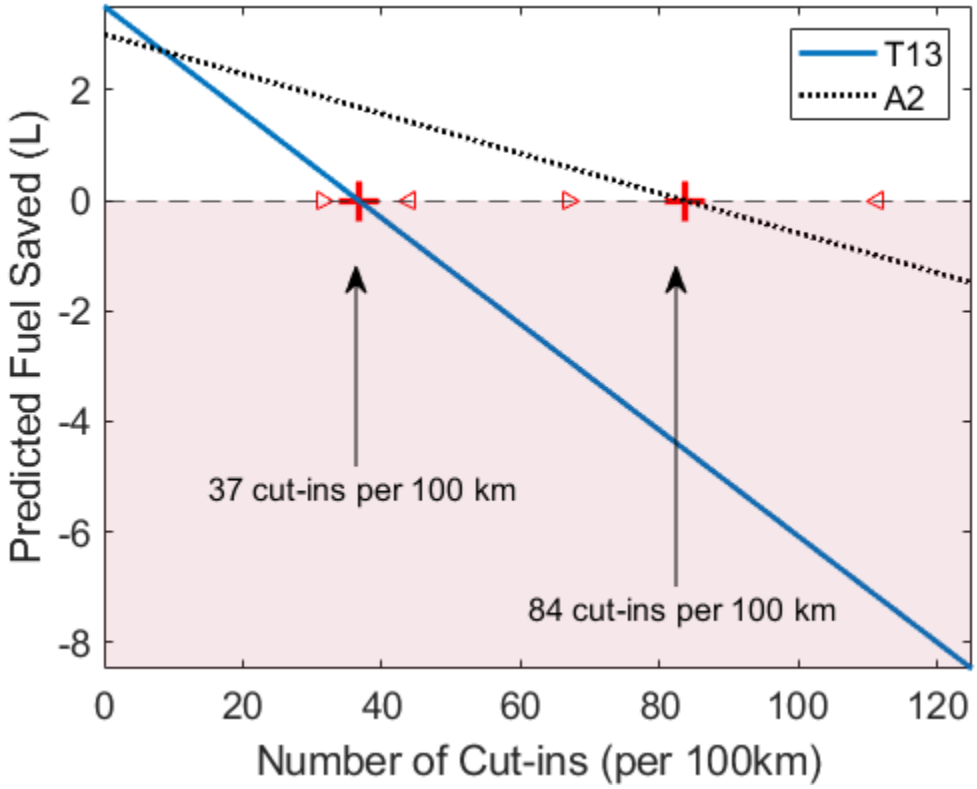

Figure 29: The number of cut-ins to nullify platoon benefits is estimated

Figure 29 shows the prediction of how many cut-ins it would take to cancel the platooning fuel economy benefits for the two trucks downstream of the cut-in location platooning at 100’ headway. For T13, it is estimated that 37 cut-ins per 100 km would nullify the 100’ platooning fuel benefit. For A2, the impact of cut-ins was less severe, and it is predicted that 84 cut-ins per 100 km would nullify platoon benefits.

3.3.3 Controller Development Prior to ACM 2021 Testing: NMPC

Following the implementation of the H-Infinity controller for NCAT 2020 testing, which displayed string-stable behavior to velocity changes, the H-Infinity controller was tested in the context of grade changes in early 2021. An out-and-back testing loop was identified on US highway 280 located near the NCAT test track. This testing loop had the following grade characteristics:

On the eastbound test section, the hills were steeper and shorter than the national average (Wood et al. 2016).
On the westbound test section, the hills were flatter and longer than the national average (Wood et al. 2016).

While the H-Infinity controller had performed well in response to velocity changes during NCAT 2020 testing, the performance over the grade on the eastbound section was found to be unsatisfactory. The unsatisfactory performance of the H-Infinity controller over grade changes spurned the development of a new Nonlinear Model Predictive Control (NMPC) strategy. The details of the NMPC development can be found in (Jacob Ward et al. 2021). In short, the NMPC designs an optimal velocity trajectory utilizing upcoming grade information. The NMPC cost function for lead vehicles considers total fuel consumption over the upcoming highway topography and the velocity error. For followers, headway and range rate replace velocity in the controller cost function.

A two-truck platoon and a control truck were driven over the testing loop and fuel economy was compared between H-infinity with fixed spacing, H-Infinity with time gap spacing, and NMPC control in April 2021. The results over the eastbound test section are shown in Table 9 and visualized in Figure 30 and Figure 31.

Table 9: Indicated Fuel Savings for Different Controllers over US 280 Eastbound versus Single-Truck Driving

	H-Infinity Following	NMPC Following
Cruise-Control Leader	0% lead/0.67% follow	1.6% lead/20.6% follow
NMPC Leader	17% lead/10.5% follow	14.0% lead/19.9% follow

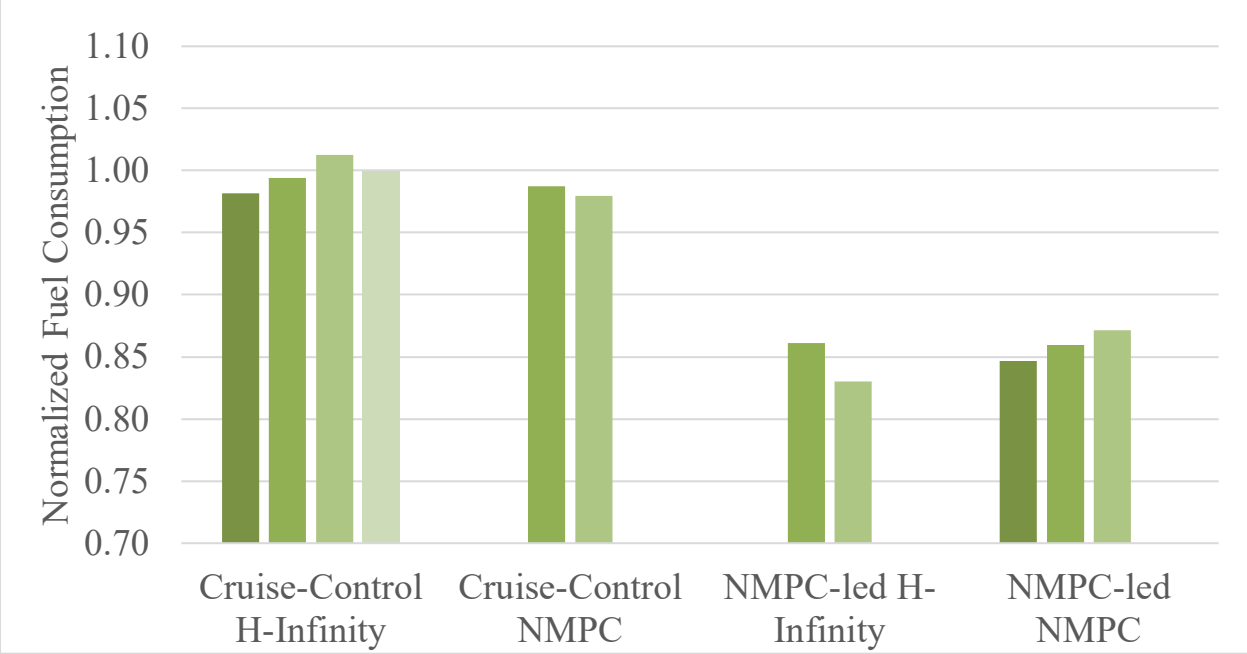

Figure 30: Leader fuel consumption during US-280 testing

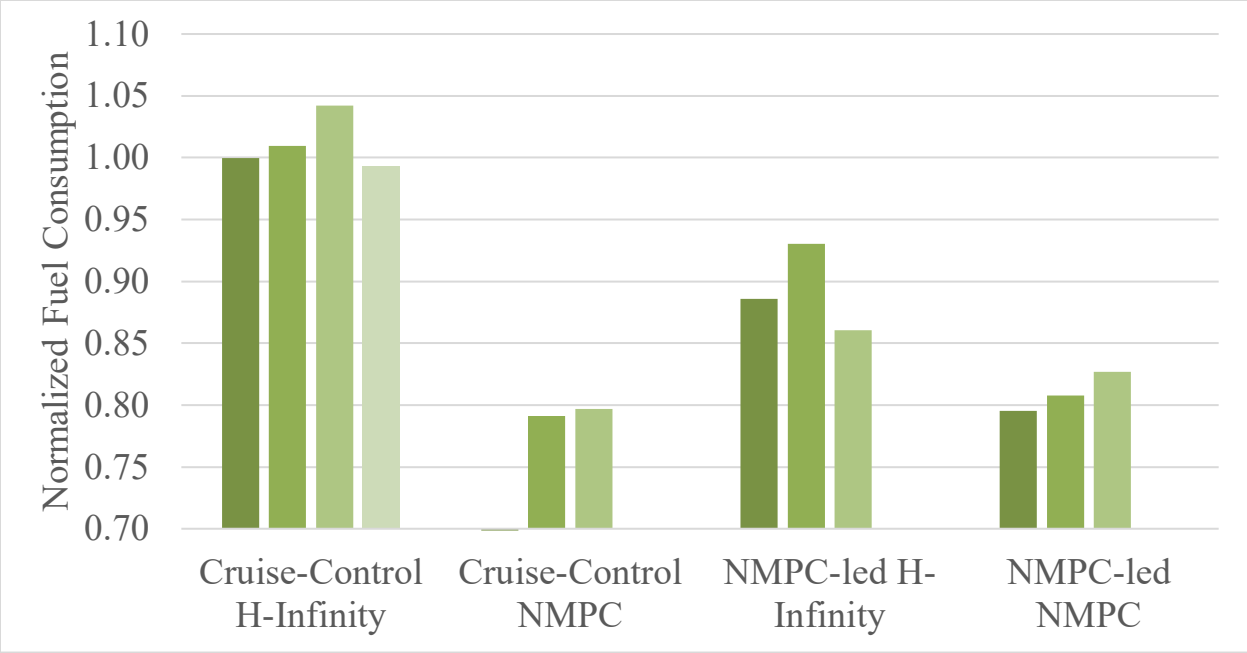

Figure 31: Follower fuel consumption during US-280 testing

The NMPC controller responded to severe grade changes significantly better than the H-Infinity controller. An NMPC follower saved 20% fuel compared to the H-infinity controller, regardless of the lead vehicle's control strategy. Also, the leader benefitted significantly from using an NMPC cruise-control strategy instead and help the follower's performance,

The NMPC controller would be further proven via ACM testing in May 2021.

3.4 ACM 2021 Results

Initial tests of the H-Infinity controller at ACM in 2021 confirmed the US-280 results: While the H-Infinity controller was satisfactory for velocity disturbances, it did not provide effective string stability when confronted with grade disturbances. Thus, the ACM 2021 testing utilized the NMPC or 'optimal' control designs. Use of the NMPC/optimal controller required a redefinition of the testing matrix. The optimal controller considers headway as just one of the cost function weights. Therefore, headway is no longer a fixed reference, as it was with the PID controller used in year 1 testing. Instead, cost function weights and references were hand tuned until the mean headway per lap approximately matched a desired value. Thus the 50', 75', and 100' results represent mean headways during those testing runs. In reality, the headway fluctuated significantly for each following vehicle. The headway statistics in Table 10 highlight this effect, which shows headway deviations far greater than those produced by the PID controller.

Table 10: ACM 2021 headway statistics

	T14 (ft, +- std)		T13 (ft, +- std)		A2 (ft, +- std)	
2T-nmpc50	55.1	11.2			53.5	16.1
2T-nmpc100	100.7	12.5			103.0	20.7
4T-nmpc50	57.1	11.2	49.5	8.5	54.1	12.8
4T-nmpc75	77.1	11.2	73.5	8.9	72.2	20.7
4T-nmpc100	104.3	12.5	96.8	18.4	99.7	26.9
CutIn	104.3	15.1	100.4	20.7	100.1	28.9
Merge	100.4	12.8	107.3	33.5	105.3	39.0

ACM 2021 results did produce more string stable operation of all trucks due to controller updates and developments. Significant improvements in fuel economy were attributed to the new 'optimal' NMPC control strategies employed. The resulting average fuel economies are tabulated in Table 11.

Table 11: ACM 2021 Fuel Economy Summary (* indicates platoon leader)

ACM Lap Fuel Economy Summary			
Truck	Configuration	Avg Fuel Economy [km/L]	Percent Difference from Baseline
A1	Baseline	5.17	-
	2T 50*	5.13	-0.84%
	2T 100*	5.30	2.38%
	4T 50*	5.38	3.91%
	4T 75*	5.14	-0.72%
	4T 100*	5.11	-1.18%
A2	Baseline	5.30	-
	2T 50	5.55	4.68%
	2T 100	5.61	5.88%
	4T 50	5.63	6.25%
	4T 75	5.41	2.01%
	4T 100	5.86	10.53%
T13	Baseline	2.76	-
	2T 50*	2.78	0.84%
	2T 100*	2.80	1.58%
	4T 50	3.28	18.96%

	4T 75	3.27	18.61%
	4T 100	3.05	10.71%
T14	Baseline	2.97	-
	2T 50	3.30	11.31%
	2T 100	3.22	8.40%
	4T 50	3.49	17.51%
	4T 75	3.39	14.22%
	4T 100	3.29	10.90%

The NMPC control strategy worked extremely well for all trucks. A1, running the stock cruise control as usual, performed as expected where its fuel economy benefits did not span far from zero. T14 performed admirably under the new controller where it benefitted in any configuration compared to baseline. With a looser restriction on headway distance, the truck was allowed to coast for longer (whether or not the headway was decreasing) and, because of this, experienced efficiency benefits between 8-18% depending on the configuration. T13 also performed admirably under 'optimal' control, producing fuel economy increases of 10-19% in 4T platoons and marginal benefits during 2T platoons, where it leads A2. A2 also experienced enhanced energy efficiency benefits in 2T and 4T configurations. Due to the increased transient behavior of the new controller style, A2 did struggle occasionally to maintain reasonable following distances, which resulted in limited fuel economy benefits relative to T14 and T13. This concern is exacerbated in 4T platoons as opposed to 2T due to the increased length of the platoon and the accordion-like manner in which transient behavior is passed down from truck to truck. Variance in headway is passed down in compounding fashion, causing follower trucks to struggle slightly more while platooning, which was seen comparing 2T results to 4T. Even with the skirmish between transient behavior and aerodynamic benefits, fuel economy remained positive throughout any configuration.

3.4.1 Cut-ins and Merges with NMPC Platoons

Cut-ins and merges were performed at ACM in 2021 with the trucks running the NMPC control software. As in other testing periods, the cut-ins and merges were performed between the second and third truck in the platoon. Each cut-in lasted approximately 30 seconds, and the vehicle remained with the platoon in the inside lane. Meanwhile, the merges lasted less than 20 seconds each, as the merging vehicle would accelerate on-track, communicate the intent to merge, merge into the platoon, and then leave the formation via an exit ramp.

Another method was used to analyze the cut-ins and merges at ACM 2021: a paired f- and t-test similar to that in (Ward et al. 2021). For each cut-in and merge run, the fuel used per lap by the third and fourth trucks was compared to that of the second and first trucks respectively, as the powertrains are similar.

For T13, the cut-ins and merges led to universal increases in fuel consumption versus pure platooning without cut-ins. One cut-in run led to over 11% worse fuel consumption than the pure platooning performance.

Results were mixed for A2, with one cut-in showing slightly better fuel economy during cut-in runs than the 100' platooning performance, but worse during the other two. The merge showed no

statistical difference in energy consumption for A2, relative to the 100' optimal NMPC platooning performance (Figure 32).

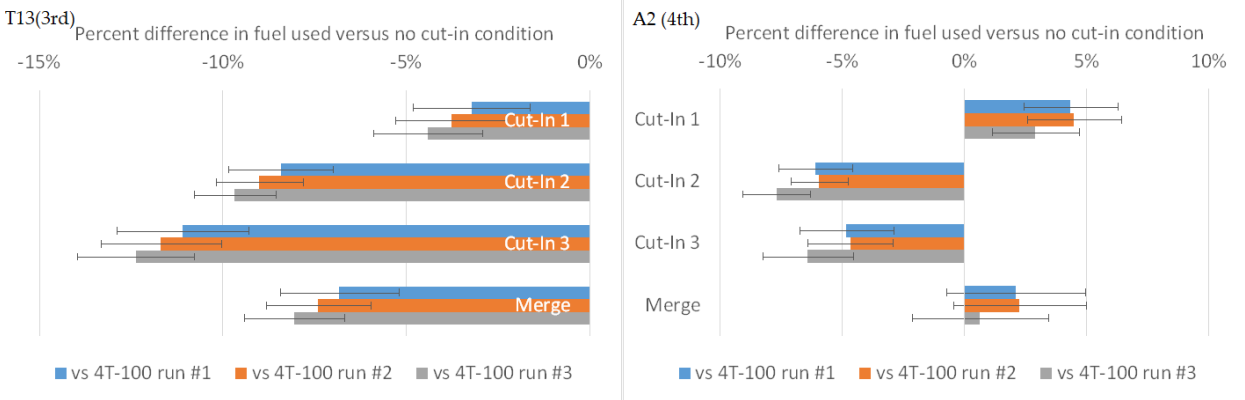

Figure 32 Cut-in fuel economy difference versus no Cut-in 100' NMPC platooning at ACM 2021 for T13 (left) and A2 (right)

3.5 V2V Communications Subsystem Performance

As mentioned in section 2.3.4, we considered seven discrete scenarios of interest, each of which is detailed in its own section below. With each scenario we include test results and discussion in line with the test and data processing descriptions.

3.5.1 Occlusions

In order to examine the effects of an occluding obstacle in the line-of-sight (LOS) between a pair of communicating vehicles, we used the NCAT test track and documented the baseline between communication effectiveness between L and F1 at a following distance of 150' and truck speed of 45 mph, as shown in Figure 33 we see a Received Signal Strength Indicator (RSSI) of about -52.8 dBm along the curves and -67.7 along the straightaways.

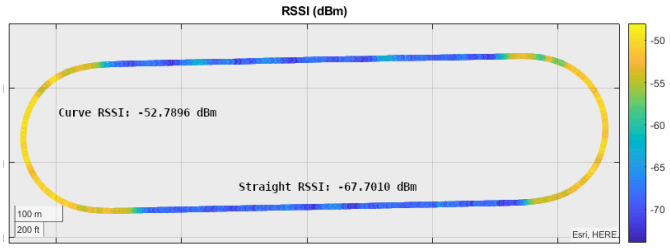

Figure 33: RSSI of packets received by F1 from L at 150' separation with no obstruction of the LOS between them

We compared this baseline performance with the results of communication effectiveness between L and F2 with a 50' following distance at the same speed, which results in close to the same total gap distance, but with the addition of F1 driving in between them, acting as a large metal obstacle and hindering a direct line-of-sight. These results are shown in Figure 34. We see an RSSI of around -52.7 dBm along the curves and -69.1 dBm along the straightaways.

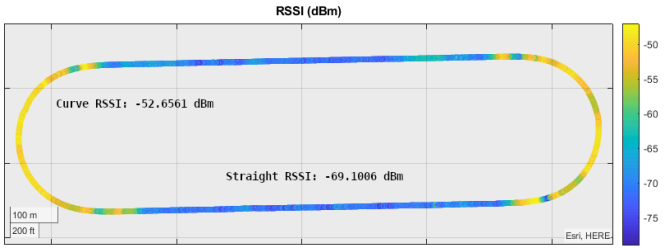

Figure 34: RSSI of packets received by F2 from L at 150' separation with F1 obstructing the LOS between L and F2

These results indicate that the presence of an additional obstructing truck between the two communicating trucks adds ~1.4 dB in additional path loss in the straight portions of the track. However, this loss becomes negligible (~0.13 dB) on the track's steep curves. This is because there is a direct LOS between L and F2 around the steep curve that is not occluded by F1.

We cross-verified these results by performing similar analysis on other vehicle pairs in our truck convoy and our conclusions are analogous. For example, Figure 35 shows the communication effectiveness between F3 and F2 at a following distance of 150' and 45 mph. Here we have -73.8 dBm curves and -70.9 dBm straights.

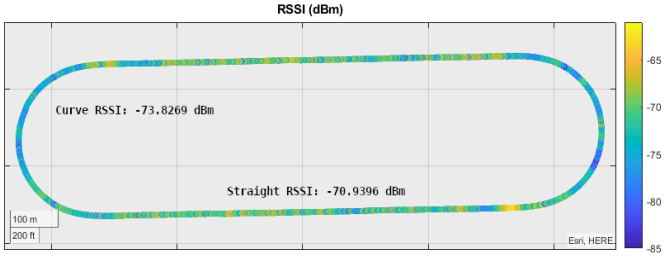

Figure 35: RSSI of packets received by F3 from F2 at 150'separation with no obstructions.

Figure 36 shows the performance between F3 and F1 at the following distance of 50', where F2 sits between them as the occluder. Here we have -74.4 dBm curves and -78.1 dBm straights.

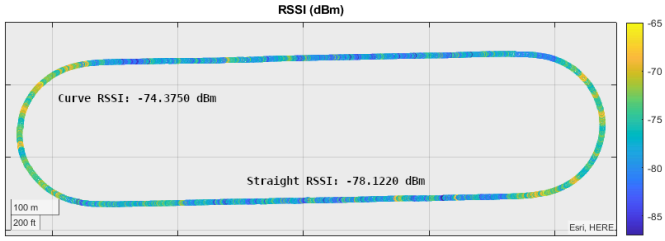

Figure 36: RSSI of packets received by F3 from F1 at 150' separation with F2 obstructing the LOS between F1 and F3

The path loss due to occlusion is much more pronounced on F3 – about ~7.2 dB on the straightaways, and ~0.6 dB on the steep curves.

The effects of an occluding truck hindering LOS are considered additionally in (Harri, et al. 2013), (CAMP LLC 2019), and in particular (Meireles, et al. 2010), which shows that for their setup with a 50m gap distance the additional loss caused by a vehicular obstruction is a little over 5 dB, results comparable to our own.

3.5.2 Rain

We compared received signal strength for laps over the ACM test track on two different days, both of which were overcast but only one of which had rain. Figure 37 shows the RSSI at each position on the ACM track, as well as the average RSSI over the loops, for the dry and rainy testing. Units are dBm and meters from the center of the track.

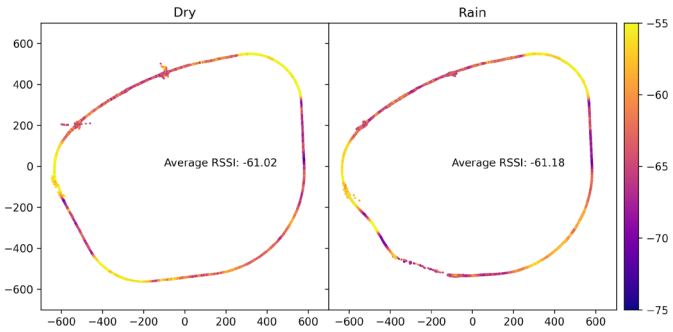

Figure 37: RSSI for the platoon in dry vs. rainy weather

There is a very slight increase in path loss of about 0.16 dB during the day that it was rainy. There is generally some attenuation due to rain because the water droplets absorb and scatter the signal, reducing how much signal reaches the receiving radio (Cheek, et al. 2020) (Kestwal, Joshi and Garia 2014). Table 12 gives the statistical analysis of the dry and rainy days, respectively.

We also considered histogram plots of every received packet's RSSI for both the dry and rainy days of testing. These can be seen in Figure 38 and Figure 39.

Table 12: Statistics for dry test loops.

	RSSI (dBm) Dry	RSSI (dBm) Rain	Latency (ms) Dry	Latency (ms) Rain
Mean	-61.053	-61.445	2.548	2.594
St Dev	4.422	4.605	0.828	0.936
Min	-76.000	-77.000	1.713	1.666
25%	-64.000	-65.000	2.156	2.174
50%	-61.000	-62.000	2.264	2.276
75%	-57.000	-57.000	2.496	2.496
Max	-48.000	-50.000	16.772	15.227

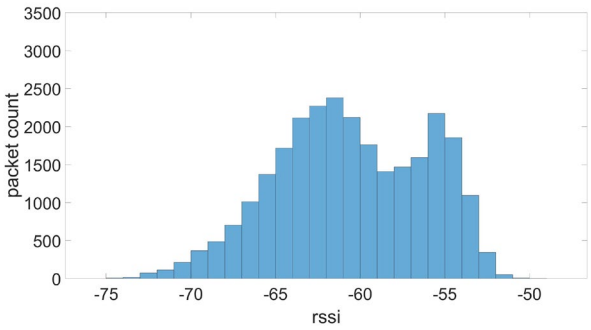

Figure 38: RSSI histogram for received packets in dry weather

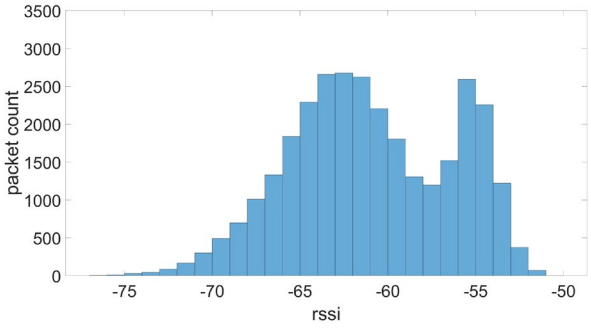

Figure 39: RSSI histogram for received packets in rainy weather

3.5.3 Antenna Position

In order to test the effects of the vertical positioning of the antennas on received signal integrity, we ran laps around the ACM track with the convoy continuously transmitting and receiving packets at 100' gap distance. For this test, we mounted the antennas to the left and right sides of the rear of the cab at 8' above ground level and monitored the GPS location of the trucks as well as the RSSI of all incoming packets, tagged with which truck transmitted them. We then repeated the test with the antennas otherwise in the same position but raised to 13' above the ground.

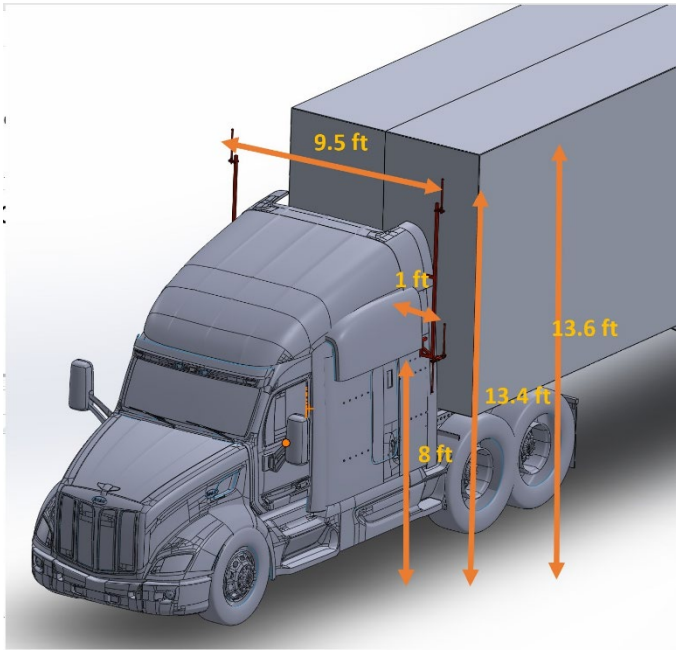

Figure 40: Antenna mounting positions on the cab of a Peterbilt truck

Figure 40 provides the antenna mounting location and Figure 41 puts into perspective the entire length of the truck shown on a Peterbilt with attached trailer.

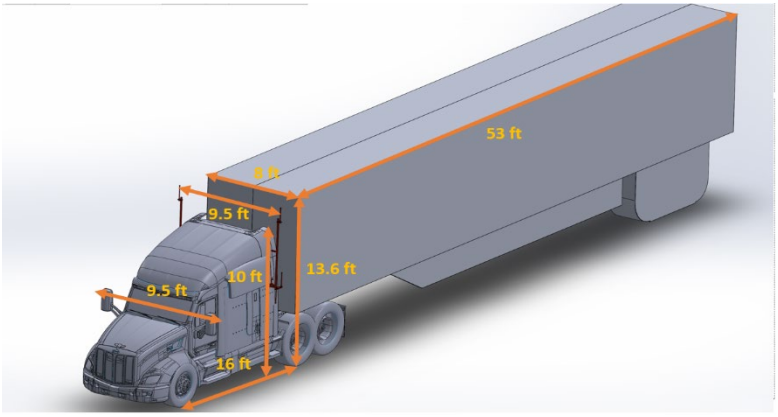

Figure 41: Overall Peterbilt truck cab with attached trailer dimensions

Figure 42 shows the mounting on the top of the other two trucks used, which were Freightliner M915A5s. They used the same standard trailer as on the Peterbilt and had the “low” antenna position mounted on top of the side view mirrors. As shown in the figure, the “high” position was instead mounted on a brace across the roof of the cab.

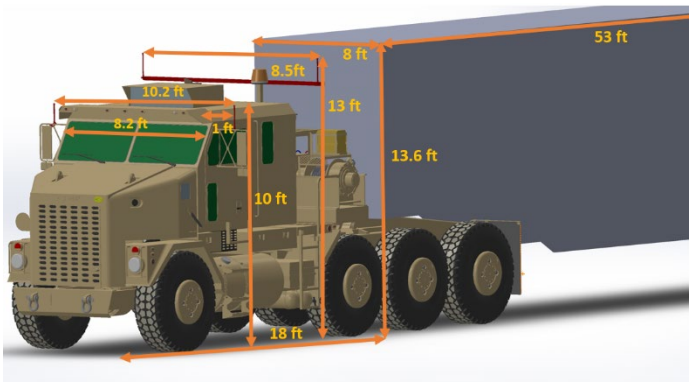

Figure 42: Antenna mounting on Freightliner truck

To begin with, we considered the overall averages for RSSI for each truck and for both the low and high antenna positions. Despite F2 not providing us any logs to analyze, we found that the higher antenna offered significant improvements of about 3 dB in RSSI for L and F1, with a very slight 0.2 dB loss on F3 at the very rear of the convoy. This is shown graphically in Figure 43, where the GPS loops have been colored according to the RSSI in dBm, as indicated by the color bar. The other axes once again give meters from the geometric center of the ACM highway loop.

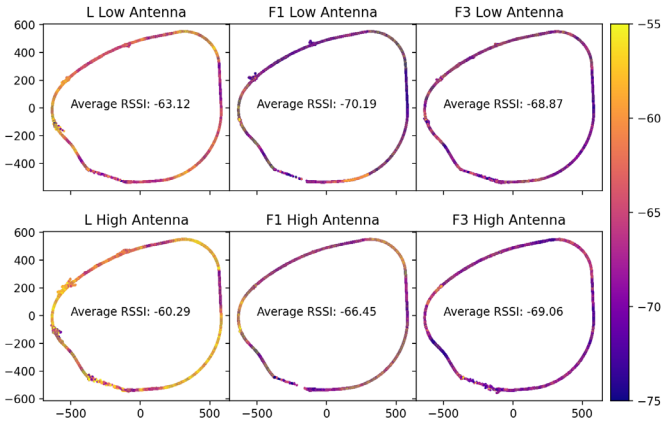

Figure 43: Overall average RSSI per truck for the 8' (low) and 13' or 13'6" (high) antenna elevations

Next, we limited our consideration to only neighboring trucks, that is, we only consider packets sent by the truck immediately in front of or behind the receiver. Figure 44 displays the results. Once again, we see significant improvement with the high antenna position for the L and F1 (about 5 dB), but this time the loss with F3 is more substantial at 4.18 dB.

We also looked at the average RSSI when only considering packets from trucks which were not adjacent to the receiver. The results as shown in Figure 45 were interesting, as they indicate an approximately uniform 2 dB of gain on all trucks.

We then considered only packets transmitted by the truck of the same kind as the receiver, Peterbilt (L) to Peterbilt (F3) and M915 (F1) to M915 (F2). The results of this are shown in Figure 46. Here, L and F3 received the least benefit from switching to higher antennas, likely because of their significant distance from each other, and F1 improved by about 4.5 dB.

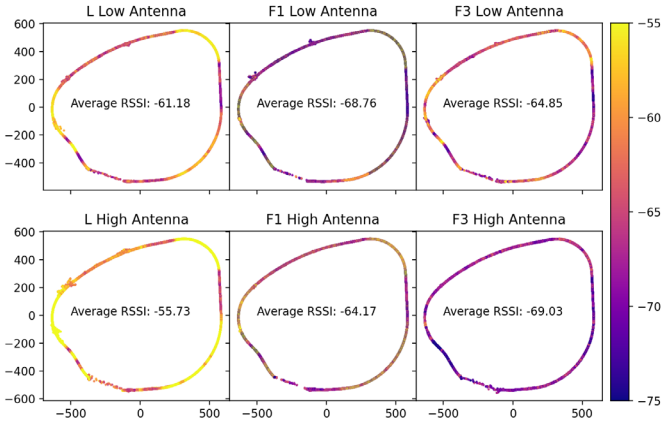

Figure 44: Average RSSI between neighboring trucks in the convoy

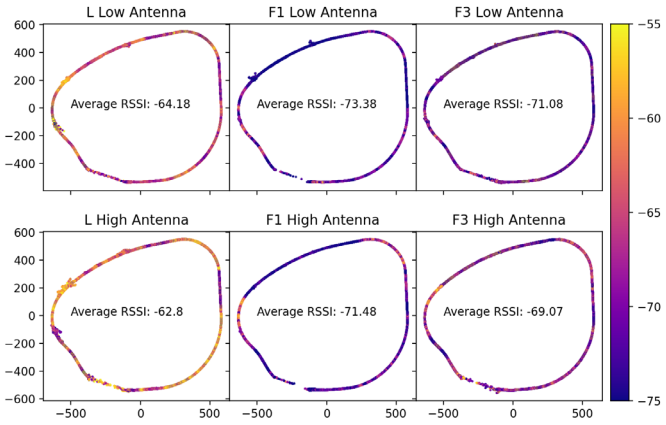

Figure 45: Average RSSI between non-neighboring trucks in the convoy

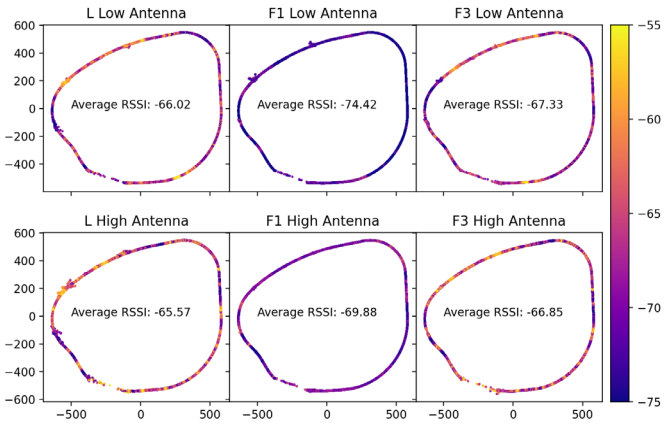

Figure 46: Average RSSI between trucks of the same type.

We proceeded to perform the complementary analysis, considering only packets transmitted by trucks of the type different from the receiver. Now we once again see L and F1 show significant improvement with the high antenna, about 3.5 dB, while F3 suffers marginally. This is shown in Figure 47.

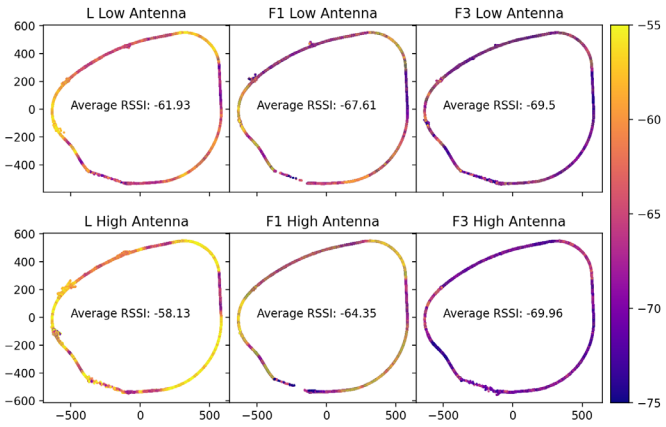

Figure 47: Average RSSI between trucks of different types.

Based on what we have seen so far, it appears that F2 brings down the average RSSI of any truck that receives packets from it. We considered the overall averages when F2 is excluded entirely in Figure 48.

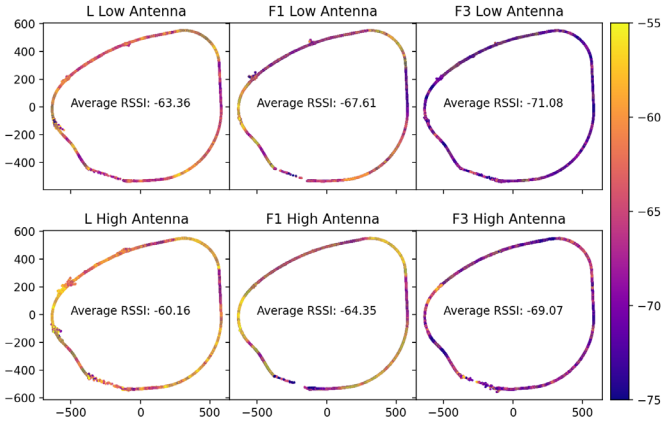

Figure 48: Average RSSI between trucks not including F2

Here we see noticeable improvement across the board with the high antenna. It is possible that F2 had some unintentionally significant cabling loss or insertion loss in the high antenna configuration which caused it to transmit at a lower signal strength. Fortunately, this was the only test affected by these problems with the F2 setup.

Overall, we can see that even a minor increase in antenna height of 3-5' offers significant benefits for received power, allowing networks to have better reliability and range. This is as expected, as greater antenna height is typically associated with better performance, for example in (Kaul, et al. 2007). The effects of antenna positioning are considered further in (Gao, Lim and Bevly 2016) and (Bogard, et al. 2017).

Future work in this area may include additional consideration of front and rear mounted antennas as opposed to the current left and right mountings. The current method was the result of discussions with automotive manufacturers who determined that side mountings were more desirable for consumers, partially due to concerns stemming from changing the connected trailer from the cab.

3.5.4 RF Interference

In order to test the effects of RF interference, we obtained a variable frequency noise transmitter, selected an RF channel close to the 5.9 GHz that our DSRC communication channel operates on, and placed it near the testing loop (Figure 49).

Figure 49: Interference source (28 dBm) placed adjacent to the test track at NCAT

This interference device was transmitting constant noise at 28 dBm and was placed at the south-east corner of the NCAT test loop. Figure 50 shows the RSSI and packet reception density for loops with the interference in place.

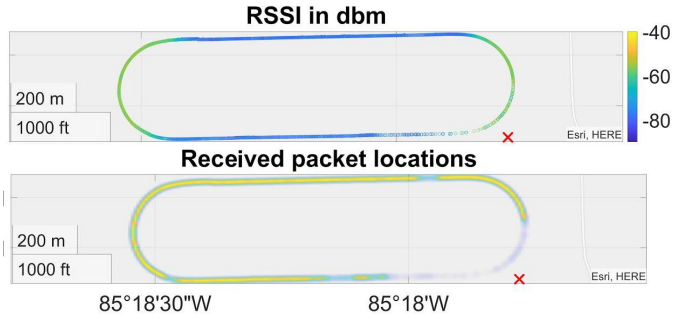

Figure 50 RSSI and received packet reception density graphs. Interference source marked with a red cross

Figure 51 shows the baseline loops, where no interference was present. In this case we see far fewer lost packets in the south-east corner. Average RSSI does not appear to be affected, which makes sense as the interference device only adds additional noise, not any additional path loss – meaning it affects the signal-to-noise ratio (SNR) but not the received signal strength.

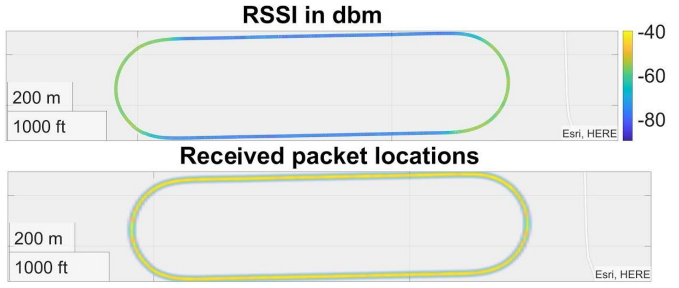

Figure 51: RSSI and received packets - Baseline (no interference).

The effects of interference on DSRC communications are explored more fully in (Cheng, et al. 2017) and (Bainwol, et al. 2020). Without either the interference device or the DSRC radio network

turned on, the noise floor was measured at approximately -90 dBm using a spectrum analyzer. Given this, there were very few dropped packets while transmitting at 23dBm and receiving at upwards of -80 dBm. However, with a 28 dBm interference device located south-east corner of the track, there is complete denial of communications in the surrounding portion of the track.

3.5.5 GPS Outage

To analyze the effects of GPS outage, we compared the results of two similar paths on the ACM test track:

- Passes through a tunnel with no GPS coverage
- Bypasses the tunnel with a parallel route which maintains GPS connection

Table 13 gives a statistical analysis of both scenarios.

Table 13: RSSI and latency statistics for the path with GPS.

	RSSI (dBm) with GPS	RSSI (dBm) no GPS	Latency (ms) with GPS	Latency (ms) no GPS
Mean	-58.528	-65.813	2.598	2.401
St Dev	3.546	3.681	0.896	0.307
Min	-73.000	-79.000	1.717	1.816
25%	-60.000	-68.333	2.182	2.245
50%	-57.000	-66.375	2.286	2.335
75%	-56.000	-62.857	2.530	2.476
Max	-52.000	-56.000	14.187	18.153

The data for determining the comparative results of GPS presence or absence was recorded over two separate days of testing. Both days had rain, although it should be noted that its severity and the fact that the tunnel would be dry inside may have caused some of the observed variations in the results.

The data was geofenced, so only radio reception events within an area slightly larger than the length of the tunnel were extracted and processed. Figure 52 shows the RSSI along the path through and around the 700' tunnel.

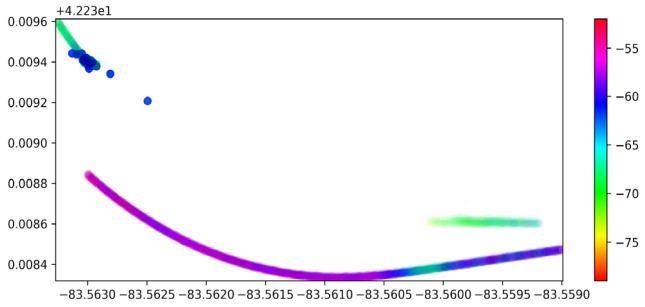

Figure 52: Visual depiction of the tunnel and bypass RSSI data. The lower path is the bypass, and the GPS-interrupted top path is through the tunnel

One thing to note is that the packets received inside the tunnel cannot be geo-located and all such packets were assigned to the last known geo-location of the receiver, which is at the entrance of the tunnel. The data inside the tunnel is otherwise perfectly valid and packets were sent and received without any problems. The tunnel's inside walls are made of metal, creating a GPS denied environment and causing internal reflections and waveguiding effects.

The RSSI data is also given as a histogram, as seen in Figure 53 and Figure 54. From these we can see that the tunnel data is bimodal, likely because of the difference between the tunnel and open-air conditions. From the open-air portion, it is clear that the larger mode in the tunnel shown in Figure 53 is the RSSI state inside the tunnel. The entire tunnel graph is shifted slightly lower in RSSI, but this might be because of road curvature effects resulting from the shape of the path inside and outside the tunnel.

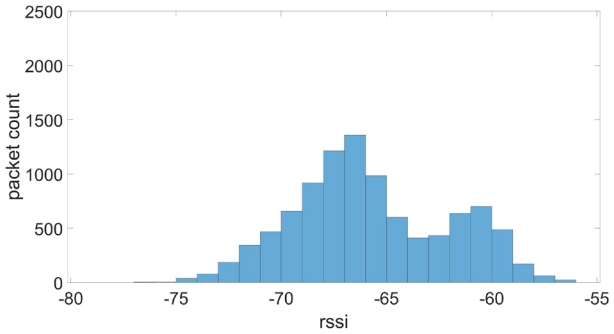

Figure 53: Tunnel RSSI data. It is bimodal, likely representing the change in conditions between the tunnel (where the most time is spent) and outside

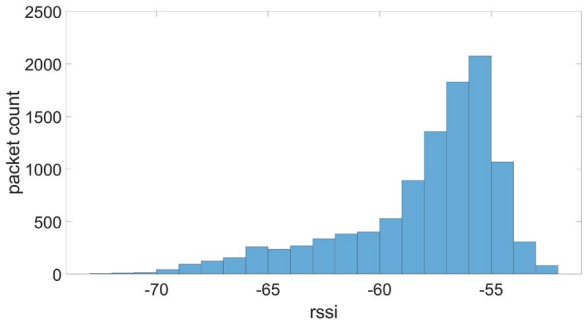

Figure 54: Tunnel Bypass RSSI data. Here, the data has one mode, representing the signal strength outside of the tunnel

3.5.6 Road Curvature

To analyze for road curvature, we filtered the NCAT data by splitting off the curved and straight sections of the track by GPS and performing our analysis on both sections separately. Table 14 shows the results for both the straight and the curved sections of the NCAT loop.

Table 14: RSSI and latency statistics for the curved sections of the NCAT test track

	RSSI (dBm) Curved	RSSI (dBm) Straight	Latency (ms) Curved	Latency (ms) Straight
Mean	-73.349	-88.553	18.283	15.107
St Dev	4.318	2.472	93.654	73.182
Min	-90	-98	1.675	1.736
25%	-76	-89	2.296	2.386
50%	-72	-88	2.528	2.834
75%	-70	-87	3.415	4.5665
Max	-68	-73	1299.465	992.392

These indicate a significant improvement in RSSI when the trucks go on a bend in the track. We believe this is related to the occlusion results, as the curve allows for line-of-sight between any pair of vehicles without the obstruction of the vehicles in between, or their own trailers.

3.5.7 Grade

To analyze the impact of grade, or elevation changes, on RSSI we selected a couple of portions from the ACM test track where we ran 45 mph tests with antennas mounted at 8'. Running a correlation coefficient matrix on the stretches, we did not find any significant correlation (< 0.2). Figure 55 is a sample of two sections of track on the east side of the test loop, one with a relatively large grade change, and one without. The colorbar shows the height of the track in meters.

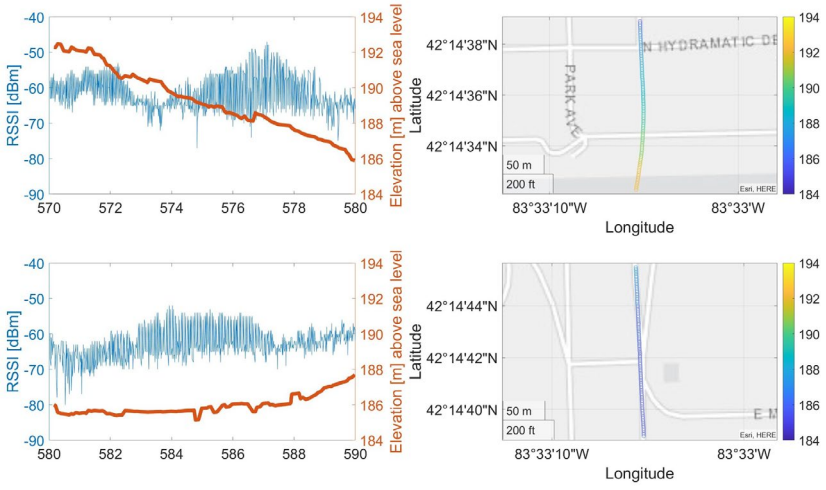

Figure 55: RSSI vs elevation in slope (above) and flat (below), 8' antenna height

As can be seen, the RSSI in blue does not appear to be correlated to the elevation shown in red which is obtained via GPS. This data was collected on the lead truck L and has an averaged sample RSSI of received packets from all the other trucks F1, F2, and F3 in the convoy.

3.6 Effect of Sensor Performance on Platooning

This section elaborates on the effect of faulty radar, degraded GPS and radio interference, on fuel economy.

3.6.1 Effect of Faulty Radar on Platooning

3.6.1.1 Sensor issue

As discussed in the Delphi radar section, the radar is tracking many different points during operation. If the radar fails to track the correct points, then the range measurement may be affected. To investigate the effect of such a scenario, a radar was installed backwards on one of the platooning trucks in the four-truck platoon, T13 from Table 1. This caused the radar to track incorrectly during the curves at the NCAT test track, as shown in Figure 56. Only several laps are shown, rather than the full span of 26 laps (an hour of operation). Filled data points represent time steps where the radar received a tracking update.

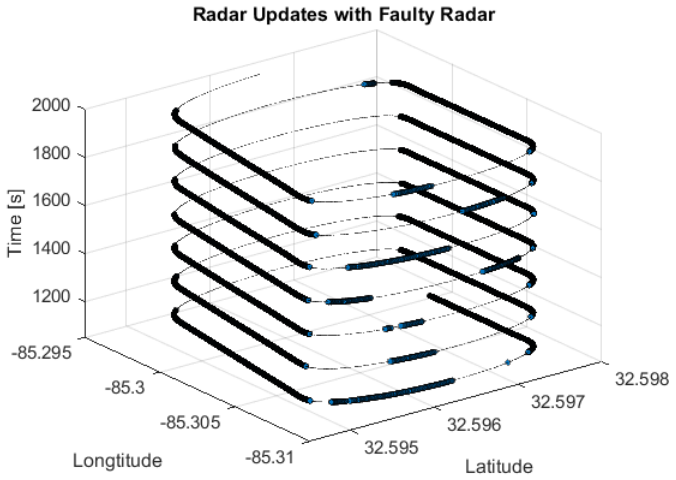

Figure 56: Radar updates with an incorrectly mounted radar. Filled points represent when radar updates were occurring.

Figure 57 shows what the lap position in the subsequent figures translates to on the NCAT test track.

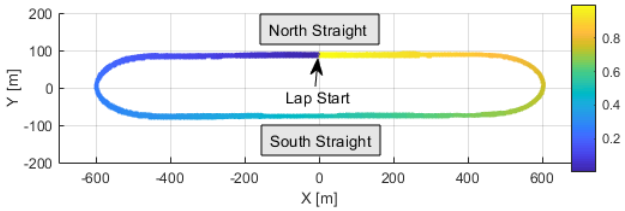

Figure 57: Demonstrating what lap position corresponds to on the NCAT test track

3.6.1.2 Control effects

The lack of radar updates creates an erroneous headway estimate, as shown in Figure 58. The headway is the estimated range of the system (distance to the truck ahead), an output of the KF.

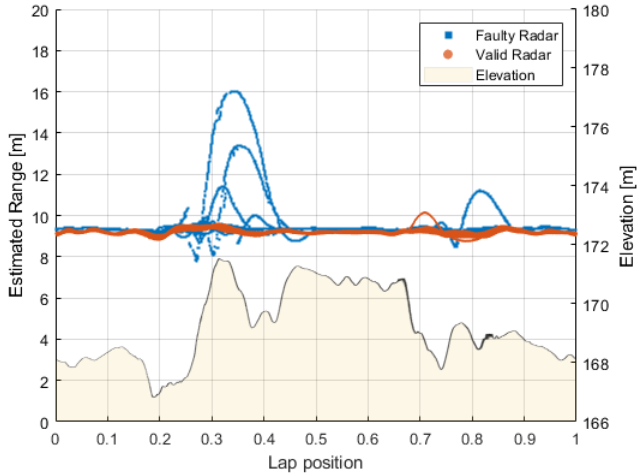

Figure 58: Headway perceived by the CACC system for valid and faulty radar

Figure 59 shows a region of interest just before the curve, highlighting a particularly incorrect range estimate. All further figures in this section will be focused on that region. As the radar updates sporadically, the range estimate chatters, leading to poor control and overshooting. The presence of a hill likely exacerbates the issue.

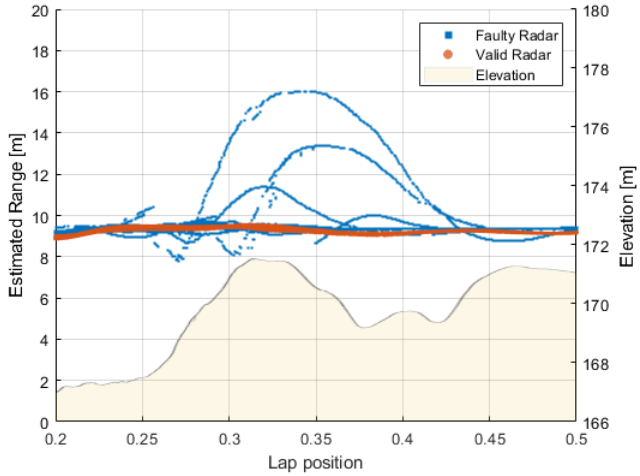

Figure 59: Range estimate in region of interest for truck T13 in a 4T 100' platoon with and without radar faults

3.6.1.3 Dynamic effects

Due to the incorrect headway estimate from faulty radar, the truck brakes aggressively, and subsequently must accelerate aggressively once true headway is realized again. Figure 60 shows

the wheel-speed sensor data for T13 for both valid and faulty radar operation. A pattern of braking and accelerating is clear in the faulty radar traces.

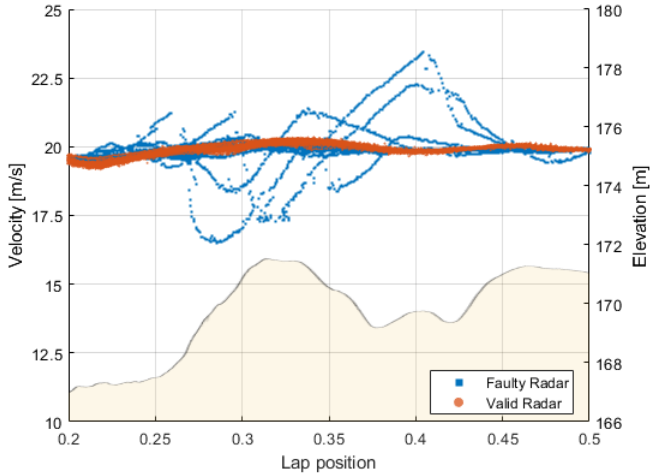

Figure 60: Velocity trace for truck T13 in a 4T 100' platoon with and without radar faults

Figure 61 shows velocity for both the preceding truck and T13 during a single lap with the radar installed backwards. In this instance, the faulty radar induced headway errors that forced braking and subsequent reacceleration. The braking event takes the truck nearly 9% under the set velocity, and the subsequent acceleration takes it nearly 10% over the set speed.

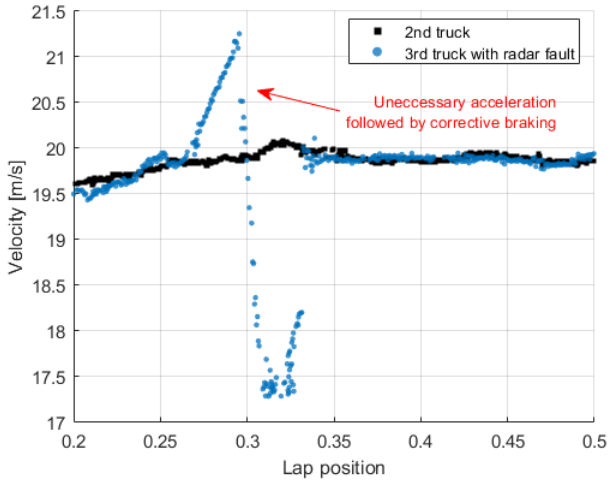

Figure 61: Velocity profile for truck T13 in 4T 100' platoon and its immediate leader during one lap, showing aggressive correction

3.6.1.4 Fuel Effects

Aggressive acceleration events induced by the reversed radar and subsequently erroneous headway measurements force the truck to waste energy on:

1. over-acceleration, especially in the event of a transmission downshift

2. the braking event itself. Any time a truck in platoon actively decelerates, it is wasted energy. Braking here is generalized to mean both the retarder and the air brakes.

Both effects can be seen in the CAN fuel rate data for the truck with faulty radar measurements in Figure 62:

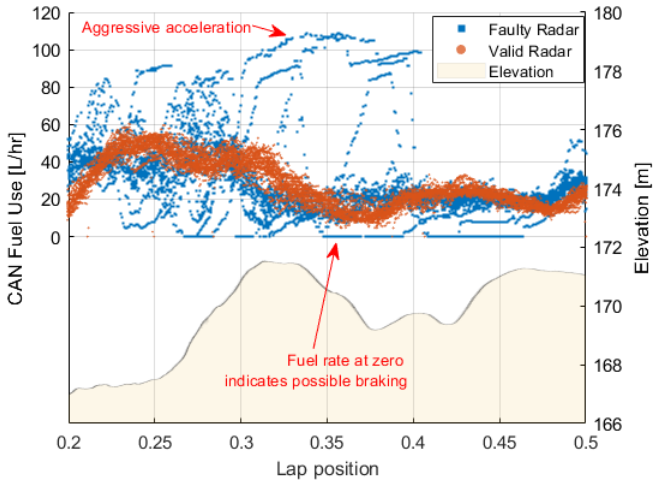

Figure 62: CAN fuel rate for truck T13 with both valid and faulty radar.

When the fuel rate data shown in Figure 62 is integrated, fuel consumption over the course of faulty radar operation was 5.68% greater. The standard deviation over the section shown in Figure 62 is much higher for the faulty radar, at $\sigma_{faulty} = 21.2\ L/hr$ vs. $\sigma_{valid} = 12.6\ L/hr$.

3.6.2 Effect of Degraded GPS on Platooning

3.6.2.1 Sensor issue

While GPS is always available, the number of satellites visible to a GPS receiver is constantly changing. A GPS receiver needs a minimum of four satellites to fix its position because the XYZ receiver position and the receiver clock bias must be estimated. While some GPS receivers have clocks stable enough to allow for positioning with three satellites, the Auburn system requires four. Additionally, four satellites do not guarantee quality estimates. Several factors can impact the measurement quality such as signal to noise ratio and elevation angle, in additional to all the other error sources stated in the DRTK section.

Figure 63 presents a scenario in which the Auburn vehicles were platooning on an overcast night in a tree-lined area. While DRTK is able to maintain a position solution when five satellites are visible, the accuracy greatly drops when the number of satellites visible is reduced to four. While

this chatter remains relatively small, some GPS solutions can degrade to the point of returning RPV's of up to a mile.

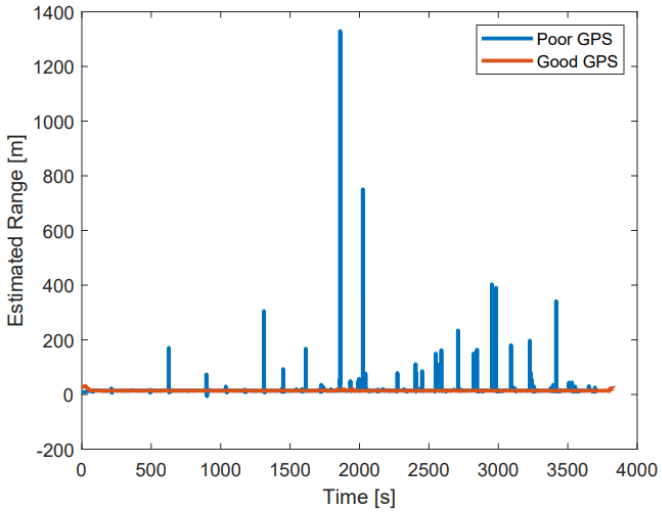

Figure 63: RPVs in poor vs. good GPS conditions

Figure 63 provides a larger time scale for context and is generated from the same data as Figure 64. A scenario in which the same truck is platooning on the same terrain but has better GPS data is also shown for comparison.

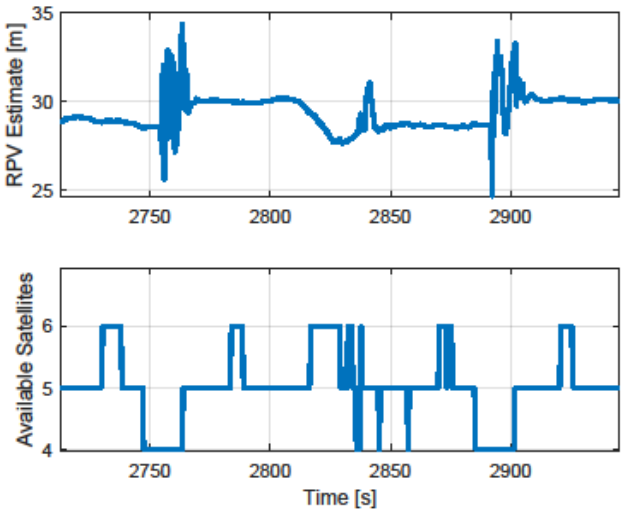

Figure 64: RPV Solution vs Available Satellites.

3.6.2.2 Control effects

While bad radar measurements were impactful enough to cause serious deviations in vehicle headway and CAN fuel rate, the sub-optimal GPS performance created almost no impact. This is primarily due to these key factors:

1. The headway controller on the vehicle penalizes range-rate errors 5X more than it penalizes range errors,
2. Radar is the dominant measurement in sensor fusion algorithm for range-rate updates, and

3. Fault rejection for DRTK measurements.

While the reduced satellite GPS does create very poor range estimation on its own, the CACC headway controller was able to successfully mitigate these disturbances. Figure 65 provides the range estimate vs normalized track position for both the "good" GPS vs "poor" GPS scenarios. Each of these runs is 26 laps of operation on the NCAT track. The scenario shows no clear signs of sub-optimal control performance except for one small deviation. The rejection of noise from the GPS signal is primarily accomplished through two methods. The first is the fusion of all available measurements as described in the sensor fusion section. The second is due to performing a 3-sigma test. Namely, if the range measurement exceeds 3σ of the expected range, the measurement is rejected by the headway controller.

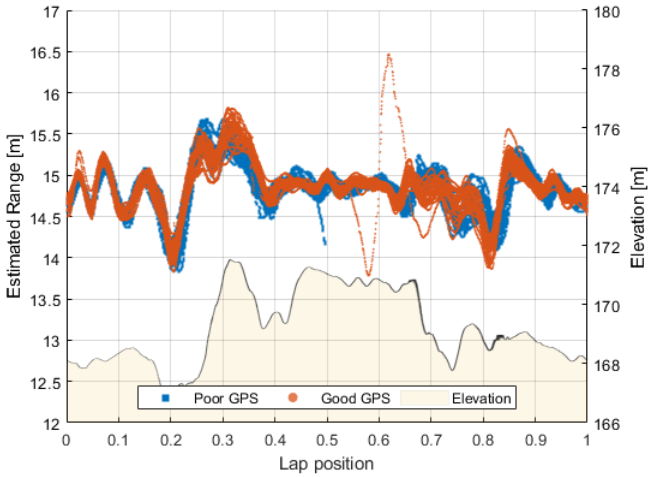

Figure 65: Estimated Range with poor GPS vs good GPS (all laps are shown)

3.6.2.3 Dynamic effects

Because the range estimate was largely unaffected, it was suspected that the velocity profile for the vehicle should also be largely unaffected. Figure 66 displays the velocity profile between the same good GPS and poor GPS runs. With the exception of one velocity perturbation on the poor GPS run, the overall trends are almost identical between the two scenarios.

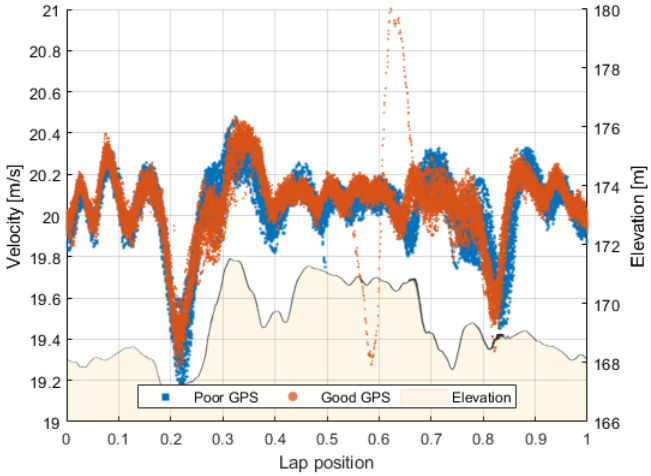

Figure 66: Vehicle velocity results for good vs sub-optimal GPS

3.6.2.4 Fuel Effects

As a result of the sensor fusion algorithm being able to reject the sub-optimal GPS points, the fuel rate data shows almost no changes on a lap-to-lap basis through the run with only one exception. While it is reasonable to assume that the large spike in fuel rate would cause a sizeable increase in the fuel consumption, but that was not the case. Surprisingly, the 'good' GPS run consumed 0.255% more fuel over an hour of operation. With a fuel consumption difference of only 0.255%, there is no clear negative platooning effects caused by the GPS (Figure 67).

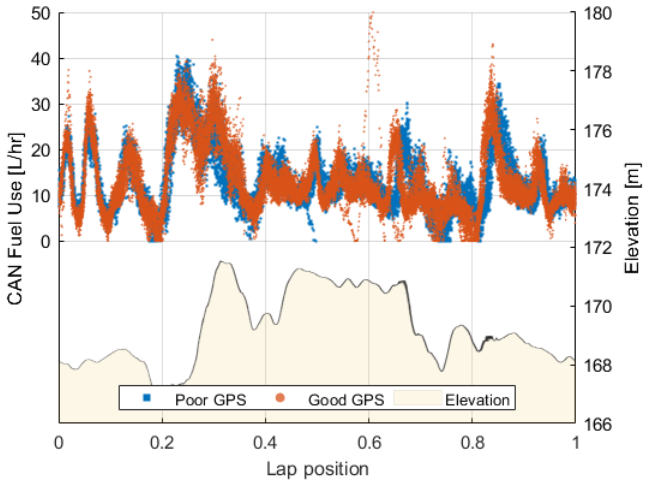

Figure 67: Fuel results for good vs sub-optimal GPS

3.6.3 Effect of Radio Interference

3.6.3.1 Sensor issue

In order to test the effects of radio frequency (RF) interference, a 5.8GHz video transmitter system was obtained. An RF channel close to the 5.9GHz that DSRC operates on was selected and the transmitter was placed near the testing loop in the South-East corner as shown in Figure 68. The frequency 5.8GHz is an industry, scientific and medical (ISM) band as defined by the Federal Communications Commission (FCC), allowing for unregulated power levels up to 1 watt (30 dBm), which is commonly used for Wi-Fi and other applications (Federal Communications Commission n.d.). This RF interference source was set to transmit at 27.5 dBm, and using the standard COTS antenna, the sideband radiation was enough to generate noticeable interference in the 5.9GHz range.

For clarity, Figure 68 depicts a single lap of operation with interference. As a comparison, a lap of nominal operation without interference is shown in Figure 69. In both tests, the data displayed are the packets received by truck T13 from the preceding vehicle, T14, while platooning at 100' headway gap distance and a platoon order of A1, T14, T13, A2. Truck T13 was chosen so the impacts of the dropped packets caused by the RF interference on vehicles both ahead and behind the selected truck can be deciphered.

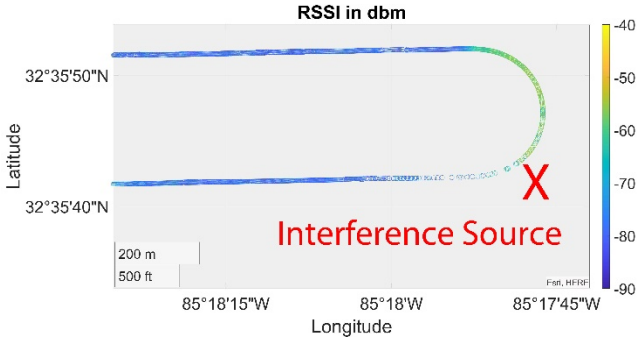

Figure 68: Received packet signal strength in RSSI with the interference source active.

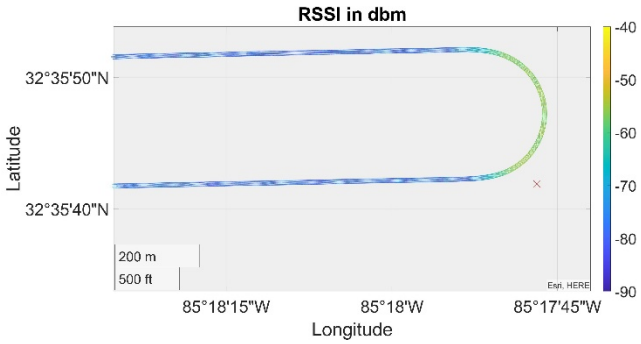

Figure 69: Received packet signal strength in RSSI by location during nominal operation,

Because the interference device increased the noise floor, the effect on RSSI is small, and does not reduce the signal power to a level that approaches the receiver's minimum sensitivity level, but does degrade the signal to noise ratio, leading to dropped packets.

3.6.3.2 Control Effect

Figure 70 and Figure 71 present headway and RSSI versus lap position for both nominal operation and operation during RF interference, respectively. The interference device is located near lap position 0.7. No appreciable performance degradation from the RF interference is noted near lap position 0.7. It is plausible that the impacts of RF interference are being outweighed by other factors impacting the following distance. Namely, greater signal strength was observed in the curved area of the track, see Figure 68 and Figure 69, and the impact of elevation changes.

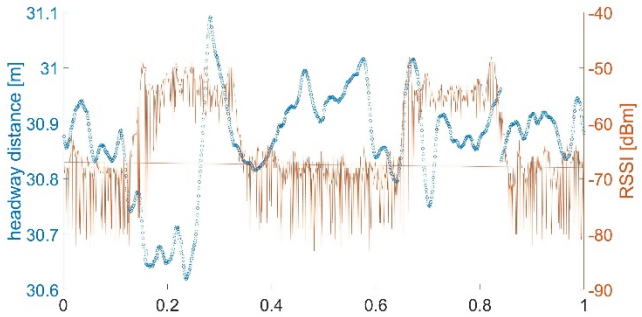

Figure 70: Range vs RSSI versus lap position with no RF interference

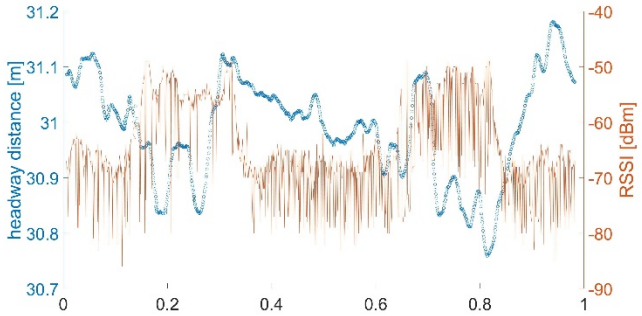

Figure 71: Range vs RSSI versus lap position with RF interference

3.6.3.3 Dynamic Effect

Because the range estimate was essentially unaffected, the velocity trace of a truck through a corner with radio interference was also unaffected relative to its velocity without radio interference. As an example, Figure 72 shows the velocity of the second truck in platoon from the four-truck platoon, T14, during operation with and without radio interference at 100' headway distance.

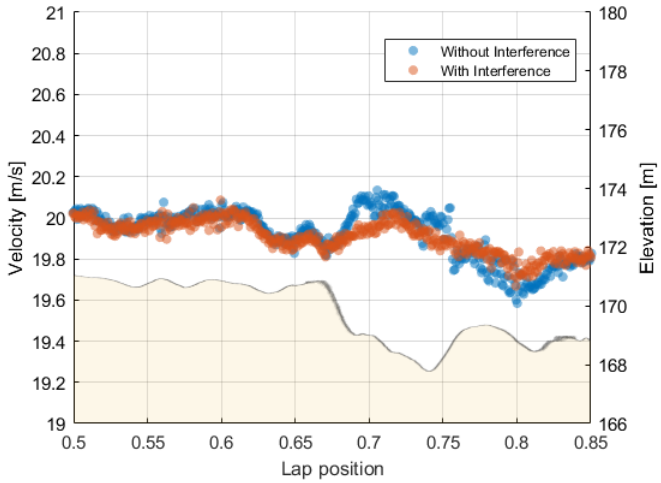

Figure 72: Velocity of second truck in platoon through a corner where radio interference is present

3.6.3.4 Fuel Effect

Because the velocity trace was unaffected by the interference, it follows that the fuel consumption was also unaffected. Figure 73 confirms that this interference strategy had no discernable impact on fuel consumption. The small differences between the 'with' and 'without' interference fuel rates could certainly be due to the influence of some other factor, such as wind, but no further effort was made to isolate this.

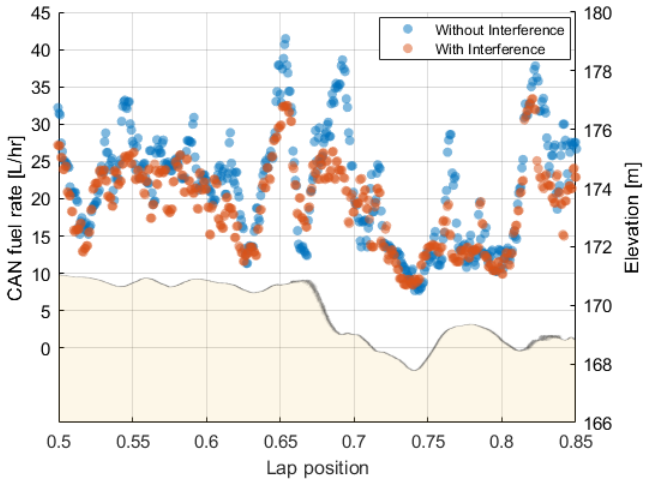

Figure 73: T14 CAN fuel rate throughout the jammed SE corner

3.7 Modeling and Simulation

This research has two parts: (i) modeling – building a computer model of truck platooning, and (ii) simulation – running that model to produce test results.

The simulation model in this paper was developed with PreScan and Matlab-Simulink. PreScan is a commercial physics-based simulation platform that is extensively used for the development of connected-autonomous vehicles (CAV) and advanced driver assistance systems applications.

3.7.1 Modeling

The model used to describe the truck-platoon has the following elements:

1. Test Roads - ACM Highway Loop (HWL)
2. Sensors - Radars, GPS, DSRC
3. Environmental Effects - Rain, Snow
4. Control and Actuation - ACC-based Throttle and Brake, also takes in DSRC input during sensor failure
5. Vehicle Dynamics - Mass, Drivetrain, Tires, Trailer
6. Test Scenarios

3.7.1.1 Test road

The test road used in this experiment is ACM as previously mentioned. A 3D model was generated by PreScan staff employed at the ACM. The ACM is a testing environment located in Ypsilanti, MI where the performance of AVs, CAVs and vehicle platoons can be evaluated. The ACM offers many different scenarios for testing your vehicles. They can be driven on the HWL which is a 3795-meter-long road that is representative to a regular highway setting with minimal buildings and sparse vegetation in the surrounding area, the User Defined Area (which can be configured by the tester to create most scenarios you would like to test), traffic light areas, tunneled areas and many others.

The HWL is the test road that is used in this experiment to evaluate the vehicle's performance. Performance of the vehicle platoon is based on the safety margins, or the minimum headway

between the leading and following vehicle. Figure 74 shows both the map of the entire ACM and a section of the 3D map of the HWL that has been created within PreScan.

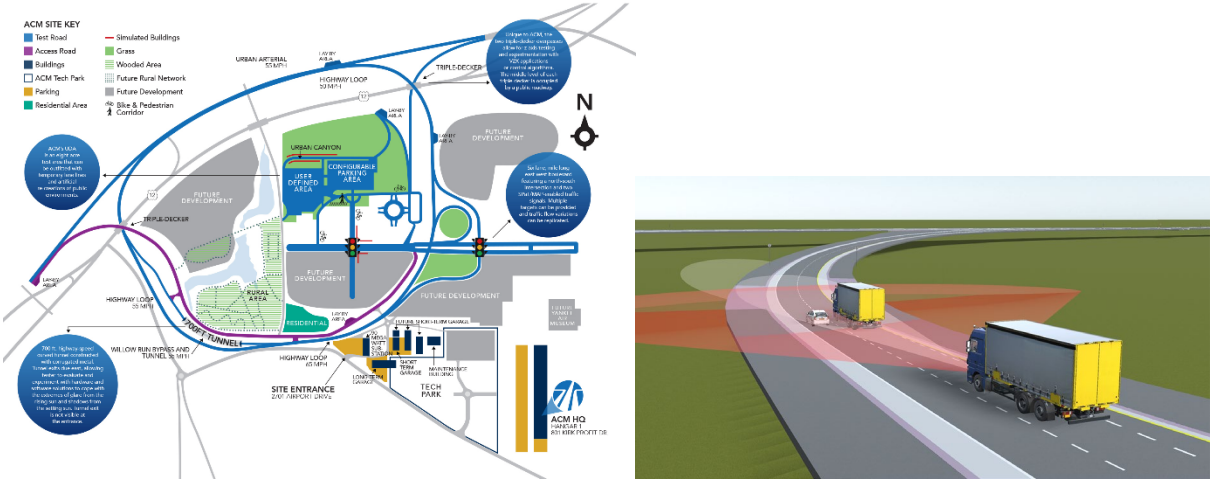

Figure 74: Actual ACM test track (left); PreScan model of the 3D ACM test track (right).

3.7.1.2 Sensors

A long-range radar is used to maintain headway with the vehicle ahead, a short-range radar is used to detect vehicle cut-ins, GPS for vehicle localization and DSRC radios are used as an extra layer of data verification in the case of sensor failure or in the case that the vehicle ahead is outside of one or both of the radar's field of view (FOV).

1. The DSRC network modelled in this experiment sends packets of a size of 1500 bytes, which is the closest available setting which matches with what was being sent over the DSRC network in the work done in (Alghodhaifi, et al. 2018). Within PreScan, a packet has a higher chance of being dropped over a certain distance as the packet size increases. This relationship is shown in Figure 76. The messages that are being sent over the DSRC network are Basic Safety Messages (BSMs) with data elements indicating sender ID, message ID, GPS location, vehicle speed, yaw rate, heading, path history as well as path prediction and other data elements (Figure 76). It should be noted however that only GPS location, vehicle speed and yaw rate are currently being taken by the ACC unit for headway control and the other parameters are merely sent to increase the size of the packet to be similar to what is being sent in the actual DSRC network between trucks tested at the ACM. Within PreScan, the packet delivery rate (PDR) is dependent on the packet size. The smaller the packet, the less likely it is to be sent erroneously. Two antennas are placed on each semi-truck, one on each of the side-view mirrors (Figure 75).

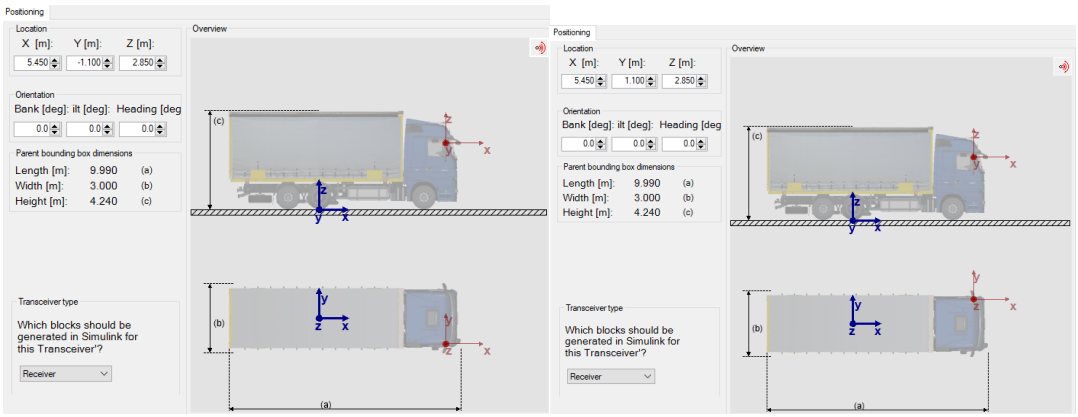

Figure 75: Placement of receiving DSRC antennas on following vehicle. Placement is identical for transmitting antenna on lead vehicle

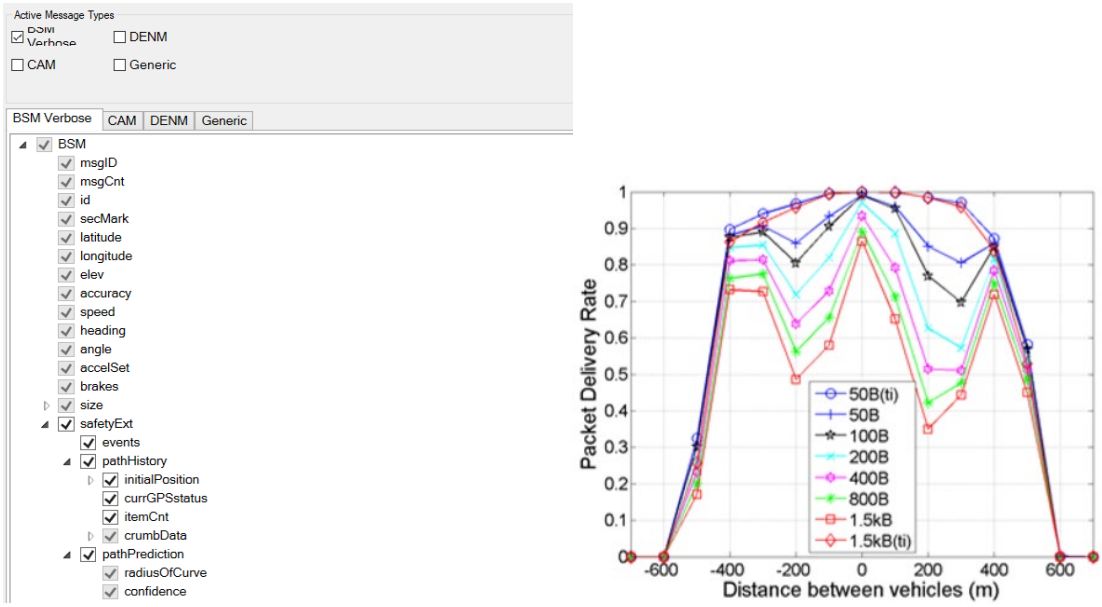

Figure 76: Data frame selection for BSM (left), PDR vs Packet Size (right)

2. The GPS information being sent over the DSRC network has a variable packet size which is proportional to the number of satellites the GPS receiver is connected to at once. For the sake of simplicity, it is assumed that a GPS receiver is constantly connected to at least 8 satellites. The GPS information is then configured to take up 800 bytes of data within the DSRC packet.

3. The long-range radar and short-range radar both have an operating frequency of 74 GHz, ranges of 175 meters and 60 meters and cover an azimuth angle of +/-10 degrees and +/-45 degrees respectively. Figure 77 shows the radar placement on the front bumper of the following semi-truck. The radar pulse's received signal power is a function of the radar cross section (RCS), antenna gain, surface area of the reflective object, the object's reflectivity, and the transmitted signal power and distance to the object (Yamada 2005). If the received signal strength is too low, then the receiver will recognize it as noise. This is implemented through the use of a Simulink block shown in Figure 78, where the energy

loss in dB is compared to a threshold value. If the energy loss exceeds the threshold value, the received signal is discarded as noise. The threshold value was determined by the transmitted power in dB of the radars used in previous studies (Alghodhaifi, et al. 2018).

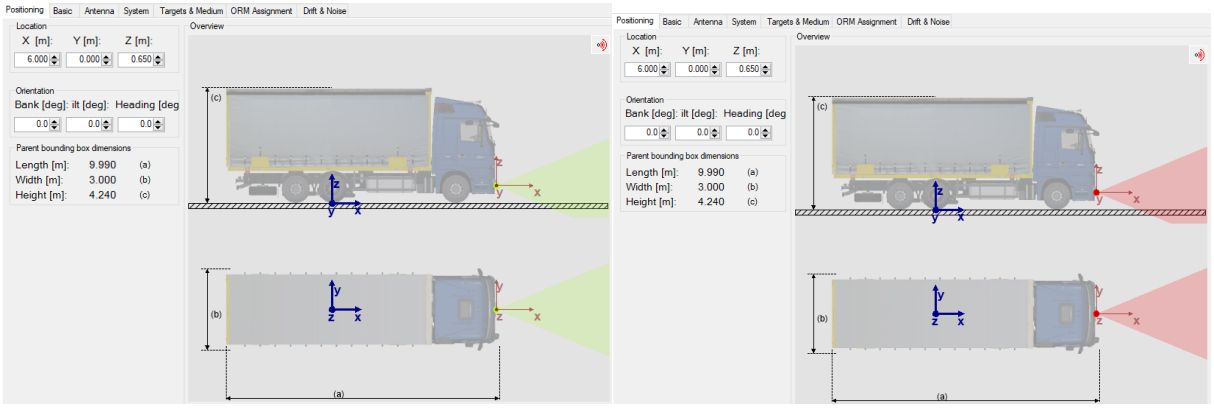

Figure 77: Placement of Long-Range Radar (Left) and Short-Range Radar (Right)

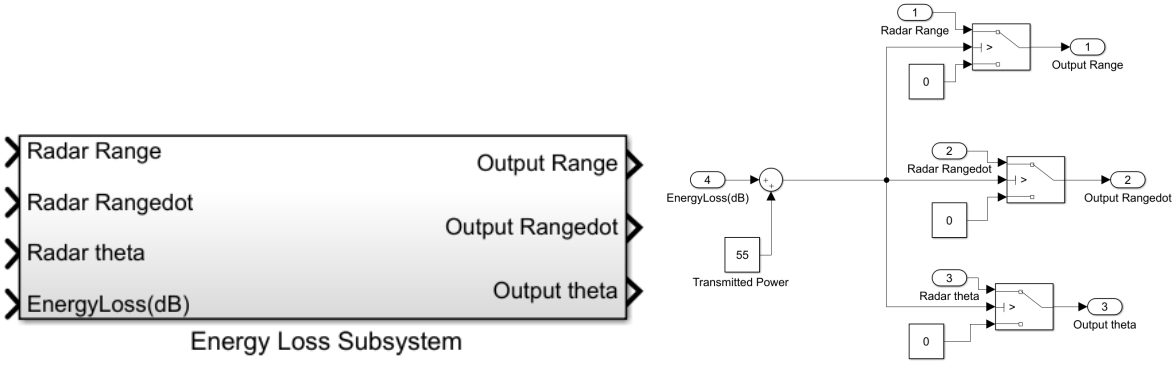

Figure 78: Energy Loss Subsystem used to filter low-power readings

3.7.1.3 Weather Conditions

The test scenarios simulated in PreScan can be set to have varying types of weather. The weather conditions ultimately affect the friction of the vehicle's tires against the road surface. With decreased tire friction against the road surface, the follower vehicle must allow for a larger headway between itself and the vehicle ahead of it to maintain adequate safety. Each of the later described test scenarios were run in dry, moderately rainy, and extremely rainy weather conditions. Increases in precipitation also have an adverse effect on the sensors utilized by the truck platoon. As a RF signal is transmitted from the radars through space, it experiences attenuation as it travels (Figure 79). This phenomenon is known as path loss (Ghassemzadeh and Tarokh 2003). This attenuation is increased when it is raining because the electromagnetic signal power is absorbed by the water molecules within the atmosphere (Chandra, Joshi and Singh 2014). Descriptions for what is considered "moderately rainy" and "extremely rainy" can be seen in Figure 80.

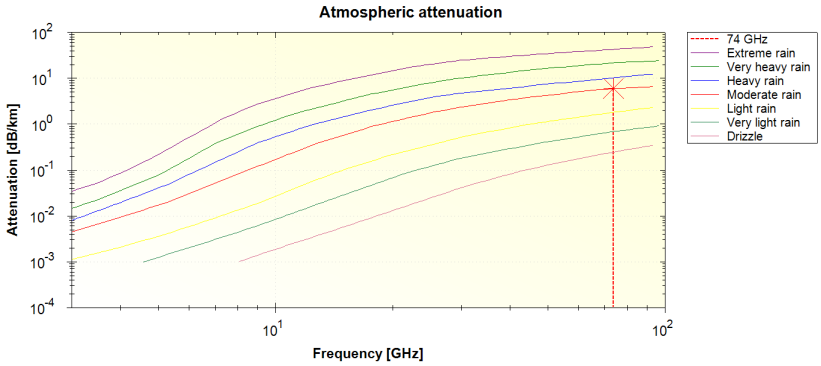

Figure 79: Attenuation vs. Operating Frequency for ACC Radar

Category	R [mm/h]	<R> [mm/h]	<Dp> [mm]
Very light	0 < R < 1	0.5	0.77
Light	1 < R < 2	1.5	0.93
Moderate	2 < R < 5	3.5	1.06
Heavy	5 < R < 10	7.5	1.23
Very heavy	10 < R < 20	15	1.57
Extreme	R > 20	40	2.03

Figure 80: Rain descriptors. R = rainfall rate, <R> = average rainfall rate, <Dp> = rain diameter

3.7.1.4 Control and Actuation

The headway control of the following semi-truck in the platoon is managed by an adaptive cruise control (ACC) system. The goal of the ACC system is to control the throttle and brake pressure of the following vehicle in order to maintain its speed in such a way that a safe headway with the following vehicle is maintained. The key input to the ACC system is the demanded headway time (HWT). This user defined input is what the ACC system uses as a reference when actuating the vehicle's throttle and brake pressure to force the measured HWT to be as close as the demanded HWT. The measured HWT is the vehicle's relative distance to the target object divided by its speed. Figure 81 is the Simulink representation of the ACC system.

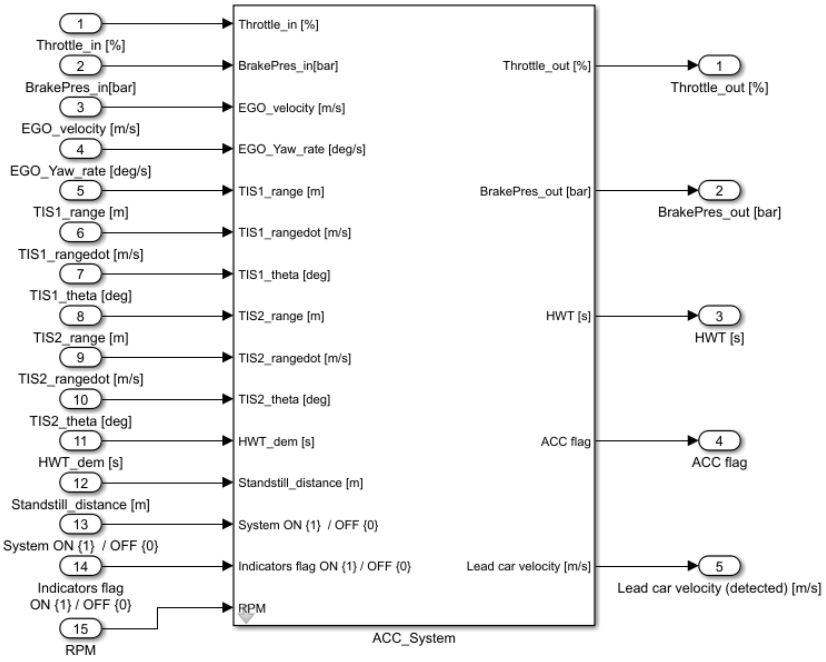

Figure 81: ACC subsystem used for headway control

Longitudinal vehicle control and steering is controlled by a PathFollower (Figure 82) algorithm designed to mimic human driver behavior. This algorithm calculates the optimal front wheel steer angle to minimize the lateral error (e_Lat) of the vehicle position and its reference path. It translates the trajectory of a given vehicle and computes an equivalent steering angle input for the vehicle dynamics model. The algorithm uses 10 preview points (pvp) to calculate the steering angle.

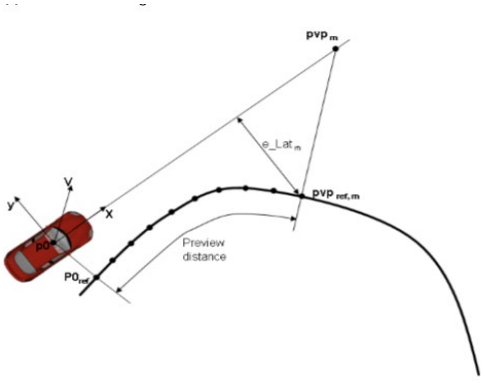

Figure 82: Path follower model for realistic longitudinal control

3.7.1.5 Vehicle Dynamics

The vehicles selected for this experiment were two Mercedes Benz Actros 2541 L 6x2 semi-trucks with attached trailers. All vehicles within PreScan come with their own pre-defined dynamics models. The 3D dynamics models within PreScan allow vehicles to traverse 3D

roadways in a realistic manner. The 3D chassis model of the semi-trucks reflects all aspects of the real world. The chassis parameters for vehicle dynamics are shown in Figure 83 and Figure 84.

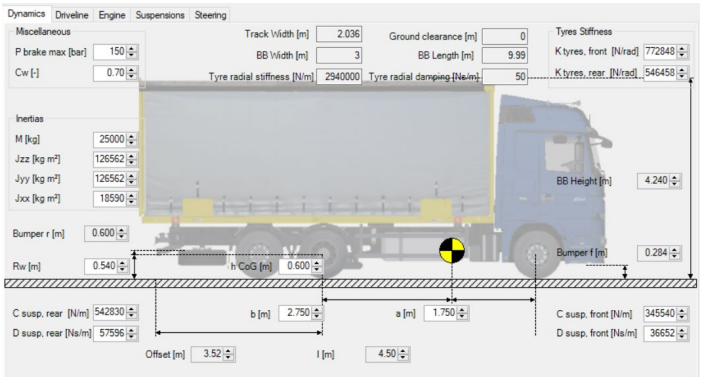

Figure 83: PreScan 3D Vehicle dynamics of Mercedes Benz trucks

Parameter	Description	Unit
P max	Maximum brake pressure	[bar]
M	Total mass of the vehicle	[kg]
Jzz	Moment of Inertia of the vehicle body, around the z axis	[kg m^2]
Jyy	Moment of Inertia of the vehicle body, around the y axis	[kg m^2]
Jxx	Moment of Inertia of the vehicle body, around the x axis	[kg m^2]
Rw	Tyre radius	[m]
Tyre radial stiffness	Tyre vertical stiffness coefficient	[N]
Tyre radial damping	Tyre vertical damping rate coefficient	[Ns/m]
C susp. rear	System stiffness of the rear suspension, both sides merged (used for roll calculation only)	[N/m]
D susp. rear	System damping rate of the rear suspension, both sides merged (used for roll calculation only)	[Ns/m]
Kfront	Cornering stiffness of the front tyres (left & right merged)	[N/rad]
Krear	Cornering stiffness of the rear tyres (left & right merged)	[N/rad]
h Cog	Height of the center of gravity	[m]
b	Distance of center of gravity to rear axle	[m]
a	Distance of center of gravity to front axle	[m]
l	Wheel base of the vehicle	[m]
Cw	Air resistance factor	[-]
C susp. front	System stiffness of the front suspension, both sides merged (used	[N/m]

Parameter	Description	Unit
	for roll calculation only)	
D susp. front	System damping rate of the front suspension, both sides merged (used for roll calculation only)	[Ns/m]
Kfront	Cornering stiffness of the front tyres	[N/rad]
TrackWidth	Track width of the vehicle (used for simple dynamics)	[m]
BB Width	Bounding Box Width of the Vehicle (used for AIR sensor)	[m]
BB Length	Bounding Box Length of the Vehicle (used for AIR sensor)	[m]
BB Heigth	Bounding Box Length of the Vehicle (used for AIR sensor)	[m]
Bumper	Position of the bumper wrt the ground (used for default sensor positioning)	[m]

Figure 84: Parameter descriptions for 3D Vehicle Dynamics

3.7.2 Simulation

The model described in 3.7.1 was run to produce test results. Four different scenarios in which the semi-truck platoon were operating were considered to reflect real-life trucking conditions at the ACM. The ultimate goal of the following test scenarios is to determine whether or not a DSRC link between vehicles makes the system more secure. Keeping this in mind, the test scenarios

should be analyzed to see if there are any moments where the platoon is operating in unsafe conditions. The test scenarios can be broken up into two sections:

1. Scenario A - Radar Only, no Vehicle Cut-In: Two Mercedes Benz semi-trucks are traveling at ~ 65 mph (speed increases and decreases around corners, traveling uphill and traveling downhill). The demanded HWT between semi-trucks is .2 seconds. When moving at ~65 mph, this corresponds to approximately 20-40 meters between semi-trucks, which is a dangerously close range for fuel savings but allows the platoon to stay closer together. The two semi-trucks are to travel one full loop around the ACM test track. The following semi-truck is equipped with one long range radar and one short range radar. Dry, moderately rainy, and extremely rainy weather conditions are used for three individual test runs.

2. Scenario B - Radar and DSRC, no Vehicle Cut-In: Exactly identical to Scenario A, except a DSRC communication link is utilized to determine lead vehicle range, doppler velocity and azimuth angle in the case that the long-range radar or short-range radar experience an instance of sensor failure or in the case that the leading vehicle is not in the radar field of view.

3. Scenario C - Radar Only, Vehicle Cut-In: Exactly identical to Scenario A, except there will be instances of a third vehicle which is not a member of the platoon cutting in between the two semi-trucks.

4. Scenario D - Radar and DSRC, Vehicle Cut-In: Exactly identical to Scenario C, except a DSRC communication link is utilized to determine lead vehicle range, doppler velocity and azimuth angle in the case that the long-range radar or short-range radar experience an instance of sensor failure or in the case that the leading vehicle is not in the radar field of view.

3.7.2.1 Scenario A

The results from Scenario A show that regardless of weather conditions, the following vehicle in the platoon is able to adequately maintain the desired headway with the lead vehicle around the entirety of the HWL. Cases where the lead vehicle is not in the following vehicle's field-of-view (FOV) can be seen by the "Adaptive Cruise Control" text in the follower vehicle's dashboard (Figure 85, Figure 86) turning from green to grey or by both of the radars reading a range of zero. No unsafe scenario was detected for the platoon, even when turning corners and traversing uphill or downhill.

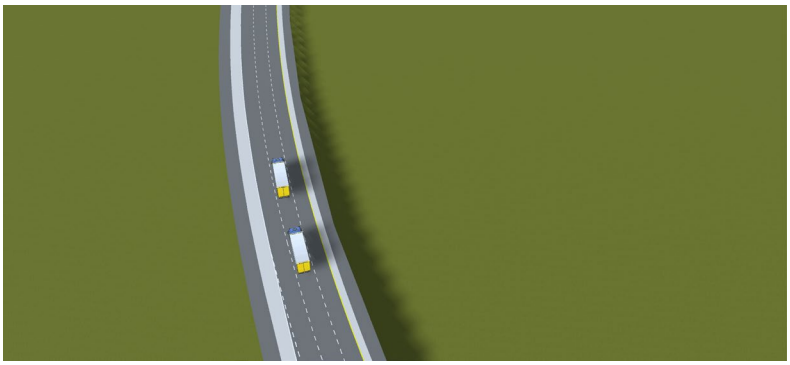

Figure 85: Leader - Follower convoy moving smoothly through turn on a dry weather run

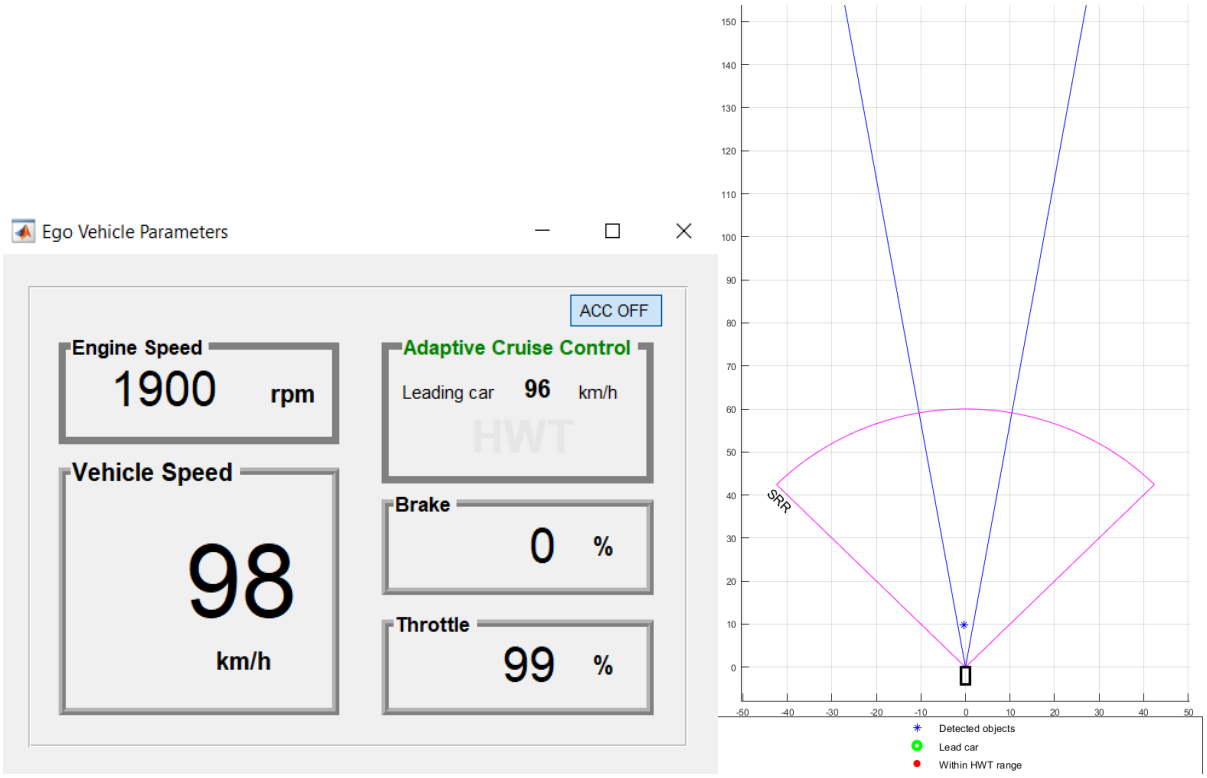

Figure 86: Radar GUI (left) and follower vehicle display (right) during safe operation

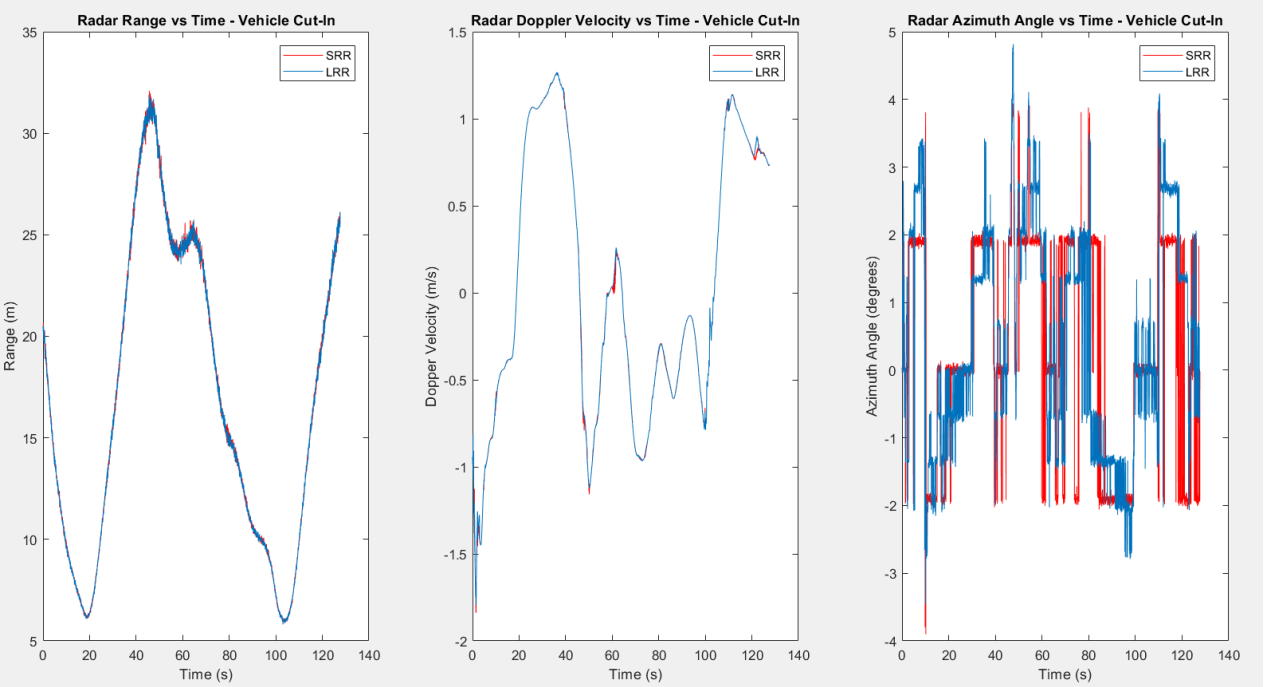

Figure 87: Radar Parameters vs Simulation Time

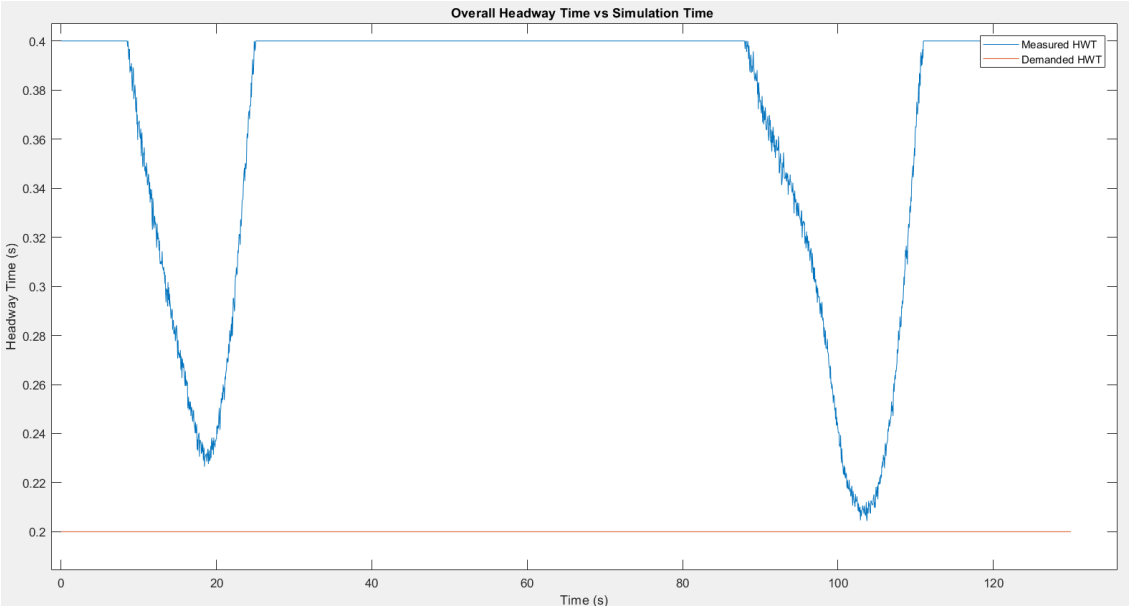

Figure 88: Measured HWT vs Simulation Time

3.7.2.2 Scenario B

The results for Scenario B were similar to Scenario A. Since no sensor failure occurred and the lead vehicle was always inside the radar FoV, the data being sent over the DSRC link never played a role in actuating the following vehicle. The values for radar range, doppler velocity, and azimuth angle were identical between test runs of scenario A and B.

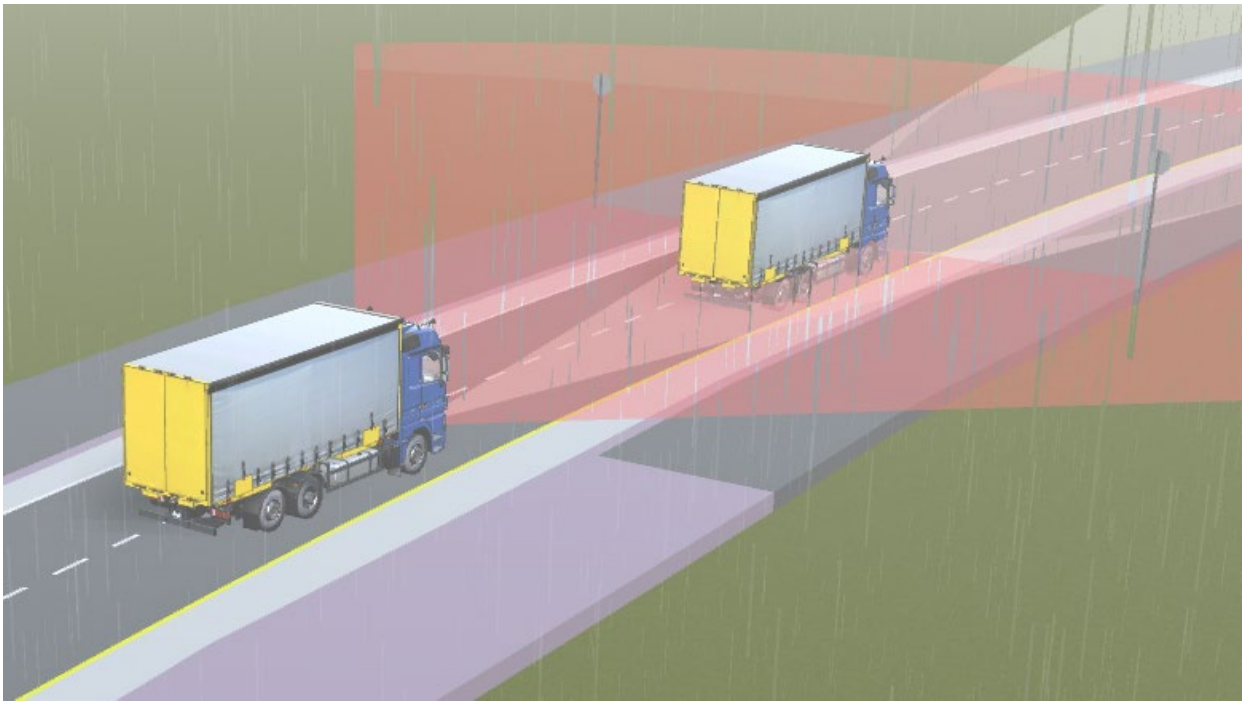

Figure 89: Lead Vehicle inside follower vehicle Radar FoV

3.7.2.3 Scenario C

In the case of vehicle cut-ins when the following vehicle only utilized ACC radars, there were some unsafe driving conditions which occurred. For example, in the case where a vehicle would cut in between the leader and follower and move slower than the lead vehicle for some period of time before exiting the lane, the following vehicle would no longer be able to locate the lead vehicle. This was the case especially when a third vehicle that did not belong to the platoon would cut in between the two semi-trucks before they approached a turn (Figure 90 and Figure 91). It was in this case that the lead vehicle was too far away from the lead vehicle to reestablish the desired headway. It can be seen from Figure 92 and Figure 93 that the following vehicle was no longer able to locate the lead vehicle during the time intervals where the radar range, doppler velocity and azimuth angle were all reported to be zero as well as the grey “Adaptive Cruise Control” text. Figure 94 shows the resulting measurements in HWT during the periods where the following vehicle was not able to locate the leading vehicle.

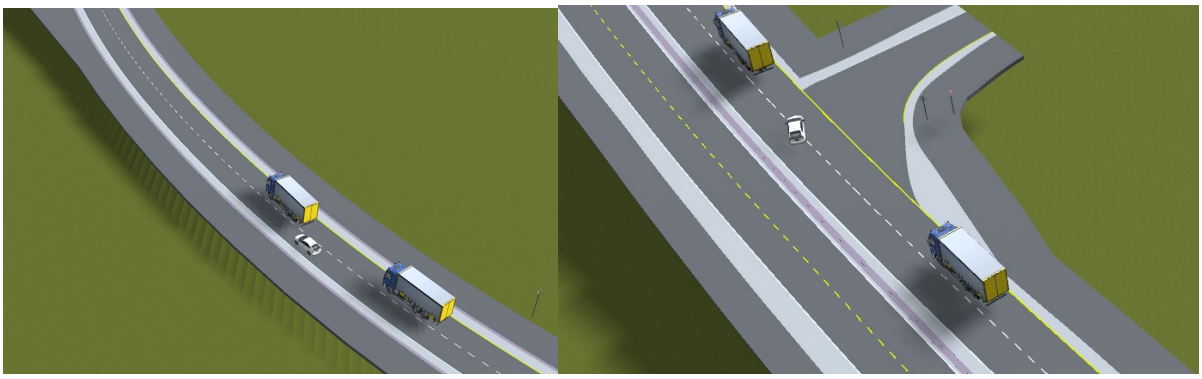

Figure 90: Non-convoy vehicle merging between leader and follower

Figure 91: Follower and leader separation due to vehicle cut-in

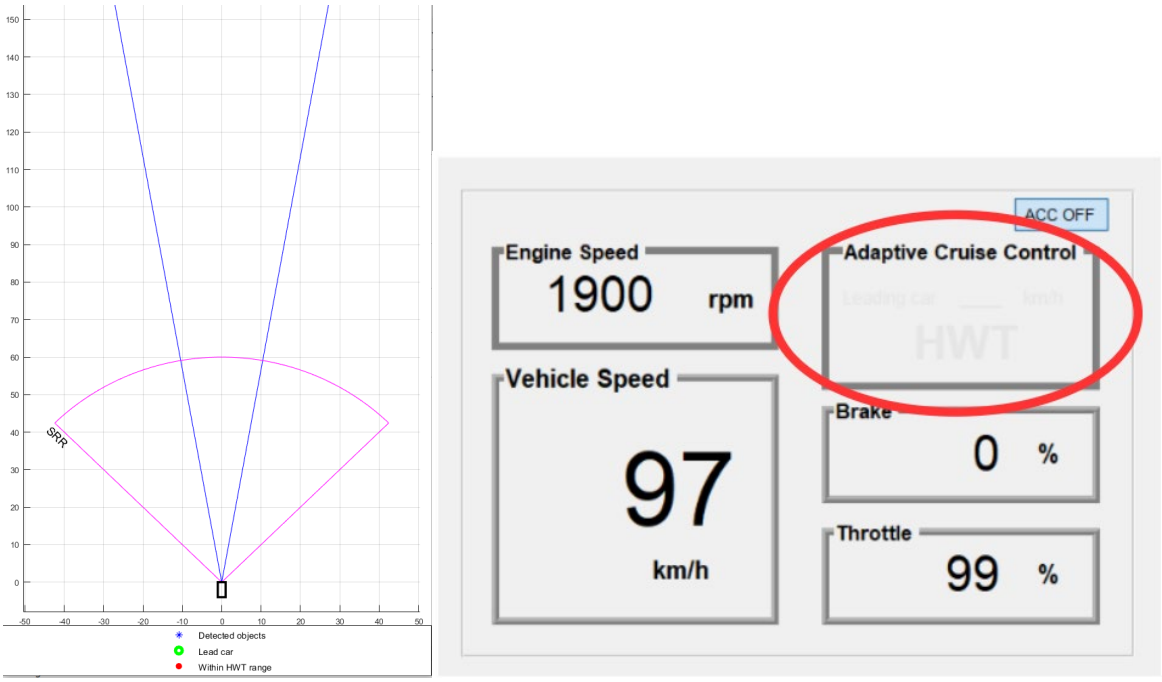

Figure 92: Radar GUI and Follower dashboard, lead vehicle out of FoV

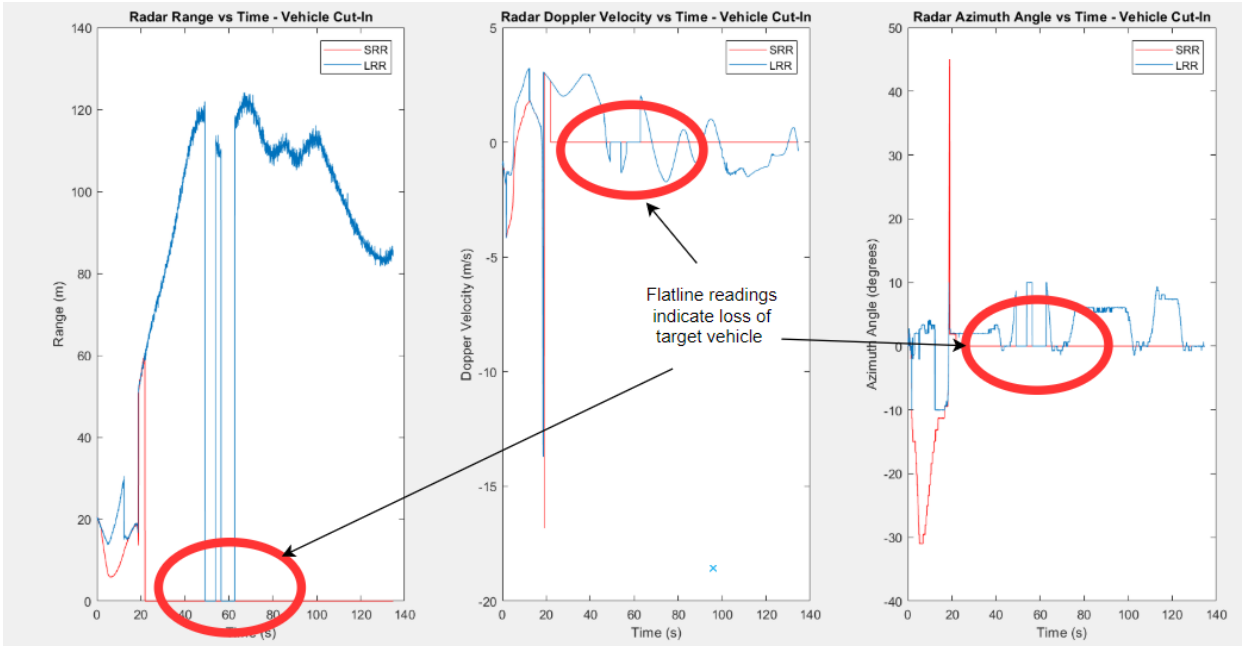

Figure 93: Lead vehicle disappears from Long-Range Radar and Short-Range Radar FoV

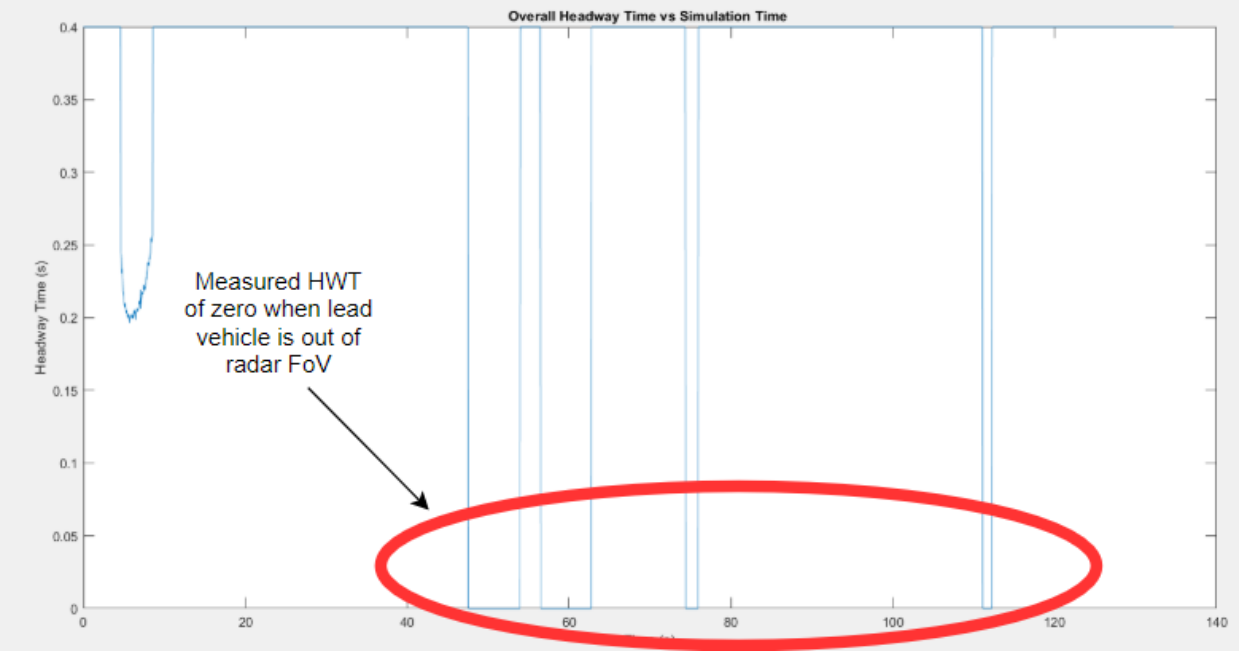

Figure 94: Loss of lead vehicle from radar FoV causes confusion to the system

3.7.2.4 Scenario D

It was proven in the previous scenario that when an alien vehicle would cut-in between the platoon that a poor HWT was observed (measured HWT was over double the demanded HWT). The performance of the platoon with the implementation of a V2V communication link improves drastically. The amount of time that the measured HWT of the lead vehicle was zero, and therefore the amount of time that the lead vehicle was outside of the ACC radar FOV and the following vehicle was not receiving GPS packets over the DSRC network was reduced by 38%.

There are still some limitations to the model, however. In the case that a packet is dropped, a junk GPS location of 0° 0’ 0” latitude and 0° 0’ 0” longitude is received by the follower vehicle, and inaccurate measurements of the follower vehicle are calculated (Figure 95). This leads to incorrect calculations in HWT between the leading and following vehicles (Figure 96).

Figure 95: Error in GPS augmented BSM packet causes faulty range estimations

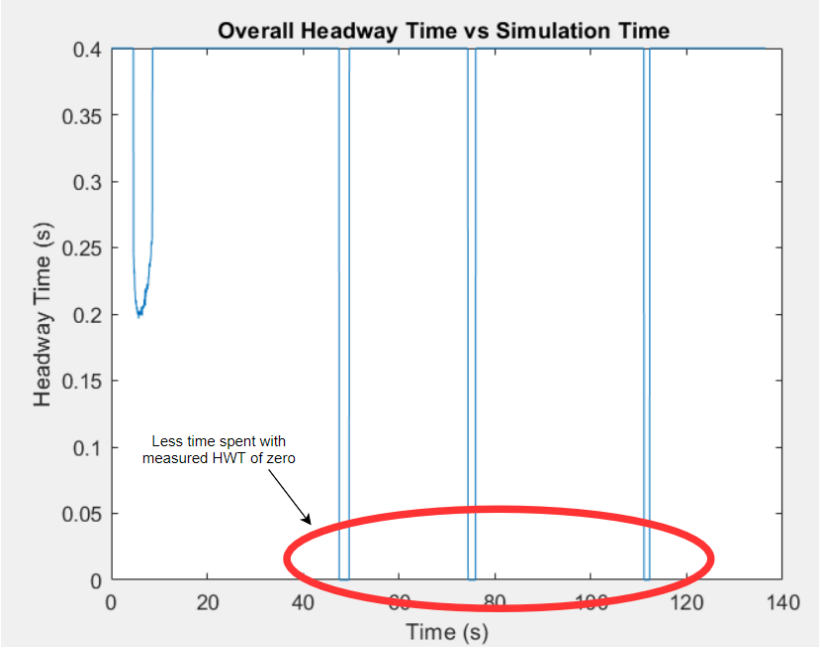

Figure 96: HWT with V2V as failsafe. Improved HWT performance

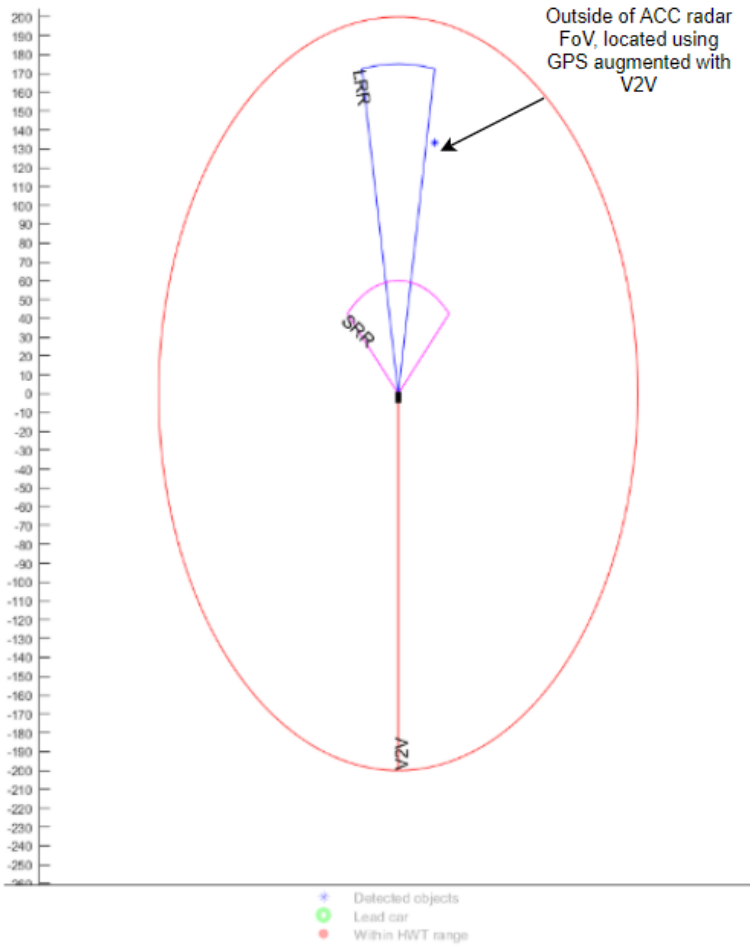

Figure 97: Lead vehicle localized by GPS sent over V2V

4 Conclusions

4.1 Overall Testing Performance

The assessment of different controllers and road grade profiles allows the team to thoroughly investigate the effects of grade and curvature on platooning vehicle fuel economy to establish whether the aerodynamic benefits outweigh the costs induced by speed and torque demand transients. The extraction of an ideal performance comparison from the NCAT data experimentally established that there are significant benefits to ideal truck platooning. When introducing grade variations, the overall fuel economy of the trucks decreased, regardless of their position in the platoon. PID-based control did not produce obvious fuel economy benefits for platooning configurations when confronted with the grade variations of ACM. Additionally, the differences in fuel economy from NCAT 2019 to NCAT 2020 were marginal, indicating the overall fuel economy benefits that could be obtained via a PID-style controller were nearly maximized. However, when the controller strategy was changed to 'optimal' NMPC for ACM 2021 testing, enhanced fuel economy benefits were observed even in the presence of grade variations. In conclusion, while operating on roads with significant grade changes, the choice of control strategy is key to obtaining energy efficiency benefits via truck platooning.

4.2 Influence of Cut-Ins and Merging

Cut-ins and merges were performed during three of the four testing periods. The differences between the periods were:

- During NCAT 2019 cut-ins, the truck downstream of the cut-in vehicle braked. Issues detecting the cut-in vehicle around curves were observed and subsequently eliminated for future iterations.
- NCAT 2020 cut-ins used the h-infinity control design and retreated from the cut-in vehicle using the retarder if necessary, opting to coast instead of brake.
- ACM 2021 cut-ins used the NMPC controller, which was very relaxed in its deceleration demands. Often, the trucks downstream of the cut-in vehicle chose to coast rather than implement brakes or retarder.

The cut-in runs in 2019 saw heavy losses in fuel economy due to lost kinetic energy (braking) and inefficient catchup behavior. During NCAT 2020 cut-ins, the impact of each cut-in was predicted, and losses were seen for all vehicles that dealt with the cut-in, especially the first truck downstream of the cut-in.

At ACM in 2021, cut-ins and merges were conducted on hilly terrain utilizing the optimal NMPC control design. A paired f- and t-test comparison was drawn between the 4T NMPC controlled platooning runs and the merges/ cut-in cases. In most instances, the cut-ins decreased fuel economy, up to 11 percent worse. One case for the last truck showed better fuel economy during cut-ins. This is not outside the realm of possibility as the cut-in vehicle rode beside the platoon and potentially provided additional aerodynamic shielding.

4.3 Influence of Grade

Attempts to elucidate the influence of grade on platooning performance must include control design details as different controllers handle grade disturbances disparately. The influence of grade on platoons will be discussed for each controller separately and then compared.

For controllers that lack lookahead capability, grade disturbances severely hampered the fuel efficiency and string stability of the platooning vehicles. The energy efficiency deterioration increased the for each truck downstream in the platoon (a characteristic of string-instability).

Once lookahead control was implemented, as in the case of the newly developed NMPC controller, the outlook was much rosier. The second and third platooning vehicles in the four-truck platoon could now easily maintain formation. The underpowered fourth truck sometimes had difficulty maintaining its gap during the latter half of the ACM 2021 experimental period. This suggests that some platoon orders will experience better fuel efficiency than others, and that further refinement of A2's controller is required.

Data indicates that the shorter and steeper hills become, the worse that disturbance impacts platoon energy efficiency. At inflection points, the platooning vehicles are experiencing disparate disturbances: a leader may be going up a hill, and a follower down, or vice versa. It was during these peaks and valleys that the platoon performance was most tested by grade.

In a brief overview of the fuel economy for A2 during operation at NCAT 2020 and ACM 2019, the most similar controller designs (both PID) with introduction of increased grade severity, the effect of road grade plays a massive role in the decline of the average fuel economy of a truck. This can be seen in Figure 98.

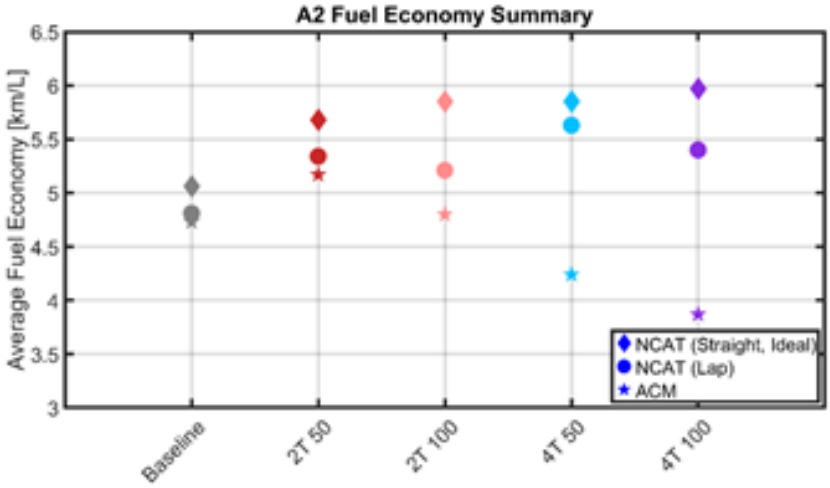

Figure 98: A2 Fuel Economy Summary

Figure 98, shows that grade influences platoons differently based on (at minimum) platoon size and following distance. Baseline operation does not experience substantial disparities in fuel economy due to the grade changes present at ACM. But overall, fuel economy still decreases as road grade severity increases from the "ideal" performance at NCAT to the whole NCAT lap analysis, and then ACM. The fuel economy range (from ideal to ACM in any configuration) is much smaller for 2T platoons than for 4T platoons, whether the following distance is 50 or 100 feet, indicating that, as the size of a platoon increases, the impact of grade on fuel economy increases. From a following distance perspective, the fuel economy range for 2T 50 is noticeably smaller than 2T 100 and can likewise be interpreted from the 4T 50 and 4T 100 data. The impact of grade on fuel economy for 4T configurations increases as the following distance increases. This signifies those platoons of greater following distances are more susceptible to decline in fuel economy due to increased road grade transients.

4.4 V2V Communications Subsystem Performance

Our work studies the influence of a wide variety of both independent and correlated determinants of RF performance in the context of DSRC V2V used to enable platooning via CACC. We have examined the impact on RSSI of occlusions, rain, antenna mounting position, RF interference, GPS dependencies, road curvature, and road grade. These measurements range from not noticeable to significant differences in performance; however, the physical real-world environment such as road curvature can overwhelm smaller subtleties when not isolated even on a closed test track such as those on which we performed our tests. Despite this, we were able to show how comparisons can be made and isolated even when environmental factors coincide together and would be difficult to observe otherwise.

4.5 Effect of Sensor Performance on Platooning

The CACC system outlined herein critically depends on GPS, radar, and V2V communications. As such, this study investigated three potential mechanisms in which sensor performance degradation could lead to degraded convoy platooning performance. The study was conducted in a controlled environment on a closed test track with minimal grade changes.

Installing a radar in reverse orientation leads to missing radar updates and allowed erroneous range estimation in the short term, resulting in unnecessary vehicle transience. Due to aggressive acceleration events, operation with faulty radar led to a 5.68 % increase in fuel consumption. However, the missing radar updates occurred during a relatively tight curve, an unlikely scenario for a real-world platooning application.

Additional scenarios where a lack of satellites caused ‘poor’ GPS performance and where RF interference was intentionally created did not produce fuel consumption impacts. During these tests, the CACC range estimate was sufficiently accurate to maintain intended platooning performance. However, the RF interference should be expanded over longer durations and to stronger intensities before broader conclusions are reached.

It is worth noting that the results herein are specific to the control system and sensor suite of these trucks, and that other commercial or research-grade platooning systems may experience different results. Still, the mechanism of disturbance remains the same in all cases: sensor degradation leading to poor dynamic performance, leading to increased fuel consumption.

4.6 Modeling and Simulation

Our modeling and simulation work shows that having a DSRC link between two trucks in a convoy is an effective means of reducing the amount of “blind time” where the following vehicle is operating without awareness of where the lead vehicle is.

5 Recommendations

5.1 For Real-World Fuel-Efficient Platoon Control

Over flat terrain, classical PID methods were found to be sufficient for platoon control. Once grade became a significant disturbance, lookahead control is essential for maintaining platoon fuel economy benefits. Recent work has used classical control methods and kinetic energy minimization to approach the benefit of lookahead control (Xu et al. 2017), and these methods warrant further investigation in the heavy-duty platooning context.

From this work, it is hypothesized that two control behaviors define the efficiency of a platoon: how much energy is wasted in slowing the platoon down, and how efficiently the power is recovered.

5.2 On Allowed Platoon Headway Variance

In this study, allowing headway variance over grade changes was essential to fuel-efficient platooning.

In this study, up to 75 feet of headway variation occurred with the lookahead NMPC controller. This is not the most useful number, since varying terrain and truck configuration will drastically impact the headway variance. The recommendation is to further investigate what quantity allowed headway variance allows braking to be avoided for a variety of platoon configurations.

During the ACM tests, the headway variance of the lookahead controller was higher than that of the PID controller, which enabled vast fuel economy improvements in 2021. Relative to its own baseline operation, truck A2, which operated last in the 4T platoon, experienced 18% worse fuel economy during platooning in 2019 (with PID) and 10% better fuel economy while platooning in 2021 (with optimal NMPC).

The more important factor was energy conservation (avoiding break/retarder) and subsequent catchup behavior. By intelligently increasing gap in anticipation of the upcoming grade disturbances, much less energy was lost to brake/retarder application.

Potential fuel efficiency benefits were the primary investigation, but any future controllers will require an in-depth safety analysis as well.

5.3 V2V Communications Subsystem Performance

Future work could include generalizing on larger data sets and being able to predict the impact of changes. It may even potentially include Cellular Vehicle-to-Anything (CV2X) technologies that have been recently emerging. The sensors used in this research are standard and well-documented for this application, and there is a research opportunity in applying more novel sensors such as Ultra-Wide-band radar, LIDAR, and cameras to platooning. Additionally, harsher environment such as rain or snow could poses unresolved challenges for the current sensors and merit further investigations.

5.4 Effect of Sensor Performance on Platooning

Further investigations are needed where the convoy experiences more disruptions caused by elevation changes, turns, tunnels, foliage, traffic, RF interference, etc. The sensors used were standard and well-documented for this application, and there is a research opportunity in applying more novel sensors such as Ultra-Wide-band radar, LIDAR, and cameras to

platooning. Additionally, harsher environment such as rain or snow could poses unresolved challenges for the current sensors and merit further investigations.

5.5 Modeling and Simulation

Future work on our modeling and simulation effort is to explore other case scenarios where having a communication link between autonomous vehicle platoons is beneficial to the safety of the platoon and surrounding vehicles on the roadway. The next steps would include testing in different environments, with different vehicles and with other sensors such as camera sensors, Lidar, ultrasonic, and others.

6 Products

6.1 Publications/Presentations

- ASME Journal of Dynamic Systems, Measurements, and Control Special Issue
  - “A Method of Optimal Control for Class-8 Vehicle Platoons Over Hilly Terrain” accepted for publication in a special issue titled “Optimal Energy Management and Control in Connected and Automated Vehicles”.
- WCX SAE World Congress Experience 2022
  - “New Metrics for Quantifying the Energy Efficiency of Platoons in the Presence of Disturbances” submitted to session PFL-0565, “Holistic Session on Fuel Consumption and Fuel Economy”
  - “Experimentally Establishing Ideal Platooning Performance as a Metric for Real-World Platooning Assessment” submitted to session AE-101, “ADAS and Autonomous Vehicle System: Safety, Fundamentals, and Driver Interface”
- GVSETS 2019
  - J. Ward, P. Smith, D. Pierce, D. Bevly, P. Richardson, S. Lakshmanan, A. Argyris, B. Smyth, C. Adam and S. Heim, "Cooperative adaptive cruise control (CACC) in controlled and real-world environments: testing and results," 2019 NDIA Ground Vehicle Systems Engineering and Technology Symposium (GVSETS), August, 2019. Awarded Conference Best Paper.
- SPIE 2020
  - E. Cheek, H. Alghodhaifi, C. Adam, R. Andres and S. Lakshmanan "Dedicated short range communications used as fail-safe in autonomous navigation", Proc. SPIE 11425, Unmanned Systems Technology XXII, 114250P (23 April 2020); https://doi.org/10.1117/12.2558925.
- SAE WCX 2021
  - C. Adam, R. Andres, B. Smyth, T. Kleinow, K. Grenn, S. Lakshmanan and P. Richardson, "Performance of DSRC V2V communication networks in an autonomous semi-truck platoon application," SAE Technical Paper 2021-01-0156, 2021, https://doi.org/10.4271/2021-01-0156.
  - C. Adam, S. Lakshmanan, P. Richardson, E. Stegner, et al., "Correlation between sensor performance, autonomy performance and fuel-efficiency in semi-truck platoons," SAE Technical Paper 2021-01-0064, 2021, https://doi.org/10.4271/2021-01-0064.
  - “Experimental Fuel Consumption Results from a Heterogeneous Four-Truck Platoon” presented in session AE100, "ADAS and Autonomous Vehicle System"
  - “Using Demanded Power and RDE Aggressiveness Metrics to Analyze the Impact of CACC on Fuel Savings for Heavy Duty Platooning” to be presented in session AE100, "ADAS and Autonomous Vehicle System"
- Book Chapter 2021
  - S. Lakshmanan, C. Adam, T. Kleinow, et al. "Semi-autonomous truck platooning with a lean sensor package," to appear in AI-enabled Technologies for Autonomous and Connected Vehicles, Editors: Y. L. Murphey, I. Kolmanovsky and P. Watta, Springer, 2021.

6.2 Patents Applications/Inventions

Newly filed Provisional Application No. 63/215,721: “A Method of Optimal Control for Class-8 Vehicle Platoons over Hilly Terrain” was submitted to the United States Patent and Trademark Office on June 28th, 2021, listed inventors are Jacob Ward, Evan Stegner, Mark A. Hoffman, and David M. Bevly. The patent invention will be submitted via iEdison by the Auburn University, Alabama legal patent office to fulfill the project close requirements. They will also perform the required reporting for the 10 year period of time specified.

6.3 Works Cited

Alghodhaifi, H., S. Lakshmanan, S. Baek, and P. Richardson. 2018. "Autonomy Modeling and Validation in a Highly Uncertain Environment." *Proceedings of the Ground Vehicle Systems Engineering and Technology Symposium.*

Amoozadeh, Mani, Hui Deng, Chen-Nee Chuah, Michael H. Zhang, and Dipak Ghosal. 2015. "Platoon Management with Cooperative Adaptive Cruise Control Enabled by VANET." *Vehicular Communications 2*, March 28: 110-123.

Bainwol, Mitch, Desi Ujkashevic, Don Butler, and John F. Kwant, Jovan Zagajac Kwant. 2020. "Comments of the Ford Motor Company before the Federal Communications Commission in the matter of use of the 5.850-5.925 GHz band."

Bergenhem, Carl, Erik Hedin, and Daniel Skarin. 2012. "Vehicle-to-Vehicle Communication for a Platooning System." *Elsevier.* doi:10.1016/j.sbspro.2012.06.1098.

Bergenhem, Carl, Rolf Johansson, and Erik Coelingh. 2014. "Measurements on V2V Communication Quality in a Vehicle Platooning Application ." *MACOM 2014: Multiple Access Communications* 35-48.

Bogard, Scott E., Shan Bao, David LeBlanc, Li Jun, Shaobo Qiu, and Bin Lin. 2017. "Performance of DSRC during Safety Pilot Model Deployment." *SAE International Journal of Passenger Cars-Electronic and Electrical Systems* 10: 165-172.

CAMP LLC. 2019. "C-V2X Performance Assessment Project."

Chandra, M., S. Joshi, and L. Singh. 2014. "Prediction of Rain Attenuation and Impact of Rain in Wave Propagation at Microwave Frequency for Tropical Region." *International Journal of Microwave Science and Technology.*

Cheek, Eric, Hesham Alghodhaifi, Cristian Adam, Russell Andres, and Sridhar Lakshmanan. 2020. "Dedicated Short Range Communications used as FailSafe in Autonomous Navigation." *Unmanned Systems Technology XXII.*

Cheng, Bin, Hongsheng Lu, Ali Rostami, Marco Gruteser, and John B. Kenney. 2017. "Impact of 5.9 GHz Spectrum Sharing on DSRC Performance." *2017 IEEE Vehicular Networking Conference (VNC).*

Crane, Carl, Jennifer Bridge, and Richard Bishop. 2018. "Driver Assistive Truck Platooning: Considerations for Florida State Agencies."

Dadam, Sumanth Reddy, Robert Jentz, Tyler Ienzen, and Herbert Meissner. 2020. "Diagnostic Evaluation of Exhaust Gas Recirculation (EGR) System on Gasoline Electric Hybrid Vehicle." *SAE.* doi:10.4271/2020-01-0902.

Delgrossi, L., and T. Zhang. 2012. *Vehicle safety communications: protocols, security, and privacy.* Hoboken, N.J: Wiley-Blackwell.

Eilbert, Andrew C., Anne-Marie Chouinard, Tim A. Tiernan, and Scott B. Smith. 2020. "Performance Comparisons of Cooperative and Adaptive Cruise Control Testing." *A&WMA's 113th Annual Conference & Exhibition.*

Ekiz, Levent, Adrian Posselt, Oliver Klemp, and Christoph F. Mecklenbrauker. 2014. "Assessment of Design Methodologies for Vehicular 802.11p Antenna Systems." *2014 International Conference on Connected Vehicles and Expo (ICCVE).*

Federal Communications Commission . n.d. Accessed 11 12, 2020. https://transition.fcc.gov/oet/ea/presentations/files/oct07/Oct_07-Basics_of_Unlicensed_Trans-JD.pdf.

Francisco, N, and M Vicente. 2019. "Mixing V2V and Non-V2V Equipped Vehicles in Car Following." *Transportation Research Part C Emerging Technologies* 108: 167-181. doi:https://doi.org/10.1016/j.trc.2019.08.021.

Gao, Song, Alvin Lim, and David Bevly. 2016. "An Empirical Study of DSRC V2V Performance in Truck Platooning Scenarios." *Digital Communications and Networks* 2 (4): 233-244.

Ghassemzadeh, S.S., and V. Tarokh. 2003. "UWB path loss characterization in residential environments." *IEEE MTT-S International Microwave Symposium Digest.*

Gonçalves, Tiago Rocha, Vineeth Varma, and Salah Elayoubi. 2020. "Vehicle platooning schemes considering V2V communications: A joint communication/control approach." *IEEE Wireless Commu-* 1-6. https://hal.archives-ouvertes.fr/hal-02448795v2.

Harri, Jerome., Hugues Tchouankem, Oliver Klemp, and Oleksandr Demchenko. 2013. "Impact of Vehicular Integration Effects on the Performance of DSRC Communications." *2013 IEEE Wireless Communications and Networking Conference (WCNC).*

Kaul, Sanjit, Kishore Ramachandran, Pravin Shankar, Sangho Oh, M Gruteser, I Seskar, and T Nadeem. 2007. "Effect of Antenna Placement and Diversity on Vehicular Network Communications." *4th Annual IEEE Communications Society Conference on Sensor, Mesh and Ad Hoc Communications and Networks* 112-121. doi:https://doi.org/10.1109/SAHCN.2007.4292823.

Kestwal, Mukesh Chandra, Sumit Joshi, and Lalit Singh Garia. 2014. "Prediction of Rain Attenuation and Impact of Rain in Wave Propagation at Microwave Frequency for Tropical Region (Uttarakhand, India)." *International Journal of Microwave Science and Technology* 2014.

Lakshmanan, S., Y. Yu, S. Baek, and A. Alghodhai. 2019. "Modeling and Simulation of Leader-Follower Autonomous Vehicles: Environment Effects." *SPIE Unmanned Systems Technology XXI.*

Li, W., J. Wu, X. Ma, and Z. Z. Zhang. 2014. "On reliability requirement for BSM broadcast for safety applications in DSRC system." *IEEE Intelligent Vehicles Symposium Proceedings.*

Liou, Chong-Yi, and Shau-Gang Mao. 2017. "Miniaturized Shark-Fin Rooftop Antenna with Integrated DSRC Communication Module for Connected Vehicles." *2017 XXXIInd General Assembly and Scientific Symposium of the International Union of Radio Science (URSI GASS).*

Liu, Sheng, Weidong Xiang, and M. Xavier Punithan. 2018. "An Empirical Study on Performance of DSRC and LTE-4G for Vehicular Communications." *2018 IEEE 88th Vehicular Technology Conference (VTC-Fall).*

Longman, O. 2019. "Mitigation of Vehicle Vibration Effect on Automotive Radar." *IEEE Xplore.* doi:10.1109/RADAR.2019.8835520.

Lu, Xiao-Yun, and Steven E. Shladover. n.d. "Automated Truck Platoon Control and Field Test." https://www.researchgate.net/publication/266390502.

Lyamin, Nikita. 2016. "Performance evaluation of." *LICENTIATE THESIS | Halmstad University Dissertations no. 26.*

Ma, Xiaomin, Xianbo Chen, and Hazem Refai. 2009. "Performance and Reliability of DSRC Vehicular Safety Communication: A Formal Analysis." *EURASIP Journal on Wireless Communications and Networking* 2009: 1-13.

McAuliffe, Brian, Michael Lammert, Xiao-Yun Lu, Steven Shladover, Marius-Dorin Surcel, and Aravind Kailas. n.d. "Influences on Energy Savings of Heavy Trucks Using Cooperative Adaptive Cruise Control." *SAE.* doi:10.4271/2018-01-1181.

McAuliffe, Brian; Arash Raeesi; Michael Lammert; Patrick Smith; Mark Hoffman; and David Bevly. 2020. “Impact of Mixed Traffic on the Energy Savings of a Truck Platoon.” *SAE International Jounal Advances and Current Practices in Mobility* 2 (3): 1472–96. https://doi.org/10.4271/2020-01-0679.

Meireles, Rui, Mate Boban, Peter Steenkiste, Ozan Tonguz, and João Barros. 2010. "Experimental Study on the Impact of Vehicular Obstructions in VANETs." *2010 IEEE Vehicular Networking Conference.*

Nardini, Giovanni, Antonio Virdis, Claudia Campolo, and Antonella Molinaro. 2018. "Cellular-V2X Communications for Platooning:Design and Evaluation." *SENSORS MDPI.* doi:10.3390/s18051527.

Onishi, Hiro, Fumio Watanabe, Fanny Mlinarsky, and Carlos Velasquez. 2013. "DSRC Performance Assessment for Crash Warning Applications." *2013 International Conference on Connected Vehicles and Expo (ICCVE).*

Ploeg, Jeroen; Nathan van de Wouw; and Henk Nijmeijer. 2014. “Lp String Stability of Cascaded Systems: Application to Vehicle Platooning.” *IEEE Transactions on Control Systems Technology* 22 (2): 786–93. https://doi.org/10.1109/TCST.2013.2258346.

Qing, X., and R. Sengupta. 2003. "Simulation, analysis, and comparison of ACC and CACC in highway merging control." *IEEE IV2003 Intelligent Vehicles Symposium Proceedings.*

Roberts, Jack, Rick Mihelic, Mike Roeth, and Denise Rondini. n.d. "Confidence Report: Two-Truck Platooning." *2016 North American Council for Freight Efficiency.*

SAE International. 2016. "Surface Vehicle Standard Dedicated Short Range Communication Message Set Dictionary."

SAE V2X Core Technical Committee. n.d. "Dedicated Short Range Communications (DSRC) Message Set Dictionary: A March 2016 Update." *Society of Automotive Engineers.* Accessed 2019. https://saemobilus.sae.org/content/j2735_201603.

Serizawa, Koichi, Manabu Mikami, Kohei Moto, and Hitoshi Yoshino. 2019. "Field Trial Activities on 5G NR V2V Direct Communication Towards Application to Truck Platooning." *IEEE 90th Vehicular Technology Conference.* doi:https://doi.org/10.1109/VTCFall.2019.8891260.

Shladover, Steven E, Christopher Nowakowski, Xiao-Yun Lu, and Raymond Hoogendoorn. 2014. "Using Cooperative Adaptive Cruise Control (CACC) to Form High-Performance Vehicle." *UC Berkeley Research Reports.* doi:Cooperative Agreement No. DTFH61-13-H-00013.

Smith, Patrick; Jacob Ward; John Pierce; David Bevly; and Rob Daily. 2019. “Experimental Results and Analysis of a Longitudinal Controlled Cooperative Adaptive Cruise Control (CACC) Truck Platoon.” In . https://doi.org/10.1115/DSCC2019-9135.

Stegner, Evan; Jacob Ward; Jan Siefert; Mark Hoffman; and David M. Bevly. 2021. “Experimental Fuel Consumption Results from a Heterogeneous Four-Truck Platoon.” In , 2021-01–0071. https://doi.org/10.4271/2021-01-0071

Sugimachi, Toshiyuki, Takanori Fukao, Yoshitada Suzuki, and Hiroki Kawashima. 2013. "Development of Autonomous Platooning System for Heavy-duty Trucks." *7th IFAC Symposium on Advances in Automotive Control* 46 (21): 52-57.

Sybis, Michal, Pawel Kryszkiewicz, and Pawel Sroka. 2018. "On the Context-Aware, Dynamic Spectrum Access for Robust Intraplatoon Communications." *Mobile Information Systems.* doi:https://doi.org/10.1155/2018/3483298.

van Nunen, Ellen, Jan Verhaegh, Emilia Silvas, Elham Semsar-Kazerooni, and Nathan Wouw. 2017. "Robust Model Predictive Cooperative Adaptive Cruise Control Subject to V2V Impairments." *IEEE 20th International Conference on Intelligent Transportation Systems (ITSC).*

Wang, Chaojie, Situan Gong, Anye Zhou, Tao Li, and Srinivas Peeta. n.d. "Cooperative Adaptive Cruise Control for Connected Autonomous Vehicles by Factoring Communication-Related Constraints." *Elsevier 23rd International Symposium on Transportation and Traffic.*

Wang, Ziran, Guoyuan Wu, and Matthew J. Barth. n.d. "A Review on Cooperative Adaptive Cruise Control (CACC) Systems: Architectures, Controls, and Applications." *IEEE 21st*

International Conference on Intelligent Transportation Systems (ITSC). doi:https://doi.org/10.1109/ITSC.2018.8569947.

Wang, Ziran, Guoyuan Wu, and Matthew J. Barth. n.d. "Developing a Distributed Consensus-Based Cooperative Adaptive Cruise Control System for Heterogeneous Vehicles with Predeessor Following Topology." (Journal of Advanced Transportation) 2017 (1023654,). doi:1023654,.

Ward, Jacob. 2019. "Cooperative Adaptive Cruise Control (CACC) in Controlled and Real-World Environments: Testing and Results." *Ground Vehicle Systems Engineering and Technology Symposium* (NDIA).

Ward, Jacob, Patrick Smith, Dan Pierce, David Bevly, Paul Richardson, Sridhar Lakshmanan, Athanasios Argyris, Brandon Smyth, Cristian Adam, and Scott Heim. 2019. "Cooperative Adaptive Cruise Control (CACC) in Controlled and Real-World Environments: Testing and Results." *2019 NDIA Ground Vehicle Systems Engineering and Technology Symposium.* Novi.

Ward, Jacob; Evan Stegner; Mark A. Hoffman; and David M. Bevly. 2021. “A Method of Optimal Control for Class 8 Vehicle Platoons Over Hilly Terrain.” Preprint. Auburn, AL: Auburn University. ResearchGate. https://doi.org/10.13140/RG.2.2.18294.32322.

Wood, Eric; Adam Duran; Evan Burton; Jeffrey Gonder; and Kenneth Kelly. 2016. “EPA GHG Certification of Medium- and Heavy-Duty Vehicles: Development of Road Grade Profiles Representative of US Controlled Access Highways.” *SAE International Journal of Commercial Vehicles* 9 (2): 79.

Xu, Shaobing; Shengbo Eben Li; Bo Cheng; and Keqiang Li. 2017. “Instantaneous Feedback Control for a Fuel-Prioritized Vehicle Cruising System on Highways With a Varying Slope.” *IEEE Transactions on Intelligent Transportation Systems* 18 (5): 1210–20. https://doi.org/10.1109/TITS.2016.2600641.

Yamada, N. 2005. "Radar Cross Section for Pedestrian in 76GHz Band." *Research Report – R&D Review of Toyota CRDL Vol. 39 No. 4.*

Yu, Tao, Shunqing Zhang, Sha Cao, and Shugong Xu. 2018. "Performance Evaluation for LTE-V based Vehicle-to-Vehicle Platooning Communication." https://arxiv.org/abs/1810.00568v1.

Zeng, Tengchan, Omid Semiari, Walid Saad, and Mehdi Bennis. 2019. "Joint Communication and Control for Wireless Autonomous Vehicle Platoon Systems." *IEEE ICC, 2018.* doi:arXiv:1804.05290v2.

Zhang, Congchi, Yunpeng Zang, Jose Angel Leon Calvo, and Rudolf Mathar. 2017. "A Novel V2V Assisted Platooning System: Control Scheme and MAC layer Designs." *IEEE.* doi:https://doi.org/10.1109/PIMRC.2017.8292186.